



Title	Studies on Characterization of Cubosomal Drug Carriers and Their Interactions with Model Cell Membranes
Author(s)	Wakileh, Ward Daoud Salim
Citation	大阪大学, 2025, 博士論文
Version Type	VoR
URL	https://doi.org/10.18910/101701
rights	
Note	

The University of Osaka Institutional Knowledge Archive : OUKA

<https://ir.library.osaka-u.ac.jp/>

The University of Osaka

**Studies on Characterization of Cubosomal Drug
Carriers and Their Interactions with Model Cell
Membranes**

WARD WAKILEH

MARCH 2025

Studies on Characterization of Cubosomal Drug Carriers and Their Interactions with Model Cell Membranes

A dissertation submitted to

THE GRADUATE SCHOOL OF ENGINEERING SCIENCE

OSAKA UNIVERSITY

in partial fulfillment of the requirements for the degree of

DOCTOR OF PHILOSOPHY IN ENGINEERING

BY

WARD WAKILEH

MARCH 2025

Abstract

Cubosomes are dispersed bicontinuous cubic phase nanoparticles that have demonstrated their potential as drug delivery carriers owing to their high drug payloads and fusogenic properties. The design process of cubosomes as drug delivery carriers requires consideration of factors such as their structure, drug release, and interactions with cell membranes which are heavily influenced by the properties of the cubic membrane. In this work, systematic characterizations of the nanoparticles' structure and membrane were performed to elucidate how changes in the membrane environment can impact the carrier's structure and dispersibility. Also, a methodology to examine the interactions of cubosomes with model cell membrane through the examination of cubic membrane and structure was established. The results of this work provide new insights that can be helpful in clarifying the cubosome uptake mechanism by cells as well as the optimal design of cubosomes as drug delivery carriers.

In chapter 2, the effects of the incorporation of the hydrophobic drug hydrocortisone (HC) on the physicochemical properties of monoolein (MO) and MO/oleic acid (OA) self-assemblies are investigated using Raman spectroscopy, cryogenic Transmission Electron Microscopy (cryo-TEM), and Laurdan fluorescent probe. The HC incorporation influenced the surface property of MO and MO/OA dispersions, causing aggregation of the self-assemblies at high hydrocortisone loading. In addition, the change in surface properties of the self-assemblies due to drug incorporation results in changes in structural changes and formation of aggregations. The characterization method in this chapter is essential to clarify the influence of the drug on the properties such as polarity, zeta-potential, and particle size etc., and how these properties correlate to colloidal stability.

In chapter 3, the methodology to elucidate the changes to the physicochemical properties of cubosomes when interacting with cell membrane lipids was established. The interactions of MO cubosomes after mixing with DOPC liposomes using time-resolved small-angle X-ray scattering (TR-SAXS) and the changes to the generalized polarization (GP_{340}) values of Laurdan probed cubosomes over time were shown. The cubic-to-

lamellar phase transition was confirmed in the time-resolved SAXS spectra. Using the GP_{340} , the kinetics of apparent lipid exchange (k_{app}) were obtained and the apparent amount of DOPC in the cubosomes over the course of interaction could be estimated.

In chapter 4, the approach developed in chapter 3 was expanded upon to examine the changes in the structural and cubic membrane of MO cubosomes when mixed with model cell membranes at different phase states. In addition, the changes induced by the cubosomal carrier on the model cell membrane were investigated. The time of the structural change of the cubic phase to lamellar phase was influenced by the fluidity of the liposome bilayers. Mixing the cubosomes with fluid membrane liposomes required less time to transition to the lamellar phase and vice versa. Examining the (GP_{340}) values of the cubosomes and liposomes after mixing revealed that the membrane hydration states of the cubosomes and liposomes transitioned to resemble the hydration state of their counterpart, and the time needed to reach the final intermediate state was influenced by the membrane hydration of the liposomes.

In chapter 5, based on the results of the characterization of the drug incorporated carrier in chapter 2 and the methodology developed in chapters 3 and 4, the effects of loading of the drug, HC, on the interactions of MO cubosomes with liposomes were showcased. Although the incorporation of the drug did not alter the duration and kinetics of the cubic to lamellar phase transition, the membrane state analysis using Laurdan fluorescence probe showed slower kinetics in the drug loaded cubosomes. This implies that the rate of lipid exchange between carriers and cell membranes was suppressed in the presence of drug molecules.

In chapter 6, the conclusions of this work are presented, and suggestions for future works by enhancing the current methodology and broadening the scope of the developed approach for other types of lipid nanoparticles are addressed.

Preface

This dissertation work was conducted under the supervision of Professor Hiroshi Umakoshi at Division of Chemical Engineering, Graduate School of Engineering Science, Osaka University from 2019 to 2025.

The objective of this thesis to elucidate the physicochemical properties of dispersed liquid lyotropic crystalline nanoparticles, more particularly the structure and cubic membrane. In addition, this work seeks to develop the methodology to examine the interaction of cubosomal carriers model cell membranes and factors affecting them such as drug incorporation.

The author hopes that this work can provide further insights into the design process of cubosomes as drug carriers for a variety of therapeutic applications. In addition, the results of this study could be generalized to study the interactions of other types of lipid nanoparticles with model cell membranes.

Ward Wakileh

Division of Chemical Engineering
Graduate School of Engineering Science
Osaka University
Toyonaka, Osaka, 560-8531, Japan

Contents

Abstract	i
Preface	iii
Contents	iv
Chapter 1: General Introduction	1
1. Self-assembled Lyotropic Nanoparticles as Drug Delivery Carriers	1
2. Dispersed bicontinuous Cubic Phase Nanoparticles (cubosomes)	3
2.1 Lipids for the Preparation of Cubosomes	4
2.2 Preparation of Cubosomes	5
3. Characterization Methods of Cubosomes	7
3.1 Characterization of Cubosome Structure	7
3.2 Characterization of Cubic Membranes	8
4. Influence of Drug Incorporation on Properties of Cubosomes	10
5. Interactions of Cubosomes with Cell membranes	10
6. Overview of this study	12
Chapter 2: Dispersibility and Surface Properties of Hydrocortisone-incorporated Self-Assemblies	15
1. Introduction	15
2. Materials and Methods	18
2.1 Materials	18
2.2 Preparation of HC Incorporated MO and MO/OA	18
2.3 Raman Spectroscopy Analysis	19
2.4 X-ray Diffraction (XRD)	19
2.5 Dynamic Light Scattering Analysis	19
2.6 Cryo-TEM Imaging of MO, MO/OA assemblies	19
2.7 Laurdan Spectra Measurements	19
3. Result and Discussion	21
3.1. Formation of HC-incorporated Self-assemblies and Effects on Hydrocarbon Chain Packing of the Self-Assemblies	21

3.2 Effects of HC-Incorporation on the Dispersibility of MO and MO/OA Self-Assemblies	25
3.3 Structure of HC-Incorporated Dispersions	26
3.4 Effects of HC Incorporation on Particle Size Distribution and Polydispersity	28
3.5 Alteration of Zeta Potential by Incorporating HC	30
3.6 Evaluation of the Polarity in HC-Incorporated Dispersions	32
4. Summary	34
Chapter 3: Interactions of Cubosomes with Cell Membrane Lipids: Revealed Through Cubic Membrane Property Analysis	35
1. Introduction	35
2. Materials and Methods	37
2.1 Materials	37
2.2 Preparation of MO/DOPC Nanoparticles, DOPC, and DPPC Liposomes	37
2.3 TR-SAXS Measurements	37
2.4 Cryo-TEM Imaging	38
2.5 Dynamic Light Scattering Analysis	38
2.6 Optical Density Measurements	38
2.7 Steady-State Laurdan Measurements	38
2.8 Steady-State Fluorescence Anisotropy Measurements	39
2.9 Time-Resolved Fluorescence Measurements	40
2.10 Time-Resolved Anisotropy of DPH	41
3. Results and Discussion	43
3.1 Structural and Nanoparticle Characterization of MO and MO/DOPC Nanoparticles	43
3.2 Evaluation of the Membrane Properties of MO/DOPC Nanoparticles	45
3.3 Structural and Membrane Property Changes of MO Cubosomes and DOPC Liposomes Upon Mixing	50
3.4 Estimation of the Apparent Lipid Exchange between MO Cubosomes and DOPC Liposomes Using GP_{340} Values	53
4. Summary	57

Chapter 4: Investigation of Cubosome Interactions with Liposomal Membranes Based on Time-Resolved Small-Angle X-ray Scattering (TR-SAXS) and Membrane Hydration State Analysis	58
1. Introduction	58
2. Materials and Methods	60
2.1 Materials	60
2.2 Preparation of Monoolein Cubosomes	60
2.3 Preparation of the Liposomes	60
2.4 TR-SAXS Measurements	60
2.5 Cryo-TEM Imaging	61
2.6 Laurdan Spectra Measurements	61
3. Results and Discussion	63
3.1 Examination of Structural Changes in MO Cubosomes Using TR-SAXS	63
3.2 Changes to the Cubic Lattice After Mixing	68
3.3 Cryo-TEM Imaging	70
3.4 Fluorescence Intensity of Laurdan Probed MO cubosomes	72
3.5 Generalized polarization GP_{340} of the cubic and liposomal membranes	74
4. Summary	81
Chapter 5: Examination of Effects of Hydrophobic Drug Incorporation on Cubosome-Cell membrane Model Interactions.	82
1. Introduction	82
2. Materials and Methods	83
2.1 Materials	83
2.2 Preparation of Monoolein Cubosomes	83
2.3 Preparation of the Liposomes	83
2.4 TR-SAXS Measurements	83
2.5 Laurdan Spectra Measurements	84
3. Result and Discussion	85
3.1 Effects of Drug Incorporation on Cubosome Structure	85
3.2 Examination of Structural Changes in MO Cubosomes Using TR-SAXS	85

3.3 Fluorescence Intensity of Laurdan Probed Drug Loaded Cubosomes and Liposomes	87
3.4 Generalized polarization GP_{340} of the Drug Loaded Cubosomes and Liposomes	89
4. Summary	91
Chapter 6: General Conclusion	92
Suggestion for Future Works	94
Nomenclatures	95
List of Abbreviations	96
References	97
List of Publications	106
Acknowledgements	108

Chapter 1: General Introduction

1. Self-assembled Lyotropic Nanoparticles as Drug Delivery Carriers

With new diseases emerging in recent times, effective treatment methods are at a huge demand. Researchers all over the world are in pursuit of developing novel technologies to successfully produce stable and effective drug delivery systems (DDS) for the treatment of various illnesses. A drug delivery system is defined as a device that designed to deliver pharmaceutical compound to achieve a therapeutic effect (Tiwari et al. 2012). Several approaches to drug delivery have been carried out using polymers, metallic and inorganic materials, and lipids. Drug carriers using lipid self-assemblies have been gaining significant attention for their high biocompatibility and biodegradation, safety, and ability to enhance the solubility of drugs with low solubility in aqueous systems (Hina Shrestha, Rajni Bala 2014). The system of self-assembly is driven by the hydrophobic interaction between the hydrocarbon tails which induces the molecules to congregate and the hydrophilic nature of the head groups which imposes the requirement of the headgroups to be in contact with water (Israelachvili et al. 1977). Amphiphilic lipids self-assemble to form various nanostructures including micelles, lamellar, hexagonal, and bicontinuous cubic phases as shown in **Figure 1-1**.

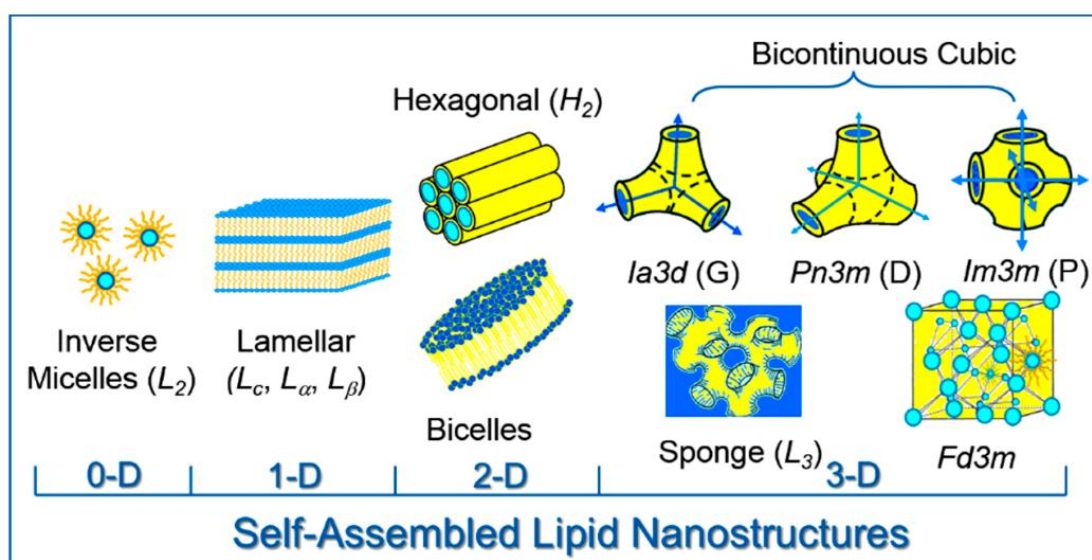


Figure 1-1 Self-assembly nanostructures of amphiphilic lipids (Kulkarni 2016).

When studying the nanostructures of lipid self-assemblies, an important parameter to be considered is the critical packing parameter (CPP). The CPP can be used to indicate how amphiphilic lipids self-assemble. Through the estimation of the CPP, the molecular packing and the resultant structure could be determined (Dutt et al. 2017). Amphiphilic lipids with a CPP=1 typically have cylindrical molecular geometry, and they adopt zero curvature, which promotes the formation of lamellar phases. The bilayer of the lamellar phase consists of planar layers where the head groups of the lipids face the aqueous phase and hydrophobic tails shielded from the aqueous phase. On the other hand, lipids with CPP>1 display inverse cone molecular geometry that display negative curvature resulting in the formation of phases with highly curved membranes such as hexagonal and bicontinuous cubic phases (Figure 1-2).

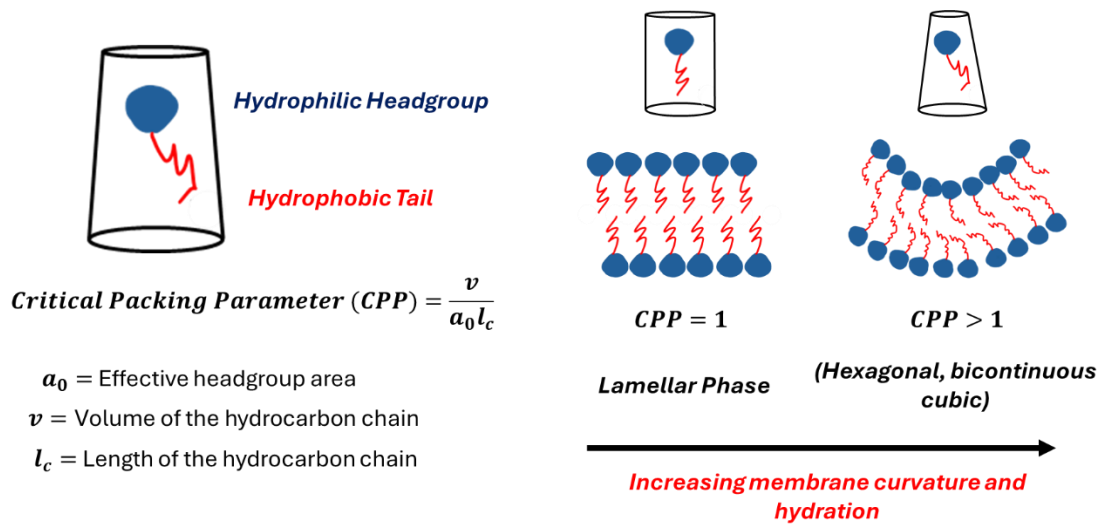


Figure 1-2 Schematic diagram of the critical packing parameter of different lipids.

The interest in lipid nanoparticles (LNPs) containing cubic and hexagonal phases have been on the rise recently because of their unique physicochemical properties. These phases are characterized by the high curvature of their lipid bilayers, adopting various complex shapes and configurations depending on conditions such as composition and temperature (Fong et al. 2009).

2. Dispersed bicontinuous Cubic Phase Nanoparticles (cubosomes)

A notable example of these LNPs are dispersions of the bicontinuous cubic phase (cubosomes), which are nanoparticles composed of cubic phases stabilized by non-ionic surfactants (Nakano et al. 2002). The cubic phases are composed of a 3D network of highly curved lipid bilayer membranes that are separated by two non-intersecting water channels (**Figure 1-3**). Due to their well-defined internal structures and large membrane surface area, cubosomes can accommodate large quantities of target molecules. The membrane surface area of the cubic phase can reach up to 400 m²/g of cubic phases (Barriga, Holme, et al. 2019). Such property makes cubosomes an attractive candidate for various therapeutic applications (Zhang et al. 2020; Sarkar et al. 2023; 2020).

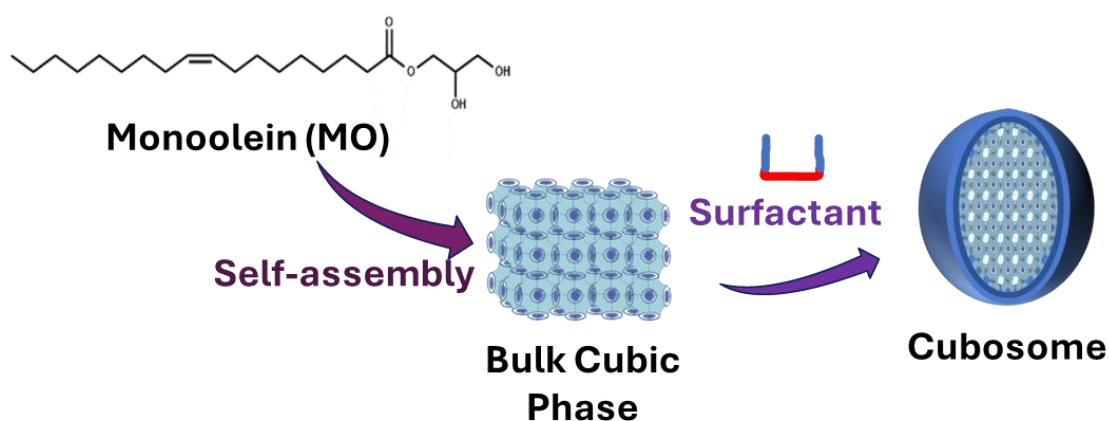


Figure 1- 3 Formation of cubic phases and cubosomes

Depending on factors such as the amphiphile composition, temperature, and pH, the bicontinuous cubic phase can adopt several conformations. The bilayer of the cubic phase can form into structures such as the gyroid, double diamond and primitive type (Larsson et al. 2005) (**Figure 1-4**).

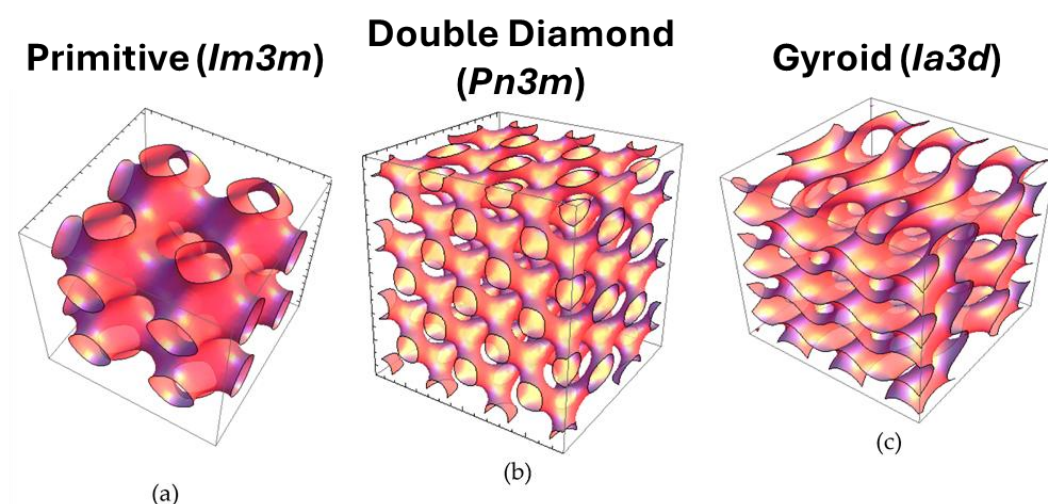


Figure 1-4 Self-assembly structures of amphiphilic lipids (Rakotoarisoa et al. 2019)

Compared to other well-researched lipid-based carriers such as liposomes and vesicles, dispersed bicontinuous phases are relatively new. Cubosomes were first discovered around 25 years ago, and since then, the number of cubosome related publications is steadily increasing every year as shown in **Figure 1-5a**. However, most of the research conducted about cubosomes is application based, while smaller percentage focuses on fundamental works on understanding the cubic phase and its behavior **Figure 1-5b**. Therefore, it is necessary to fully understand the science of cubic phases and cubic membranes to be able to exploit these phases for therapeutic delivery in the future.

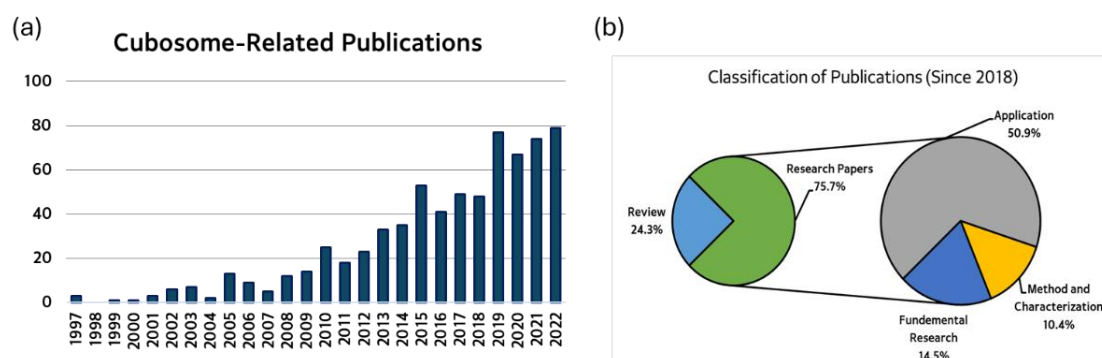


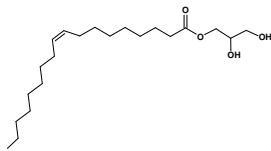
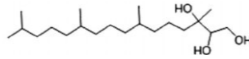
Figure 1-5 (a) Number of cubosome related publications in the past 20 years (b) Distribution of the latest 500 cubosome related publications (Obtained from Scopus 2023).

2.1 Lipids for the Preparation of Cubosomes

Although a variety of lipids can form bicontinuous cubic phases under specific conditions, few lipids can spontaneously self-assemble into bicontinuous phases in excess

water. Among these lipids, glycerol α -monooleate commonly referred as monoolein (MO) and 3,7,11,15-tetramethylhexadecane-1,2,3-triol (phytantriol) are commonly used to prepare cubosomes. Both of MO and phytantriol molecules are “wedge” shaped and of the inverse cone molecular geometry, which in turn promotes the formation of highly curved cubic membranes (Abourehab et al. 2022). **Table 1-1** lists different studies utilizing MO and phytantriol for cubosome-based DDS carriers for a variety of therapeutic applications.

Table 1-1 Commonly used lipids for the formation of cubosomes

Lipid	Chemical Structure	Description	Reference
Monoolein		Drug delivery systems for percutaneous administration of indomethacin	(Esposito et al. 2005)
		Monoolein-based ophthalmic delivery system for dexamethasone	(Gan et al. 2010)
		Monoolein-based hydrogels for topical treatment of burns	(Morsi et al. 2014)
Phytantriol		Assessment of effect of vitamin E Acetate and F127 polymer on liquid crystal nanostructure.	(Dong et al. 2006)
		Enhancement of the delivery of the poorly water-soluble drug cinnarizine from phytantriol cubosomes.	(Nguyen et al. 2011)

2.2 Preparation of Cubosomes

Cubosomes can be prepared through different methods as shown in **Table 1-2**. However, the most common method for the preparation of the dispersed cubic phases is the high-pressure homogenization method. A key process in this preparation method is fragmenting the bulk cubic phases into uniform nanosized particles.

Table 1-2 Methods of cubosome preparation

Preparation Method	Description	Reference
High-Pressure Homogenization	Preparation of colloidal dispersions of cubic monoglyceride-water phases	(Siekmann et al. 2002)
	Cubosomes for ophthalmic delivery of flurbiprofen	(Gan et al. 2010)
	Characterization of cubosomes as a targeted and sustained transdermal delivery system for capsaicin	(Peng et al. 2015)
Hydrotrope method	Preparation of cubosomes using a hydrotrope	(Spicer et al. 2001)
	Preparation of phytantriol cubosomes by solvent precursor dilution for the delivery of protein vaccines	(Rizwan et al. 2011)
Dry Powder Precursor	Dry powder precursors of cubic liquid crystalline nanoparticles (cubosomes)	(Spicer et al. 2002)

Bulk cubic phases contain interconnected lipid bilayers that are arranged in periodic three-dimensional structures. The interconnectedness of the structures of these phases causes bulk cubic phases to have high viscosities and gel-like properties that limit their applicability. To overcome this limitation, surfactants are used to improve their dispersibility (Siekmann et al. 2002; Nakano et al. 2002; Barauskas et al. 2005; Dong et al. 2006; Nakano et al. 2001). Surfactants reduce the surface tension between water and organic phase and which stabilizes the cubosomes. **Table 1-3** shows the different types of surfactants used to prepare cubosomes.

Table 1-3 Commonly used surfactants for the preparation of cubosomes

Surfactant	Property	Description	Reference
Pluronic	Non-ionic surfactants consisting of poly (ethylene oxide) and poly(propylene oxide) block copolymers.	Evaluation of Pluronic triblock copolymers on the stability and integrity of monoolein and phytantriol cubosomes.	(Chong et al. 2011)
		Disposition and association of the steric stabilizer Pluronic F127 in monoolein cubosomes	(Tilley et al. 2013)
		Impact of preparation method and variables on the internal structure in phytantriol-Pluronic® F127 cubosomes	(Akhlaghi et al. 2016)
Tween 80	Non-ionic surfactant that is derived from polyethoxylated sorbitan and oleic acid.	Piperine-loaded Tween-integrated monoolein cubosomes as brain-targeted oral nanomedicine	(Elnaggar et al. 2015)
		Stabilizing cubosomes with Tween 80 as a step towards targeting lipid nanocarriers to the blood-brain barrier	(Azhari et al. 2016)
		Tween 80 stabilized cubosomes enhance drug permeability across the blood-brain barrier in zebrafish	(Azhari 2018)

3. Characterization Methods of Cubosomes

3.1 Characterization of Cubosome Structure

Although cubosomes have been characterized through several methods as shown in **Table 1-4**, the golden standard for the characterization of the structure of cubosomes is employing small-angle x-ray scattering (SAXS) and cryogenic transmission electron microscopy (cryo-TEM) (Li et al. 2019; Angelov et al. 2013; Demurtas et al. 2015). By utilizing SAXS, the morphology of the well-defined interior structure of the cubosomes could be determined through assignment of the x-ray scattering vectors. Information about the lattice spacing as well as the water channel size could be estimated. Cryo-TEM on the other hand, allows for direct visualization of the interior structure of the cubosomes (Barriga, Holme, et al. 2019). The main disadvantage of these techniques is that they require elaborate setup and specialized sample preparation like in the case of cryo-TEM (Tran et al. 2018). Also, since the cubic phase is influenced by factors such as the temperature of its surroundings, which might change when subjecting the cubosomes to such methods, it is worthwhile to examine the properties of cubosomes using less invasive means.

Table 1-4 Cubosome Characterization Methods

Characterization Method	Description	Reference
Small-angle x-ray scattering	Assessment of surfactant and pH on the morphology and internal structure of MO/OA cubosomes	(Nakano et al. 2002)
	Characterization of MO cubosomes prepared using hydrotrope method using SAXS	(Spicer et al. 2001)
Nuclear magnetic resonance (NMR)	Small-angle X-ray scattering and ^{13}C NMR investigation on the internal structure of cubosomes	(Nakano et al. 2001)
Cryo field emission scanning electron microscopy	Characterization of Phytantriol cubosomes using Cryo field emission scanning electron microscopy	(Rizwan et al. 2007)
Cryo-transmission electron microscopy	Crystallography of cubosomes studied by cryo-transmission electron microscopy	(Sagalowicz et al. 2006)
	Direct visualization of dispersed lipid bicontinuous cubic phases by cryo-electron tomography	(Demurtas et al. 2015)

3.2 Characterization of Cubic Membranes

In the study of the properties of lipid membranes, the utilization of fluorescent probes presents many advantages. These probes can indicate the properties of lipid membranes in their native state without introducing any disturbances or alterations (Suga et al. 2018; 2016). Properties such as membrane hydration and membrane fluidity are important in the study of LNPs for drug delivery applications. The polarity of lipid membranes of LNPs can affect the degree of drug release (Bompard et al. 2020). The modulation of the membrane fluidity of liposomes was previously shown to selectively target cancer cells (Bompard et al. 2020) as well as having significant influence on the interactions with pulmonary physiological barriers (Zhao et al. 2020). Compared to other types of LNPs, the membrane properties of cubosomes have not been fully elucidated yet. More specifically, the changes in relation to their interactions with cell membrane lipids.

Membrane bound fluorescent probes such as 2-dimethylamino-6-lauroylnaphthalene (Laurdan) and 1,6-diphenyl-1,3,5-hexatriene (DPH) are effective in the examination of membrane hydration and fluidity, respectively. Laurdan is widely used to examine the membrane hydration state, with emissions peaks at 440 and 490 nm, corresponding to the hydrophobic and hydrophilic components (Parasassi et al. 1998). The calculation of the steady-state generalized polarization (GP_{340}) of Laurdan is used to indicate the membrane hydration (Parasassi et al. 1991). DPH, on the other hand, is allocated in the hydrocarbon chain region of the membrane, and the reciprocal of its polarization (I/P) reflects the membrane fluidity (Watanabe et al. 2017). Employing these probes to examine the cubic membrane can further clarify the phase behavior of the cubosomes. Previously, the influence of the membrane properties of 2-hydroxyoleic acid/MO system on their structural properties during the lamellar-to-cubic phase transition was elucidated using membrane probes (Rui, Watanabe, et al. 2024).

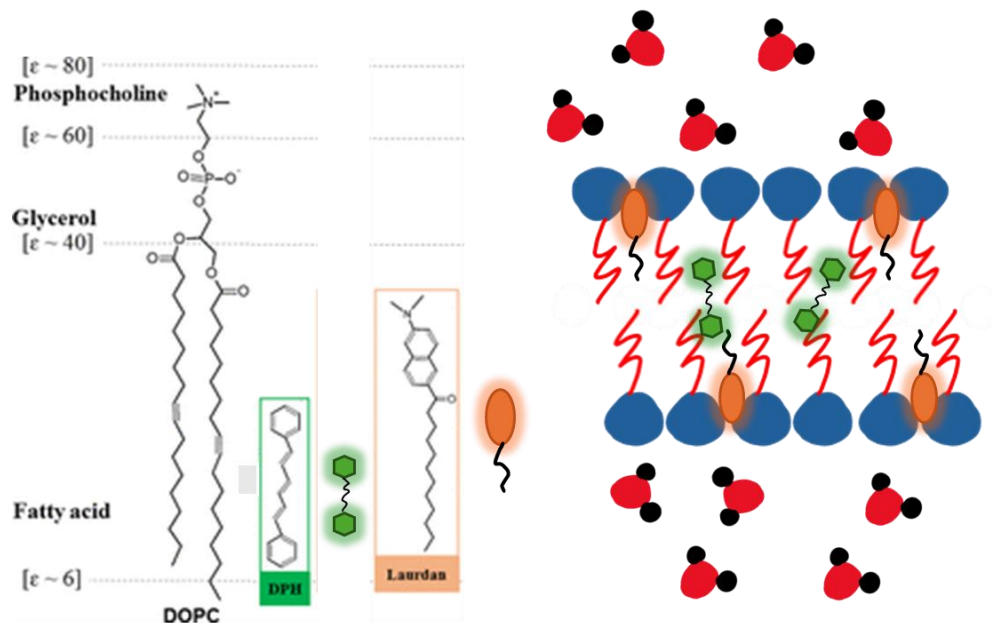


Figure 1-6 Structure of Laurdan and DPH in respect to DOPC (Bui et al. 2016) and possible allocation in the lipid bilayer.

Therefore, using these probes can provide more insights into the changes that occur in the cubic membrane in the context of cubosomes interacting with cell membrane lipids. Although the steady-state GP_{340} value of Laurdan can provide the means to estimate the membrane hydration states, this approach can leave plenty of information about the multiple fluorescence components of Laurdan. To account for the multiple excited states that Laurdan experiences, the examination of fluorescence lifetime and associated decay curves can be leveraged (Watanabe, Suga, et al. 2019; Watanabe, Goto, et al. 2019). Previously, the deconvolution of the decay associated spectra (DAS) of Laurdan and Prodan in different liposomal compositions was used to evaluate distribution of the different fluorescent components. The different fluorescence lifetimes (τ) and emission peaks (λ) were visualized using τ - λ plots (Watanabe, Suga, et al. 2019), and using different solvent mixtures, a solvent model representing the different regions of the membrane was established (Ito et al. 2023). Since properties of the cubic membrane are still not fully understood yet, the examination of their properties using time-resolved fluorescence and DAS can provide more detailed information regarding the changes in specific regions of the cubic membrane. More specifically, highlighting the changes in property due to the incorporation of cell membrane lipids.

4. Influence of Drug Incorporation on Properties of Cubosomes

One of the major problems in the delivery of many drug and nutraceutical molecules is their low solubility and bioavailability. Due to their hydrophobic nature and high molecular weights, the delivery of such molecules can be suboptimal (Kalepu et al. 2015). To improve the solubility and bioavailability of hydrophobic molecules, lipid-based formulations can be utilized. The amphiphilic nature of lipids allows them to form self-assemblies that can solubilize hydrophobic molecules, thus increasing their bioavailability (Kashapov et al. 2020). Cubosomes were shown previously to enhance the delivery of poorly water soluble drugs (Chang et al. 2021; Mulet et al. 2010).

The effects of drug loading into cubosomes, and its effects on release kinetics (Boyd 2003), stability (Esposito et al. 2005), and cubosome structural information were examined (Boge et al. 2019). Depending on the properties of the loaded drug molecule, the structure of the assembly may change. Some drug molecules can affect the lipid bilayer membrane via physical interactions and change its properties (Alsop et al. 2016). The effects of drug molecules on the cubosome structure have been assessed using small-angle x-ray scattering (SAXS) (Boge et al. 2019) and x-ray diffraction (XRD) (Esposito et al. 2005). Although some researchers studied the effects of drug molecules on the structure of cubosomes, there are few works focusing on the effects of drug loading on the membrane of cubosomes and their interactions with cell membranes.

5. Interactions of Cubosomes with Cell membranes

The potential of cubosomes for drug delivery is promising due to their fusogenic properties to cell membranes (Angelov et al. 2013). However, the uptake mechanisms of cubosomes by cells are still under investigation. Previously, researchers have taken different approaches to examine the interactions of cubosomes with cell membranes and cell membrane models. Jabłowska et al. have demonstrated the behavior of monoolein (MO) cubosomes with 1, 2-dipalmitoyl-sn-glycero-3-phosphocholine (DPPC) monolayer. Their results have shown that the interactions of the cubosomes depended on the surface pressure, and the incorporation of the cubosomes material resulted in changes to the membrane fluidity of the monolayer (Jabłowska et al. 2016). Supported lipid bilayers (SLB) were used by Dyett et al. to examine the behavior of the cubosomes under flow conditions. It was revealed that the fusion of the cubosomes with the SLBs was

influenced by the surface charge and the composition of the monolayer(Dyett et al. 2019). However, the unaddressed area in these works is the time-evolution of the structural changes in the cubosome structure when interacting monolayer/bilayer, which is an important aspect to consider for the design of drug delivery carriers. To examine such changes with high time resolution, time-resolved small-angle-X-ray scattering (TR-SAXS) is an effective method. In previous studies, this technique has been used to examine changes due to the complexation of ionizable lipid (SM-102), monoolein, and nucleic acids(Yu et al. 2023) as well as changes due to neurotrophic BDNF protein loading(Angelov et al. 2014). Vandoolaeghe et al. used time-resolved small-angle X-ray diffraction to elucidate the changes in the cubosome structure over time when interacting with unilamellar and multilamellar vesicles. Their results revealed a decrease in the cubic lattice and a transition from the cubic phase to the lamellar phase over time(Vandoolaeghe et al. 2009). Although some of the kinetics of the structural change in the cubosome structure were elucidated, there is still a missing gap regarding the changes in the cubic and vesicular membranes during the interaction. Furthermore, since the cell membrane exhibits different lipid compositions at different regions, deeper examination of the structure and membrane condition changes of the cubosomes with a wider range of lipid compositions is needed.

6. Overview of this study

The aim of this study is to systematically characterize the structure and membrane of dispersed cubic phase nanoparticles to clarify how the changes in the membrane environment influences the carrier's structure and dispersibility. This study also seeks to develop the methodology to examine the interactions of cubosomes with model cell membrane through the examination of cubic membrane and structure. The results of this work provide new insights that can be helpful in clarifying the cubosome uptake mechanism by cells as well as the optimal design of cubosomes as drug delivery carriers.

In chapter 2, by employing Raman spectroscopy, cryogenic Transmission Electron Microscopy (cryo-TEM), and fluorescent probes, examination of the changes to the self-assembly properties of MO and MO/OA self-assembly was conducted. Aggregation of the particles and reduction of the dispersibility of the self-assemblies was caused by high drug loading. The alterations in the surface properties of the particles manifested in structural changes and formation of aggregations. By examining the polarity, zeta-potential, and particle size of the self-assemblies, a systematic characterization of the carrier in relation to drug loading and stability was established.

In chapter 3, by utilizing TR-SAXS and the changes to GP_{340} values of Laurdan probed MO cubosomes after mixing with DOPC liposomes, the methodology to indicate changes to the physicochemical properties of cubosomes when interacting with cell membrane lipids was established. TR-SAXS diffractograms confirmed the cubic-to-lamellar phase transition. In addition, the kinetics of apparent lipid exchange (k_{app}) and estimation of the apparent amount of DOPC in the cubosomes could be obtained.

In chapter 4, building on the methodology in chapter 3, the interactions of MO cubosomes with model cell membranes at different phase states were investigated. The effects of the carrier on the model cell membrane were also elucidated. The fluidity of the liposome bilayer was shown to influence the time of the structural change of the cubic phase to lamellar phase. After mixing the cubosomes and liposomes, the membrane hydration states of the cubosomes and liposomes transitioned to resemble the hydration state of their counterpart. Also, it was shown that by the membrane hydration of the liposomes was an important factor in dictating the time needed to reach the final intermediate state after mixing.

In chapter 5, the effects of loading of the hydrophobic drug, HC, on the interactions of MO cubosomes with POPC cell membrane models (liposomes) were elucidated with considerations to the characterization of the drug incorporated carrier in chapter 2 and the methodology developed in chapters 3 and 4. TR-SAXS diffractograms showed that the incorporation of the drug did not alter the duration and kinetics of the cubic to lamellar phase transition. On the other hand, the Laurdan fluorescence results revealed slower kinetics in the drug loaded cubosomes compared to blank cubosomes. These results show that drug incorporation in cubosomes suppresses the rate of lipid exchange between carriers and cell membranes.

In chapter 6, the conclusions of this study are presented, along with suggestions for future work aimed at improving the current methodology and expanding the application of the developed approach to other types of lipid nanoparticles.

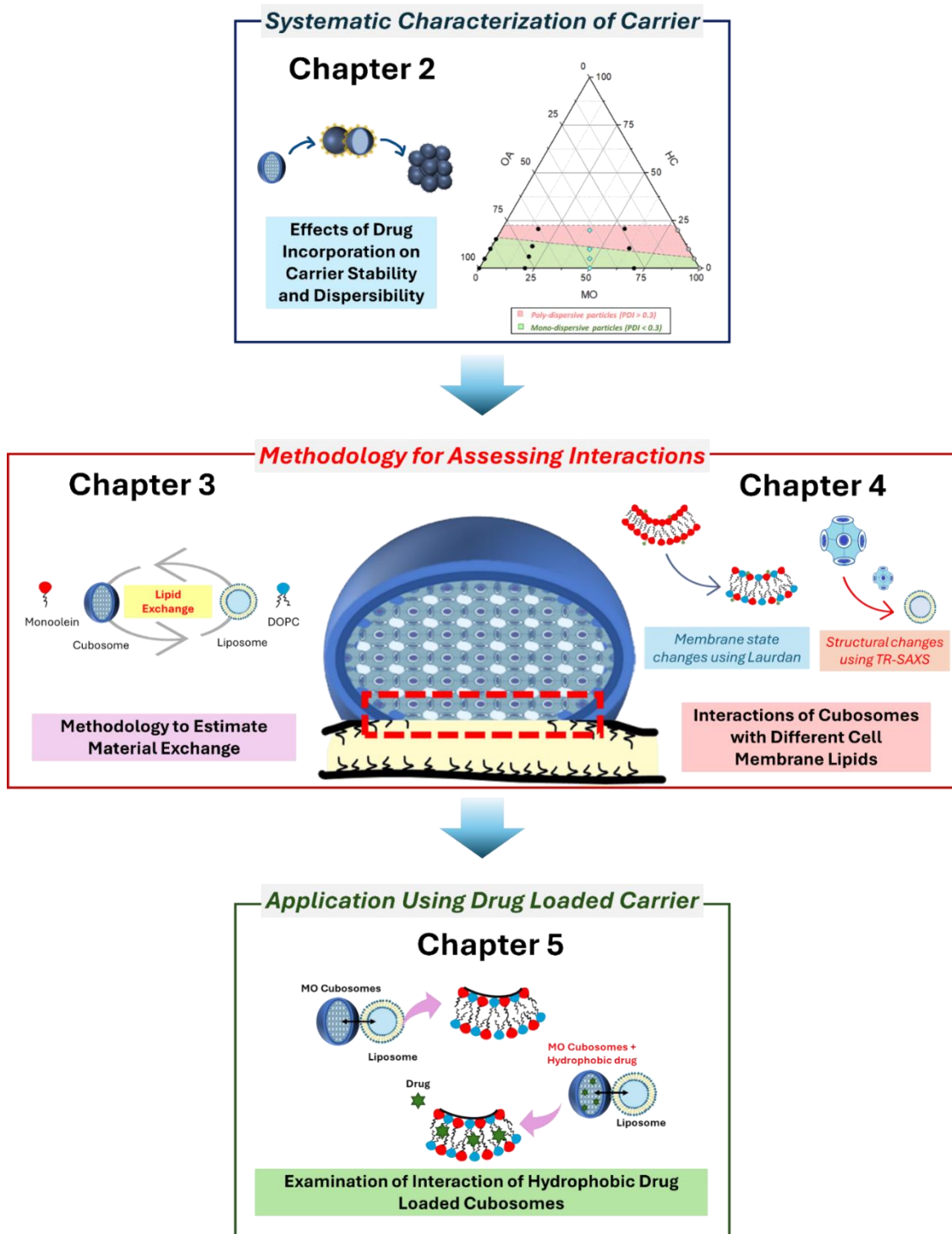


Figure 1-7 Concept map of the present study

Chapter 2: Dispersibility and Surface Properties of Hydrocortisone-incorporated Self-Assemblies

1. Introduction

Dispersibility and colloidal stability are important aspects of the design of drug delivery carriers. The carrier must be stable to retain its applicability and deliver the desired therapeutic effects. The non-dispersed (bulk) phase of monoolein has high viscosity and gel-like properties that limit its application. To overcome this limitation, surfactants, e.g., Pluronic F127 (F127), are used to improve its dispersibility (Siekmann et al. 2002; Nakano et al. 2002; Barauskas et al. 2005; Dong et al. 2006; Nakano et al. 2001). Surfactants can lower the interfacial tension, resulting in a reduction of the mechanical stress (or energy) required for downsizing particles (Tadros et al. 2004). Commonly, nonionic triblock copolymers, like Pluronic® series, are used to kinetically stabilize the particles (Wik et al. 2020). F127, consisting of poly(ethylene oxide)-poly(propylene oxide)-poly(ethylene oxide) (PEO-PPO-PEO) blocks, is commonly used to disperse particles by steric stabilization (Chong et al. 2011). The surface properties of self-assemblies are crucial to understand their stability (Jones 1995). Properties such as zeta potential and hydration states are vital in understanding the behavior of lipidic assemblies in the aqueous medium. Zeta (ζ) potential is an indicator of the surface charge of a particle, which is one of the essential surface characteristics for understanding the particle dispersibility. Usually the particles with greater absolute zeta potential values are employed to suppress inter-particle aggregation (Heurtault et al. 2003). The hydration of the self-assemblies is also an important factor in the aspect of dispersion stability. For example, a modification of liposomes with poly(ethylene glycol) (PEG) is an effective technique, because the hydration shell derived from PEG surrounding the liposome allows the particles to be well-dispersed improving blood-circulation time and preventing merging or adhesion with other proteins (Tirosh et al. 1998). Surface properties such as ζ potential and hydration are strongly related to the properties of the constituent molecules in the system. Similarly, the properties of self-assembly systems can be altered by the molecules to be incorporated in them. Therefore, it is important to investigate the changes of the surface properties of the self-assemblies while accounting for the contribution of all component molecules (lipid (as scaffold), surfactant (as stabilizer), drug etc.).

Even though surfactants like F127 provide enough steric stabilization to disperse the particles, depending on the properties and amount of the loaded drug molecules and the interaction of the loaded drugs and lipid molecules, the stability of the self-assemblies can be affected. Hydrocortisone (HC) is one of the insoluble hydrophobic drugs that is used for the treatment of swelling, rash, and allergies (Fini et al. 2008). To increase the therapeutic effects and to reduce the side effects of corticosteroids, the use of dispersed nanoparticles as carriers has been studied (Mulet et al. 2010; Rosado et al. 2013). Lyotropic liquid crystalline dispersed nanoparticles using monoolein (MO) and phytantriol (PT) succeeded to load 15 mol% of HC with high entrapment efficiency (Mulet et al. 2010). However, the drug loading caused changes to the lattice parameters of the lyotropic liquid crystalline structure. In other systems of lipid bilayer membranes, the effects of HC incorporation were also observed to change the membrane fluidity (Kaddah et al. 2018) (Alsop et al. 2016). At the lipid bilayer level, it is suggested that the incorporation of hydrophobic molecules into membranes could alter the lateral interaction between membrane lipids. However, there are few reports that clarify the correlation of the changes in the internal structural properties and the particle dispersibility. Therefore, it is important to investigate the relation of colloidal stability and the self-assembly properties with respect to the drug loading.

The difficulty in discussing the internal structure and colloidal stability is to determine the appropriate properties to reveal the correlation between them. Although the ζ potential of the colloidal particles is a typical parameter to describe colloidal stability, the electrostatic interactions are not the only determining factor. This is because even the ζ potential can be influenced by the internal structure. Therefore, characterization from the molecular level is necessary. To clarify the internal properties of a lipid self-assembly system, Raman spectroscopy and fluorescence analysis are effective tools. Raman spectroscopy provides various information about the lipid chain packing and torsion (Suga et al. 2016; Brown et al. 1973), and Laurdan fluorescence probe is used to examine the polar environment of lipid membranes. In previous research, a series of characterizations was performed for oleic acid (OA)/MO self-assemblies and OA/oleate (Suga et al. 2018; 2016). It was shown that gel-phase-like membranes display tightly packed membranes and a hydrophobic membrane surface. Utilizing this membrane

property analysis method with the assessment of surface properties can provide further insights on the effects of loading drugs on the self-assemblies.

In this chapter, the incorporation effects of the hydrophobic drug HC on MO-based self-assemblies were investigated. The effects of the surfactant F127 were also examined. The incorporation of HC in the dispersions and the molecular packing states of the lipids were confirmed using Raman spectroscopy. The particle morphology and the internal structure of HC-loaded dispersions were confirmed by cryogenic transmission electron microscopy (cryo-TEM). The effects of the incorporation of the surfactant and hydrophobic drug on the surface properties and dispersibility were examined using dynamic light scattering (DLS) and fluorescence measurements. Through a systematic characterization, this work aims to clarify; (1) how the incorporation of the hydrophobic drug, HC, affects the self-assembly properties of the dispersions, especially the effects on internal structure and surface properties such as packing state, polarity, ζ potential, and particle size; and (2) how these properties correlate to the colloidal stability, which will be helpful to consider non-equilibrium changes in the self-assembly systems including MO, OA, and hydrophobic drugs.

2. Materials and Methods

2.1 Materials

MO (glycerol α -monooleate) (purity > 40 %) was purchased from Tokyo Chemical Industry Co., Ltd. (Tokyo, Japan). OA (Oleic acid) (purity > 65 %), and hydrocortisone (HC) were purchased from Wako Pure Chemical Industries (Osaka, Japan). Pluronic F127 was purchased from Sigma-Aldrich (St. Louis, MO). Sodium chloride (NaCl) was purchased from Kanto Chemical Co., Inc. (Tokyo, Japan). Stock MO and OA were obtained by introducing MO and OA to chloroform/water two-phase system and evaporating the solvent of the collected organic phase. All chemicals were used without further purification.

2.2 Preparation of HC Incorporated MO and MO/OA

MO, OA, F127 (weight ratio: 0-12 wt% to the total lipid mixture), and HC (0-0.23 mmol corresponding to 0-20 mol%) were added to a round-bottom flask. Chloroform was added until all the F127 and HC were completely dissolved. Then the chloroform was evaporated using a rotatory evaporator at 60 °C. After the evaporation, the clear lipid film was hydrated with 100 mM NaCl solution (pH = 7.0) to reach a final lipid concentration of 100 mM. The self-assemblies were sonicated for two minutes using a probe sonicator (TOMY Ultrasonic Disruptor UD-200). The dispersions were stirred vigorously and incubated in the dark at room temperature (25°C) overnight. A schematic diagram of the preparation method is shown in **Figure. 2-1**. The total lipid concentration ([MO]+[OA]) used for the Raman, DLS, and cryo-TEM measurements is 100 mM. After sample preparation, measurements were performed within 24 h.

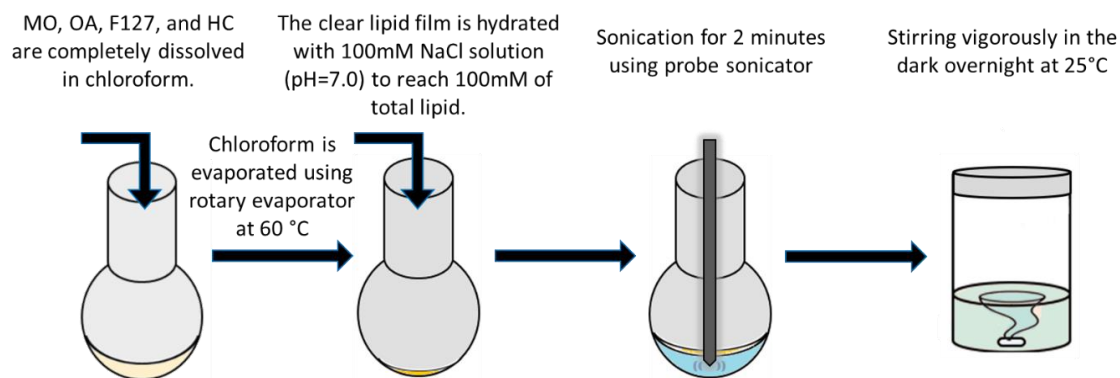


Figure 2-1 Schematic diagram of the self-assembly preparation method

2.3 Raman Spectroscopy Analysis

The Raman spectra of the self-assemblies were obtained using a confocal Raman microscope (HR-800, Horiba, Ltd., Kyoto, Japan), with an exciting laser wavelength of 532 nm. The spectra of the samples were obtained by removing the background signals. Three measurements were conducted for each sample. The hydrocarbon chain packing density can be indicated by calculating the peak intensity ratio, $R = \frac{I_{2890}}{I_{2850}}$, where the peaks at 2850 cm⁻¹ and 2890 cm⁻¹ correspond to symmetric and asymmetric vibrational modes of the -CH₂- group, respectively (Fox et al. 2007).

2.4 X-ray Diffraction (XRD)

XRD experiments were performed using a Rigaku Smart Lab X-ray diffractometer (Rigaku, Tokyo, Japan), with monochromatic Cu K α radiation (λ) of 0.1542 nm at 40 kV, and 30 mA graded elliptical multilayer optics. 100 μ L of the sample was transferred to the bottom of the glass plate. The diffraction pattern was recorded using an imaging plate and at 25 °C for 14 minutes.

2.5 Dynamic Light Scattering Analysis

The particle size, poly dispersity index (PDI), and ζ -potential of the particles were analyzed by measuring the dynamic light scattering and M3-PALS method using a Malvern Zetasizer Nano series (Malvern, UK). The samples were diluted with ultrapure water 100-fold before the measurement. For the zeta potential measurements, the samples were prepared using pH-adjusted solution (pH=7.0).

2.6 Cryo-TEM Imaging of MO, MO/OA assemblies

The sample vitrification was performed using a semi-automated vitrification device (Vitrobot Mark IV, Thermo Fisher Scientific). 2.4 μ L of 100 mM of the sample solution was deposited on to glow-discharged Quantifoil R2/2 in the Vitrobot at 100% humidity at 25°C. The samples were blotted for 4 s from both sides and submerged in liquid ethane immediately. The cryo-TEM imaging was conducted using a Titan Krios (Thermo Fisher Scientific) operating at 300 kV by a Falcon2 (Thermo Fisher Scientific) CMOS camera.

2.7 Laurdan Spectra Measurements

10 μ L of MO/OA dispersions were mixed with 1 mL of 100 mM NaCl solution (pH = 7.0) and with 10 μ L of Laurdan solution (1.0 mM, in ethanol), and then incubated

for 30 minutes. The Laurdan fluorescence spectra were obtained by exciting the samples at 340 nm and measuring the intensities in the wavelength range of 400 nm to 600 nm.

3. Result and Discussion

3.1. Formation of HC-incorporated Self-assemblies and Effects on Hydrocarbon Chain Packing of the Self-Assemblies

Raman spectroscopy is a vibrational molecular spectroscopy that is used to obtain information about the constituent molecules and their properties. Especially in the self-assembly systems composed of surfactants and lipids, Raman spectroscopy is useful to assess the packing state/ density of acyl chains (Suga et al. 2016; 2018; Watanabe et al. 2017; Faried et al. 2019). In **Figure. 2-2**, the Raman spectra of F127, MO/OA, and MO/OA with 8 wt% of F127 were compared. F127 (solid powder) displays characteristic peaks at 1143 cm^{-1} and 1483.5 cm^{-1} corresponding to C–O stretch and CH_2 scissoring, respectively (Guo et al. 1999). These peaks were not observed in the spectrum of MO/OA with 8 wt% of F127, thus it can be concluded that the spectrum mainly displays the signal from the lipids (MO and OA).

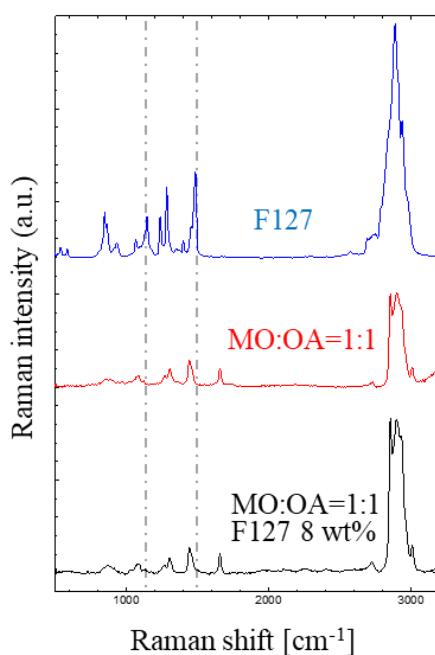


Figure 2-2 Raman spectra of F127 (solid powder), MO/OA=1:1 (dispersion), and MO/OA=1:1 with 8 wt% of F127 (dispersion).

The hydrocarbon chain packing density, R value, obtained from Raman analysis is a good indicator of the lipid packing state. In lipid self-assembly systems, membranes with $R > 1$ are highly packed (ordered state), while membranes with $R < 1$ are less packed (disordered state) (Suga et al. 2018). The hydrocarbon chain packing density showed no

difference with increasing F127 amount (**Figure 2-3** and **Table 2-1**), which shows that the surfactant F127 might have no significant influence on the packing of the self-assemblies.

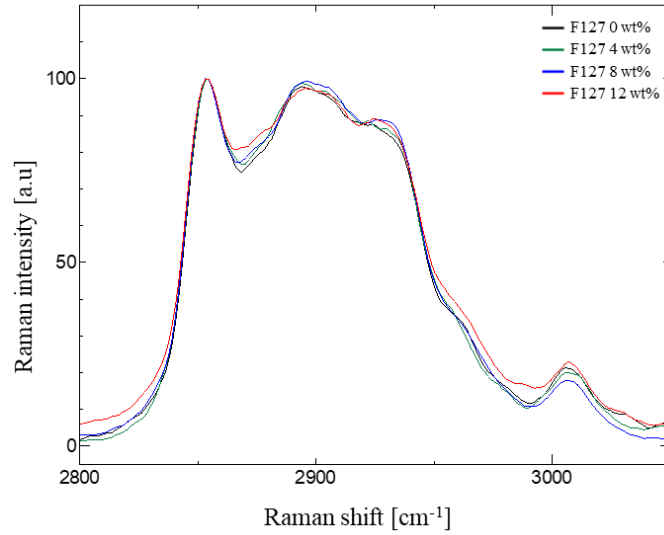


Figure 2-3 Raman spectra of MO/OA nanoemulsions with different concentration of F127.

Table 2-1 R values for MO/OA nanoemulsions with different F127 amount.

F127 [wt%]	$R = \frac{I_{2890}}{I_{2850}}$
0	0.98 ± 0.004
4	0.98 ± 0.017
8	1.01 ± 0.028
12	1.00 ± 0.034

The Raman spectra of HC, MO/OA with F127, and MO/OA with F127 and HC are shown in **Figure 2-4**. HC has characteristic Raman peaks at 1611 cm^{-1} and 1644 cm^{-1} arising from the aromatic C=C and C=O stretching vibrations, respectively (Moore et al. 2020). These peaks appear as a weak shoulder peak in the spectrum of MO/OA with F127 and HC (dispersion), indicating the incorporation of HC into the self-assemblies.

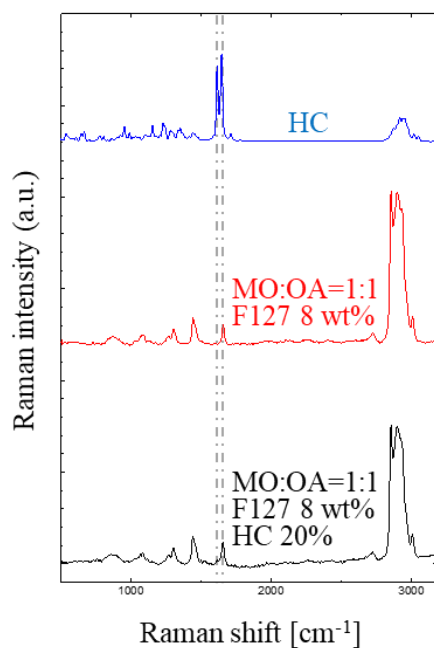


Figure 2-3 Raman spectra of HC (solid powder), MO/OA=1:1 with 8 wt% of F127 (dispersion), and MO/OA=1:1 with 8 wt% F127 and 20 mol% HC (dispersion).

When assessing the R values of MO/OA dispersions with different concentrations of HC, there were no significant changes observed (**Figure 2-4 a-b**). Pure OA assemblies at pH 7.0 form O/W emulsions (Suga et al. 2016), and pure OA and HC-incorporated OA assemblies exhibited $R < 1$. It is therefore concluded that the incorporation of HC brings small impact on the hydrocarbon chain packing in the dispersions. Additionally, to confirm the state of HC in the dispersions, X-ray diffraction analysis (XRD) spectroscopy was utilized (**Figure 2-5**). Crystalline HC displays characteristic diffraction peak around $2\theta=14.5$ (Lei et al. 2016). XRD diffractograms of all series of the self-assemblies had no HC derived peaks. Thus, it can be concluded that HC is solubilized by MO or MO/OA self-assemblies in the dispersions.

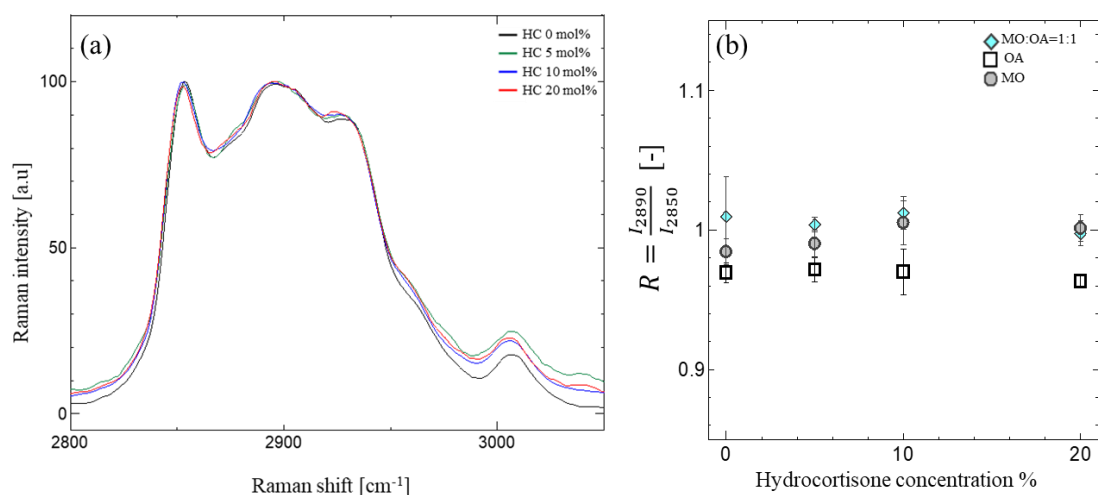


Figure 2-4 (a) Raman Spectra of MO/OA F127 8wt% nanoemulsions with different concentration of HC, (b) R values for MO:OA=1:1 with 8 wt% F127, OA with 8 wt% F127, and MO with 8 wt% F127 dispersion at different concentration of HC.

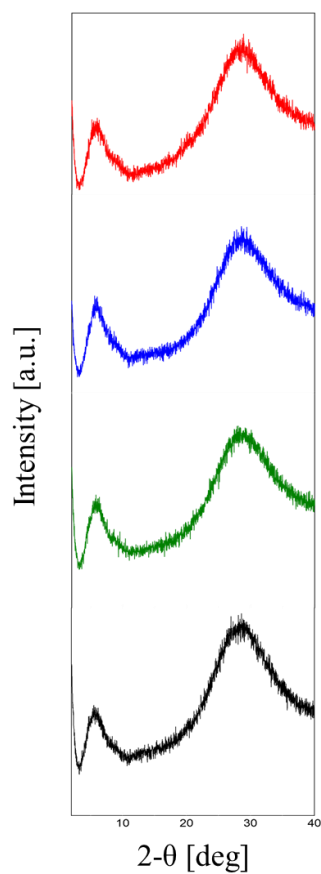


Figure 2-5 XRD patterns of MO without HC (black), MO/OA without HC (green), MO with 20 mol% HC (blue), and MO/OA with 20 mol% HC (red).

3.2 Effects of HC-Incorporation on the Dispersibility of MO and MO/OA Self-Assemblies

MO and MO/OA self-assemblies without F127 formed large gel-like aggregations occasionally, while homogeneous dispersions were formed in samples containing F127. Such characteristics have been seen in the cubic phase self-assemblies [37]. After long-time stirring (over couple days), the sample with 20 mol% of HC formed gel-like large aggregate (agglomerate) even with F127 (**Figure 2-6a**). The Raman spectrum of the gel-like aggregates of MO/OA with F127 and HC was analyzed (**Figure 2-6b**), revealing that the intensities of the HC-derived peaks were increased. The experiments in the previous section, where all the measurements were conducted using dispersions, exhibited very weak peaks of HC. It is assumed that the dispersed sample with 20 mol% of HC is in an unstable intermediate state that could transition into heterogeneous gel phase by external factors such as physical shear stress. Besides, noticeable changes occurred to the Raman spectrum, where the chain packing density increased ($R=I_{2890}/I_{2850}>1$) reflecting a change to an ordered packing state.

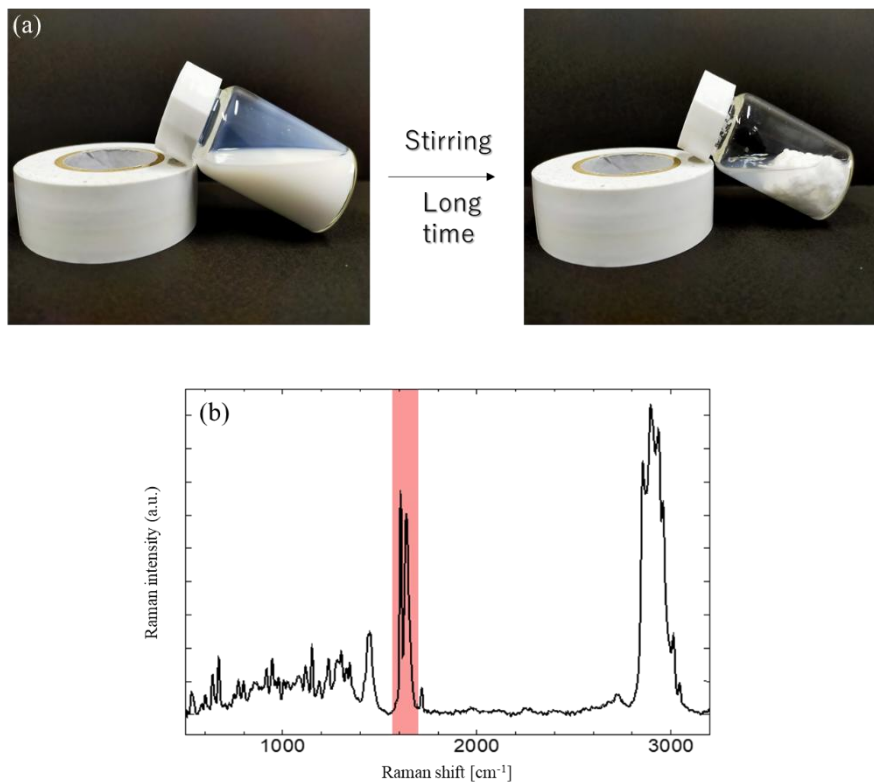


Figure 2-6 (a) Picture of MO/OA F127 8 wt% with HC 20 mol% dispersion after stirring for long-time (couple of days), (b) Raman spectra of gel-like aggregates. Half-tone region (1611 and 1644 cm⁻¹) indicates a characteristic peak of HC.

3.3 Structure of HC-Incorporated Dispersions

Cryo-TEM is commonly used to observe the structure of dispersions. The cryo-TEM images of MO with F127 shown in **Figure 2-7a** had particles containing a multilamellar-like patterned internal structure which resembles the inverse hexagonal phase. On the other hand, MO/OA with F127 dispersions (**Figure 2-7b**) showed no visible internal structure. Additionally, the dispersions displayed an emulsion-like appearance. The diffractogram using fast Fourier transform (FFT) of the MO system further confirmed the existence of a patterned internal structure (**Figure 2-7c**). The difference in the structure between MO/OA and MO self-assemblies could be attributed to the presence of the oleic acid which acts as an emulsifier that disturbs the patterned internal structure. The inner multilamellar-like structure was still present after incorporating 20 mol% HC in MO dispersions (**Figure 2-8a**). As for the MO/OA sample with 20 mol% HC, most of the particles resembled that of the emulsion-like particles (**Figure 2-8b**).

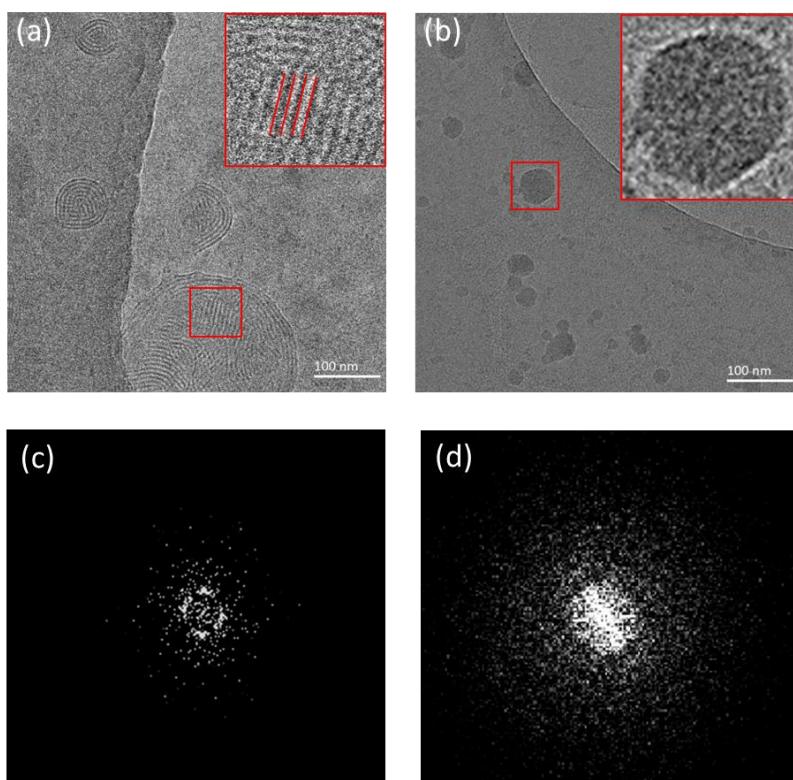


Figure 2-7 Cryo-TEM image of (a) MO without HC, (b) MO/OA without HC, Inset is closed-up picture at the marked region; Diffractogram of (c) MO without HC, (d) MO/OA without HC, Each FFT diffractogram corresponds to the inset. All samples include 8 wt% F127.

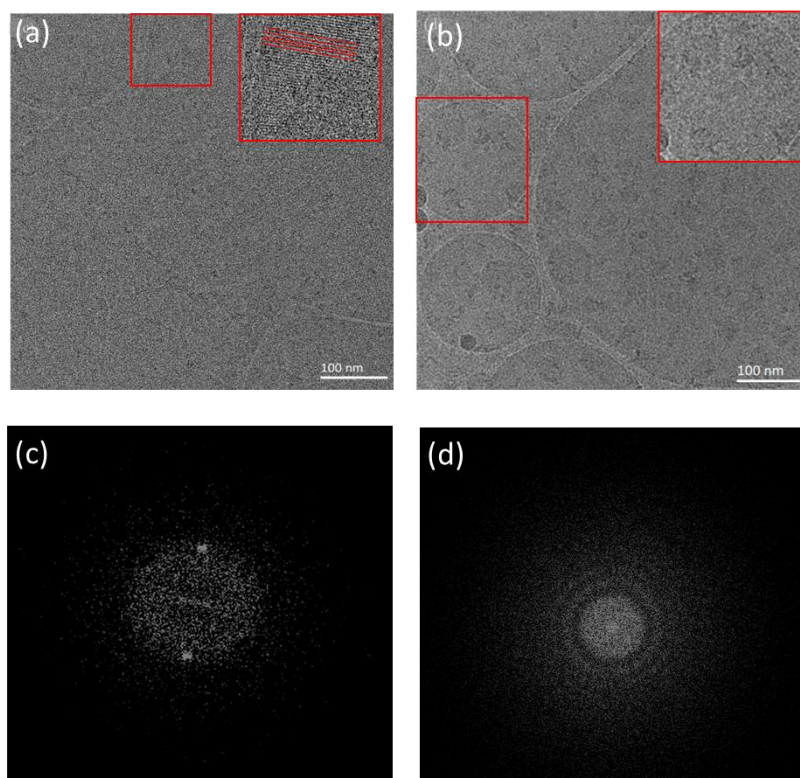


Figure 2-8 Cryo-TEM image of (a) MO with 20 mol% HC (b) MO/OA with 20 mol% HC, Inset is closed-up picture at the marked region; Diffractogram of (c) MO with 20 mol% HC, (d) MO/OA with 20 mol% HC, Each FFT diffractogram corresponds to the inset. All samples include 8 wt% F127.

Interestingly, in some instances, the MO particles with 20 mol% HC were shown to be connected to each other while still retaining their original spherical shape (**Figure 2-8a** and **Figure 2-9a**). The images confirm the assumption that incorporation of the HC at higher concentrations promotes the increase in particle size, thus the aggregation and potential gelation of the self-assemblies. It can be also observed that the two particles were connected through a well-defined internal structure that is similar to the internal structure of the particles themselves (**Figure 2-9b**). This could mean that the internal structure of each particle is likely to be reorganized with the internal structure of an adjacent particle as they aggregate. This behavior resembles the properties of bulk cubic phases exhibited by monoolein assemblies where a continuous periodic membrane lattice structure is formed. Such assemblies have very high viscosities and gel-like appearance (Barriga, Holme, et al. 2019). The metastable structure of the self-assembly system can be induced by external hydrophobic molecules, such as drugs and nanoparticles (Mulet et al. 2010; Meikle et al. 2020). Therefore, it is considered that the incorporation of hydrophobic drug molecules such as HC affected the property of the

dispersions shifting their dispersion state to be unstable. In addition, the external stimuli during preparation such as inducing strong shear stress (sonication in this study) might have accelerated the transition of the dispersions to reach an aggregation state. The structural transition triggered by HC incorporation could be supported with detailed analysis, using DLS and Laurdan fluorescence analysis.

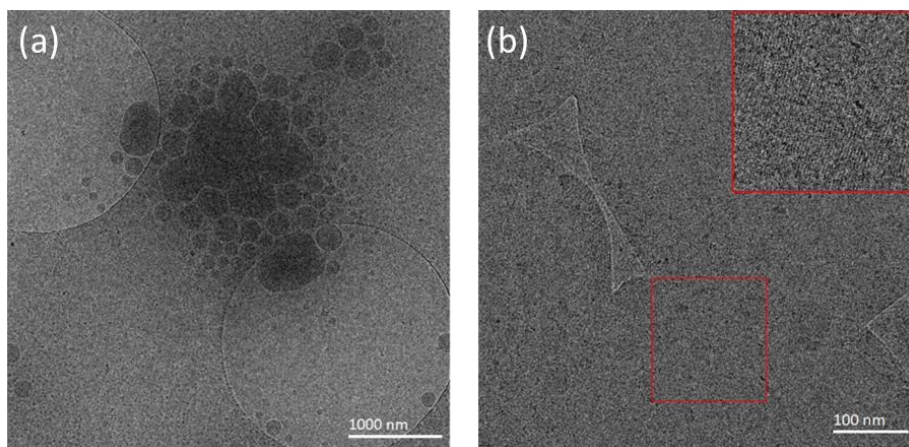


Figure 2-9 Cryo-TEM image of (a) aggregation of MO F127 8 wt% with 20 mol% HC particles (b) Reorganized internal structure of merged particles. Inset is close-up picture at the marked region.

3.4 Effects of HC Incorporation on Particle Size Distribution and Polydispersity

Herein, the particle size distribution was measured with different concentrations of HC. First, the effects of different concentrations of the surfactant (F127) were investigated as a standard. As shown in **Table 2-2**, the particle size of MO particles decreased with increasing F127 concentrations from 622 nm to 123 nm, while the PDI decreased from 0.23 to 0.15 (Entry 1-4). Values of PDI indicate the dispersibility; a PDI less than 0.3 resembles mono-dispersive property of colloidal solutions (Badran 2014). Similarly, the size and PDI of MO/OA particles decreased to 220 nm and 0.22, respectively, with the increase of F127 up to 8 wt% (Entry 5-7). The decrease in particle size is attributed to the steric stabilization caused by the adsorbed F127 on the self-assemblies. The hydrophobic PPO block of F127 anchors on the lipid membranes of the self-assembly surface, resulting in the exposure of the hydrophilic PEO block to the surrounding water, which provides significant steric repulsion between the particles (Nakano et al. 2002; Gustafsson et al. 1996). In previous works, it was shown that the

concentration of the surfactant can affect the steric stability of dispersions (Nakano et al. 2001; El-Enin et al. 2018; Esposito et al. 2003). Generally, the dispersion size decreases with an increase of surfactant (like F127), however, an opposite effect was observed at MO/OA with F127 12 wt% (Entry 8) where both the size and PDI increase to 338 nm and 0.25, respectively. A similar phenomenon was observed in self-assemblies dispersed with Poloxamer 407 (Nakano et al. 2001; El-Enin et al. 2018; Esposito et al. 2003), thus the increase in size shown in this study could be due to the high concentration of F127.

Table 2-2 Effect of F127 and HC on size distribution and PDI of MO and MO/OA particles.

Entry	Lipid	F127 [wt%]	HC [mol%]	Particle size [nm]	PDI [-]
1	MO	0	0	622.0 ± 64.8	0.23 ± 0.01
2		4	0	222.0 ± 1.2	0.22 ± 0.009
3		8	0	188.8 ± 0.4	0.15 ± 0.004
4		12	0	122.9 ± 0.5	0.15 ± 0.03
5	MO/OA	0	0	570.1 ± 31.2	0.22 ± 0.063
6		4	0	250.5 ± 2.2	0.25 ± 0.013
7		8	0	220.1 ± 2.8	0.22 ± 0.006
8		12	0	337.7 ± 15.0	0.25 ± 0.01
9	MO	8	5	167.0 ± 0.8	0.2 ± 0.008
10		8	10	142.9 ± 6.1	0.29 ± 0.021
11		8	20	246.1 ± 1.7	0.37 ± 0.014
12	MO/OA	8	5	169.8 ± 2.7	0.12 ± 0.02
13		8	10	214.0 ± 0.4	0.19 ± 0.003
14		8	20	242.4 ± 5.5	0.35 ± 0.026

When HC is incorporated, the MO and MO/OA dispersions showed a decrease in particle size compared with HC 0 mol% (Entry 9-14). For example, the size of the particles decreased from 189 nm to 143 nm by incorporating 10 mol% HC in the MO particles (**Figure 2-10a**). The decrease in size can be attributed to the increased hydrophobic interaction between molecules at outer membranes due to the incorporation of HC. This results in a decrease in the surface free energy which causes smaller dispersions to be produced (Nowroozi et al. 2018). Furthermore, an increase in the

particle size and PDI was observed at 20 mol% HC for both MO and MO/OA particles. This suggests that the maximum capacity of the membrane to incorporate HC is around 10 mol%. Beyond this point, the HC is allocated in a different location, most likely at the surface of the particle. Also, at 10 mol% HC, the PDI values of the MO and MO/OA particles are 0.29 and 0.35, respectively, which might lead to the polydispersity of self-assemblies. Based on the present results, a diagram representing the dispersity of MO/OA/HC ternary mixtures in the water is shown in **Figure 2-10b**. Herein, the criteria for determining mono-dispersive and poly-dispersive are $PDI < 0.3$ and $PDI \geq 0.3$, respectively.

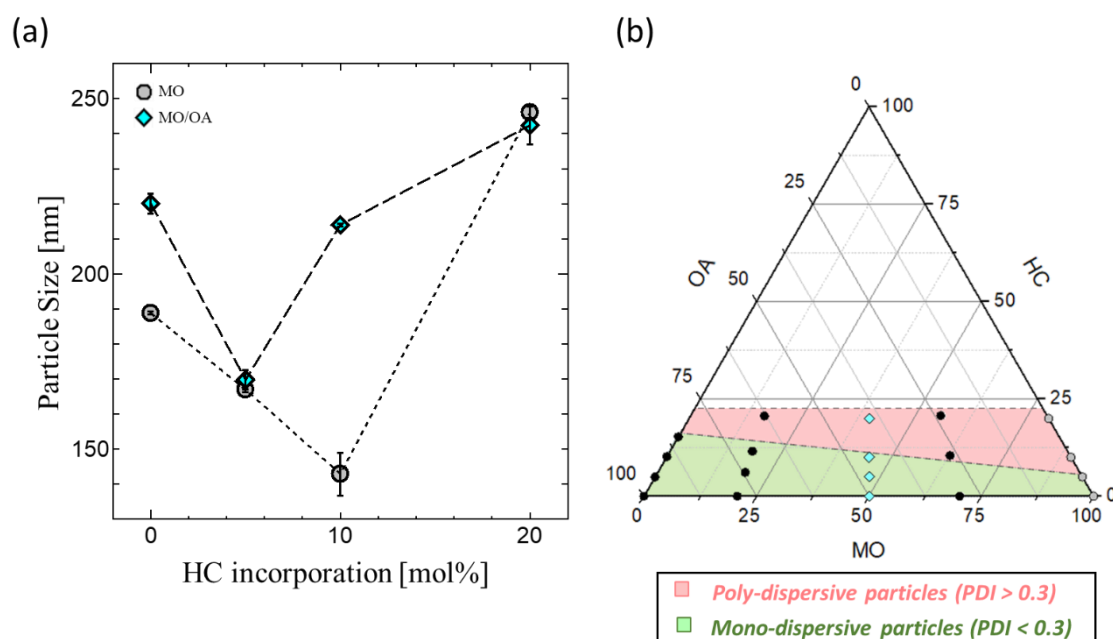


Figure 2-10 (a) Effect of HC on the particle size of MO and MO/OA dispersions (b) Trigonal diagram representation dispersity of MO/OA/HC system. All self-assemblies were stabilized with 8 wt% F127.

3.5 Alteration of Zeta Potential by Incorporating HC

To better understand the influence of HC on the stability of the dispersions, the ζ potential values of MO particles were measured. Only MO samples were used to omit any possible interferences from the ionizable OA. **Figure 2-11** shows the effects of the HC on the surface charge of MO dispersions. Blank MO dispersions (without F127) showed a zeta potential value of -0.07 mV, implying that the MO dispersions are instable. When F127 is added, the magnitude of the zeta potential values increased up -40 mV because the steric stabilization from PEO blocks is enhanced, and the values plateaued at

8 wt% F127 (**Table 2-3**). The zeta potential values were negative, most likely due to the absorption of hydroxyl ions on the surface of the particles (Zhang et al. 2020; Rizwan et al. 2011).

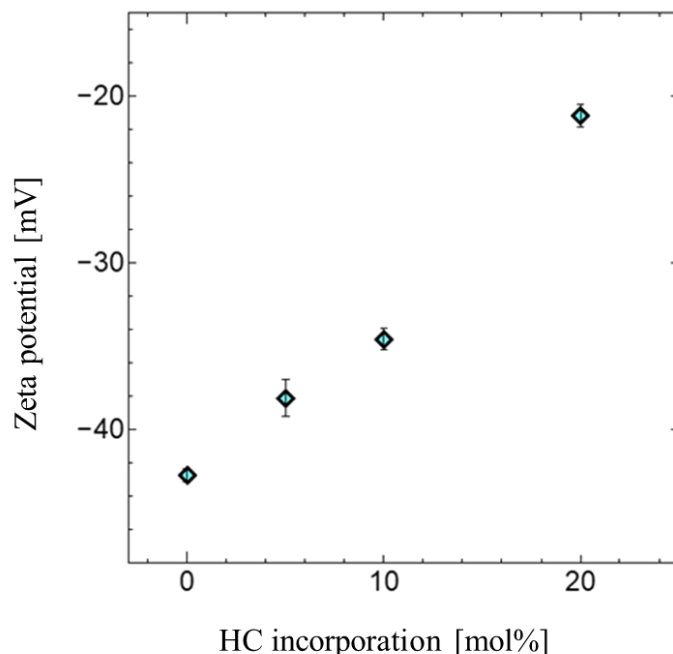


Figure 2-11. Effect of HC on the zeta potential values of MO dispersions

Table 2-3 Effect of F127 on the zeta potential values of MO nanoemulsions

Entry	F127 [wt%]	Zeta Potential [mV]
1	0	-0.07 ± 0.02
2	4	-18.87 ± 0.26
3	8	-42.73 ± 0.40
4	12	-41.23 ± 1.08

Regarding the effect of the incorporation of HC at F127 8 wt%, the magnitude of the zeta potential values dropped from -42.7 mV to -21.2 mV (at 20 mol% HC). The decline can be explained by HC causing the triblock copolymer to be detached from the surface of the particles. In previous studies, increased cholesterol concentration was shown to inhibit the partitioning of Pluronics in liposomes (Johnsson et al. 1999). This was due to the property of cholesterol to increase the strength of lateral interactions

between the hydrocarbon chains of the lipids which makes it harder for the surfactant to partition in the bilayer (Johnsson et al. 1999; Duff Putu, Jean Shoveller., Julio Montaner., Cindy Feng., Rachel Nicoletti., Kate Shannon . 2016). HC, having structural similarities with cholesterol, could interact with the MO hydrocarbon chains, which causes less free surface for the anchoring of the PPO block of F127. The decrease of the absolute zeta potential values with increasing HC concentration is consistent with the increase of particle size (**Table 2-2**). These results mean that the incorporation of HC altered the surface property of the MO dispersions, due to the existence of HC molecules in the outer membrane surface of the self-assemblies. This could suppress the stabilizing effect of F127, and then alter the dispersion stability of the self-assemblies.

3.6 Evaluation of the Polarity in HC-Incorporated Dispersions

The incorporation of Laurdan into the lipid membranes results in emission peaks at 440 nm and 490 nm corresponding for hydrophobic and hydrophilic membrane environments, respectively (Parasassi et al. 1998; Bui et al. 2016; Izza et al. 2021). Herein, the fluorescence analysis using Laurdan was adopted to reveal the polarity (hydrophobic/hydrophilic) in this self-assembly system. The effect of F127 as dispersion stabilizer and HC as coagulant on the polarity are compared (**Figure 2-13**). In both MO and MO/OA system, the increase of F127 concentration resulted in an enhanced 440 nm peak, thus, indicating that the surrounding environment of Laurdan was shifting to be more hydrophobic. The transition of the molecular environment can be explained by the increased hydrophobic PPO block anchoring on the particle surface. The Laurdan spectra with increasing HC blue-shifted both in MO and MO/OA systems, which revealed the increase of the surface hydrophobicity by incorporation of HC. These results are attributed to the hydrophobic nature of HC. It is worth noting that the spectra of the emulsions with high HC content (10 or 20 mol%) and with high F127 content (12 wt%) were similar, where the peaks around 440 nm were dominant, suggesting that the membranes of systems, enriched with HC and F127, turned to be hydrophobic. Since F127 allocates on the membrane surface and results in increased hydrophobic environment, it can be concluded HC also preferably allocates also at the surface of the particle. The Raman spectroscopy results, where the addition of HC did not have an effect on the acyl chain packing, also support the HC allocation on the particle surface.

Regarding the dispersive properties of the self-assemblies, F127 and HC showed different effects. As investigated by zeta potential analysis, the incorporation of F127 increased the absolute zeta potential, which resulted in more stable dispersions. In contrast, HC made the dispersions unstable as shown in the results of zeta potential analysis and cryo-TEM observations. Therefore, regarding the preparation of HC-incorporated dispersions, both increased hydrophobicity and decreased absolute zeta potential could be critical factors for the dispersibility of self-assemblies. With a high concentration of HC (20 mol%), a transition from a metastable dispersion state to a gel-like aggregate could occur. It is suggested that such dispersions, including the self-assemblies with hydrophobic membranes, might have a potential to form interparticle aggregation under shear stress.

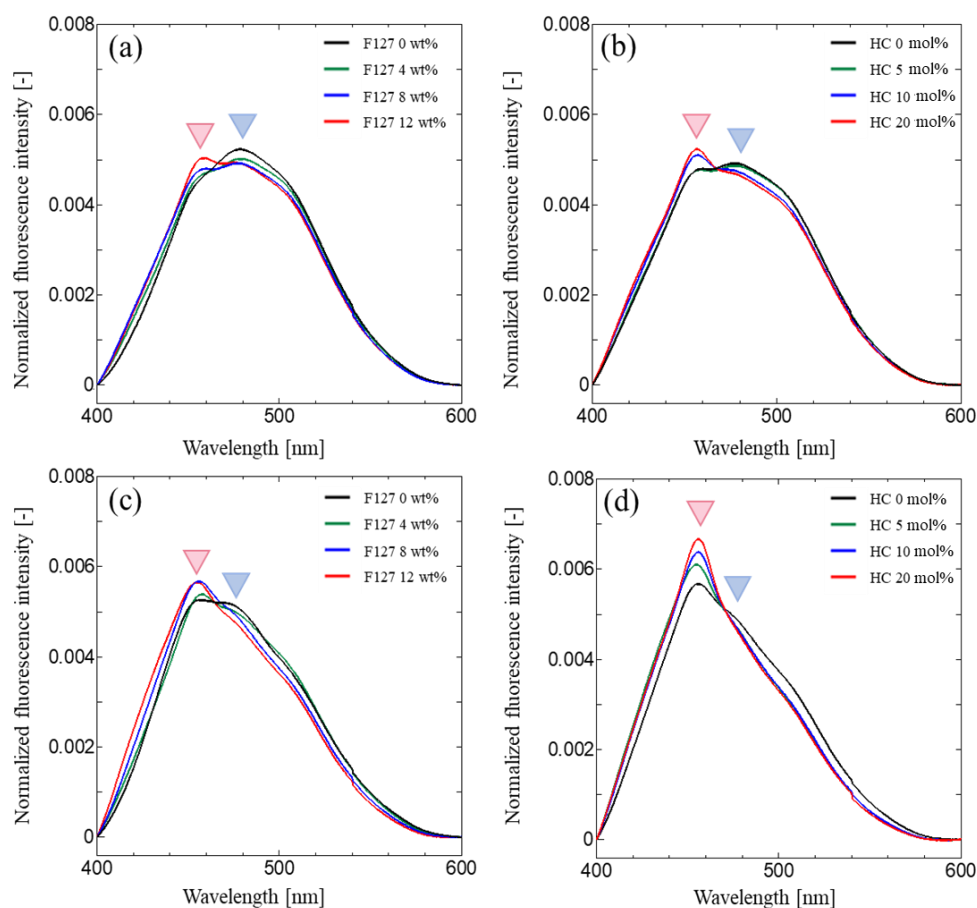


Figure 2-13. Normalized Laurdan fluorescence spectra showing the effect of F127 and HC. (a) MO with varied F127. (b) MO+8wt% F127 with varied HC. (c) MO/OA with varied F127. (d) MO/OA +8wt% F127 with varied HC. All measurements were carried out at 25 °C.

4. Summary

In this chapter, the effects of the incorporation of HC on the properties of MO, OA, and MO/OA self-assemblies were investigated. The HC incorporation was confirmed using Raman spectroscopy. It showed that HC was homogeneously distributed in the dispersed self-assemblies with less effects on the hydrocarbon chain packing. Gel formation in the samples with high amount of HC was occasionally confirmed, indicating that the HC-loading affected the surface properties of the dispersions making them unstable. Cryo-TEM microscopy images showed the particles aggregating at high HC content, providing further evidence of aggregation promoted by incorporation of HC. According to the DLS analysis, excess loaded HC was likely allocated at the surface of the particles and increasing their size. This was further confirmed from the zeta potential values where dispersibility decreased with increased drug concentrations. The allocation of HC at the particle surface was further confirmed with Laurdan fluorescence spectroscopy measurements, where the polarity of the dispersions shifted to a hydrophobic state with increased HC concentrations. Therefore, the loading of the hydrophobic drug altered the surface properties to become more hydrophobic, resulting in a metastable colloidal system. This work provides insights about how hydrophobic drug molecules affect the properties of self-assemblies by examining surface properties and inner structure. The results of this work reveal that the assessment of microscopic properties such as polarity, packing, and ζ potential can be important indicators in predicting the macroscopic properties of drug-loaded particles. The relationship between drug loading capacity and the stability of self-assemblies is a critical issue for designing LNPs as drug carriers.

Chapter 3: Interactions of Cubosomes with Cell Membrane Lipids: Revealed Through Cubic Membrane Property Analysis

1. Introduction

The structure of cubosomes is heavily influenced by the molecular geometry of their constituent lipids. Typically, monoolein (MO) forms cubic phases spontaneously in excess water. This could be attributed to their critical packing parameter (CPP), in which phases with high negative membrane curvature are formed when the $CPP > 1$ (Kulkarni et al. 2011). On the other hand, the formation of lamellar phases is more favorable in bilayers consisting of lipids with $CPP = 1$ such as 1,2-dioleoyl-*sn*-glycero-3-phosphocholine (DOPC), a biologically relevant phospholipid commonly used in cell membrane studies (Van'T Hag et al. 2017). As potential delivery carriers, the implications of the changes to the properties of cubosomes due to the exchange of lipids with cell membrane materials are important factors to study in their design process.

Previously, the phase and membrane behavior of MO/1-Palmitoyl-2-oleoyl-*sn*-glycero-3-phosphocholine (POPC) cubosomes were examined. It was shown that introduction of POPC into MO cubosomes resulted in phase transition to the lamellar phase. Also, the examination of packing stress using DPH showed that it resulted in an increase in packing stress of the cubic membranes (Nakano et al. 2005). Similarly in another work, the binary compositions of MO and DOPC showed an increase in the generalized polarization of Laurdan with increasing DOPC fraction, which was attributed to the transition from the cubic $Pn3m$ to the lamellar phase (Mangiarotti et al. 2021a). The results from these studies show that the study of the cubic membrane, which is well-hydrated and fluidic, using membrane bound fluorescence probes is effective in understanding the changes in its structure. Therefore, the utilization of such probes can be effective to elucidate the changes in cubic membrane and structure during the exchange of lipids with cell membranes.

In the first part of this chapter, the effects of the incorporation of cell membrane lipids on the cubosome structure and membrane are examined using different MO/DOPC compositions. The structure and membrane of the MO cubosomes with increasing DOPC

concentration are investigated to mimic the lipid exchange of DOPC into the cubosomes. Then, to confirm the results in the first part, examination of the interaction of MO cubosomes and DOPC liposome is done using time-resolved SAXS and GP_{340} . Also, a new approach to estimate the kinetics of apparent lipid exchange is developed. The aim of this chapter is to highlight the importance of deeper analysis of the cubic membrane in the context of lipid exchange with cell membrane lipids.

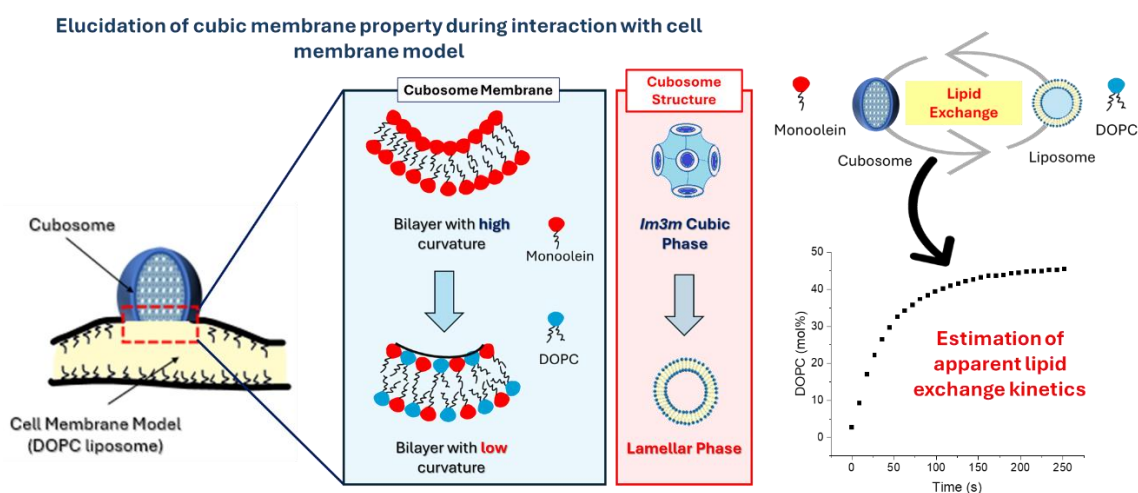


Figure 3-1 Schematic illustration of this study.

2. Materials and Methods

2.1 Materials

Glycerol α -monooleate (MO) (purity > 99 %), Pluronic F127 (F127), 6-dodecanoyl-2-dimethylaminophthalene (Laurdan), and 1,6-diphenyl-1,3,5-hexatriene (DPH) were purchased from Sigma-Aldrich (St. Louis, MO). 2-dioleoyl-sn-glycero-3-phosphocholine (DOPC) and 1,2-dipalmitoyl-sn-glycero-3-phosphocholine (DPPC) were purchased from Nippon Oil & Fats Corporation (Tokyo, Japan).

2.2 Preparation of MO/DOPC Nanoparticles, DOPC, and DPPC Liposomes

The MO/DOPC LNPs were prepared by dissolving different molar ratios of MO and DOPC in chloroform. The samples were placed under vacuum for 48 hours to remove the chloroform and create lipid films. After hydrating the lipid films with preheated F127 solution (lipid to F127 weight ratio = 100:1). Using a probe sonicator (TOMY Ultrasonic Disruptor UD-200), the samples were homogenized in an ice bath for 3 minutes. The cubosomes were heated at 70°C for 3 minutes. The samples were incubated in the dark at room temperature until further use. For the preparation of the liposomes, either DOPC or DPPC powders were dissolved in chloroform. Thin lipid films were obtained after evaporating the chloroform and were kept under vacuum for at least 24 hours. The films were hydrated with ultrapure water and agitated in a water bath for 15 minutes at 60°C. Finally, the liposome suspensions were extruded 11 times through a polycarbonate 100 nm membrane filter (Liposofast; Avestin Inc., Ottawa, ON, Canada). The prepared liposome solutions were stored at 4°C. The final concentration of the cubosomes and liposomes were 50 mM and 25 mM, and all measurements were performed at a temperature of 25 °C.

2.3 TR-SAXS Measurements

The SAXS measurements were conducted at beamline BL40B2 at SPring-8 synchrotron facility, Japan. The X-ray wavelength and sample to-detector distance were 0.100 nm and 0.578 m, respectively, corresponding to an accessible q -range of 0.24 to 3.2 nm⁻¹. The detector used is photon-counting X-ray detectors (PILATUS 3 S 2M, Dectris ltd., Baden, Switzerland) (Specifications: max. 25 Hz, 1475 * 1679 pixels, 0.172 mm/pixel). Equal volumes of the cubosome and liposome solutions were using stopped-flow apparatus (SFM-CD10, UNISOKU, Osaka, Japan). The setup was attached to the

X-ray environment with a scattering cell consisting of a quartz capillary (1.5 mm diameter, wall thickness 10 μm). The flow time and deadtime of the rapid mixing of the cubosome and liposome solutions was 50 and 1.4 ms, respectively. The size of the X-ray beam at the sample position was around 300 μm (vertical) by 400 μm (horizontal) (full width at half maximum) with photon flux of 3×10^{10} photons/s. Exposure time is 1 s, a measurement time of 180 s, and an interval of 3 ms between each measurement. The background signals were subtracted and the SAXS diffractograms were normalized.

2.4 Cryo-TEM Imaging

2.4 μL of the MO cubosomes were deposited on to glow-discharged Quantifoil R2/2 in semi-automated vitrification device (Vitrobot Mark IV, Thermo Fisher Scientific) at 100% humidity. The samples were blotted for 4 s from both sides and submerged in liquid ethane immediately. The cryo-TEM images were captured under cryogenic conditions at a magnification of 59,000 \times using a Titan Krios (Thermo Fisher Scientific, MA) and operating at 300 kV and a Falcon2 CMOS camera.

2.5 Dynamic Light Scattering Analysis

The MO/DOPC nanoparticles were diluted 1000-fold with ultrapure water. Then, the particle size, poly dispersity index (PDI), and zeta potential (ζ -potential) were obtained by measuring the dynamic light scattering and M3-PALS method using a Malvern Zetasizer Nano series (Malvern, UK). The same dilution and measurement conditions were applied for characterization of the mixing of the cubosomes and liposomes, where equal volumes of the cubosomes and liposomes were mixed and incubated for 5 min, the measurement was started immediately.

2.6 Optical Density Measurements

The measurement of optical density (OD_{400}) of the MO/DOPC particles was conducted by measuring their absorbance at 400 nm using an xMark™ Microplate Spectrophotometer (Bio-Rad, Hercules, CA). In the mixing experiment, equal volumes of the cubosomes and liposomes were mixed and incubated for 5 min, and the measurement was started immediately.

2.7 Steady-State Laurdan Measurements

The MO/DOPC compositions were probed with 15 μL of Laurdan solution (1 mM, in ethanol) after diluting 100-fold with ultrapure water. After 30 minutes of incubation in

the dark, the Laurdan spectra were obtained by exciting the samples at 340 nm and measuring the intensities in the wavelength range of 400 nm to 600 nm using FP-8500 spectrofluorometer (JASCO, Tokyo, Japan). The same procedure above was performed for the mixing experiment where either the cubosomes or liposomes were probed with Laurdan and after 100-fold dilution, the samples were mixed and incubated for 5 min, then, the Laurdan measurement was started immediately.

The generalized polarization of Laurdan (GP_{340}) was calculated according to the following equation:

$$GP_{340} = \frac{I_{440} - I_{490}}{I_{440} + I_{490}} \quad \text{Eq. 3-1}$$

where I_{440} and I_{490} are the fluorescence intensities at 440 and 490 nm, respectively.

For the examination of the changes of the GP_{340} value over time, the Laurdan probed cubosomes were mixed with liposomes after 100-fold dilution, and Laurdan spectra over the time course of 1680s were collected. The final concentration of the cubosomes and liposomes is 0.5mM and 0.25mM, respectively.

2.8 Steady-State Fluorescence Anisotropy Measurements

3 μ L of 1 mM DPH dissolved in ethanol were added to 15 μ L of MO/DOPC particles that were 100-fold diluted with ultrapure water. The fluorescence polarization of DPH (excitation = 360 nm, emission = 430 nm) was measured using fluorescence spectrophotometer (FP-6500; JASCO, Tokyo, Japan). The samples were incubated for 30 min in the dark. The samples were excited with vertically polarized light (360 nm), and emission intensities both perpendicular (I_{\perp}) (0 °, 0 °) and parallel (I_{\parallel}) (0 °, 90 °) to the excited light were recorded at 430 nm. The polarization (P) of DPH was then calculated by using the following equations:

$$P = \frac{I_{\parallel} - GI_{\perp}}{I_{\parallel} + GI_{\perp}} \quad \text{Eq. 3-2}$$

$$G = \frac{i_{\perp}}{i_{\parallel}} \quad \text{Eq. 3-3}$$

where i_{\perp} and i_{\parallel} are the emission intensities perpendicular to the horizontally polarized light (90 °, 0 °) and parallel to the horizontally polarized light (90 °, 90 °), respectively, and G is the correction factor. The membrane fluidity was calculated by the reciprocal of

polarization (I/P). The same procedure above was performed for the mixing experiment where either the cubosomes or liposomes were probed with DPH and after 100-fold dilution, the samples mixed and incubated for 5 min, then, the fluorescence anisotropy measurement was started immediately. The final concentrations of the cubosomes and liposomes are 0.5 mM and 0.25 mM, respectively.

2.9 Time-Resolved Fluorescence Measurements

The MO/DOPC compositions were probed with 15 μ L of Laurdan solution (1 mM, in ethanol) after diluting 100-fold with ultrapure water. After 30 minutes of incubation in the dark, the time-resolved fluorescence spectra were measured using DeltaFlex (Horiba, Kyoto, Japan). The same procedure above was performed for the mixing experiment where either the cubosomes or liposomes were probed with Laurdan and after 100-fold dilution, the samples were mixed and incubated for 5 min, then, the measurement was started immediately. The samples were excited with a light source of 373 nm. The emission decays were obtained from 420 to 540 nm in 5 nm steps. The acquisition time was 60 s for each emission wavelength. Obtained data were analyzed using the EzTime software (Horiba, Kyoto, Japan). The data fitting of the collected emission wavelengths was done using the multiple exponential fitting equation below:

$$I(t) = \int_{-\infty}^t \text{IRF}(t') \sum_{i=1}^n A_i e^{\left(\frac{-t-t'}{\tau_i}\right)} dt' \quad \text{Eq. 3-4}$$

where $I(t)$ is the intensity at decay time t , n is the number of components ($n = 3$) and A_i is the amplitude in counts at time zero.

Using a custom code written in python, the fitting and the determination of the lifetimes was followed by finding the DAS for each component in which the amplitude of each lifetime component in the experimental wavelength range was plotted as a function of wavelength as DAS. The components of DAS were deconvoluted using lognormal amplitude function similar to previous reports (Watanabe, Suga, et al. 2019; Ito et al. 2023). The fitting of each component was done to satisfy the highest coefficient of determination value ($R^2 > 0.95$). The final concentrations of the cubosomes and liposomes are 0.5mM and 0.25mM, respectively.

2.10 Time-Resolved Anisotropy of DPH

The time-resolved anisotropy measurements were conducted by the DeltaFlex (Horiba, Kyoto, Japan). 3 μL of 1 mM DPH dissolved in ethanol were added to 15 μL of MO/DOPC nanoparticles that were 100-fold diluted with ultrapure water. Similar to the steady-state measurements, either the cubosomes or liposomes were probed with DPH after 100-fold dilution, the samples were mixed and incubated for 5 min, then, the measurement was started immediately. The emission decays of DPH were measured at directions parallel (I_{\parallel}) and perpendicular (I_{\perp}) to the polarization of the vertically polarized excitation. The time-resolved anisotropy was calculated according to the equations below:

$$r(t) = \frac{[I_{\parallel}(t) - G(\lambda)I_{\perp}(t)]}{[I_{\parallel}(t) + 2G(\lambda)I_{\perp}(t)]} \quad \text{Eq. 3-5}$$

$$G(\lambda) = i_{\perp}(t) / i_{\parallel}(t) \quad \text{Eq. 3-6}$$

where $G(\lambda)$ is the geometry factor at the wavelength λ of emission. The G factor of the emission collection optics was determined using the emission at directions parallel (i_{\parallel}) and perpendicular (i_{\perp}) to the polarization of the horizontally polarized excitation. The acquisition time was 60 s for each emission decay. The emissions were fitted to multi-exponential decay model shown below using the EzTime software (Horiba, Ltd., Kyoto, Japan).

$$r(t) = r_{\infty} + (r_0 - r_{\infty}) \sum_j \alpha_j \exp(-t/\theta_j) \quad \text{Eq. 3-7}$$

where r_{∞} is the limiting anisotropy, r_0 is the initial anisotropy, α_j is the fraction amplitudes of each rotational correlation time, and θ_j is the individual rotational correlation time. The apparent microviscosity (η) of the membrane was calculated using the Stokes-Einstein-Debye equation:

$$\eta = \frac{k_B T}{6D_{\perp} V_{eff}} \quad \text{Eq. 3-8}$$

where k_B is Boltzmann constant, T is the temperature, V_{eff} is the effective volume of DPH = 360 \AA^3 , D_{\perp} is the rotational diffusion coefficient of DPH which was determined according to previous reports as follows (Scanavachi et al. 2021):

$$D_{\perp} = \frac{0.1674 - 0.1066\left(\frac{r_{\infty}}{r_0}\right) - 0.062\left(\frac{r_{\infty}}{r_0}\right)^2}{\phi} \quad \text{Eq. 3-9}$$

where ϕ is the average correlation time obtained from the area under the anisotropy decay curve. The final concentrations of the cubosomes and liposomes are 0.5 mM and 0.25mM, respectively.

3. Results and Discussion

3.1 Structural and Nanoparticle Characterization of MO and MO/DOPC Nanoparticles

The molecular geometry of the lipid constituents of dispersed lyotropic liquid crystalline nanoparticles has a great influence on their structural properties (Van'T Hag et al. 2017). For cubosomes, the bicontinuous cubic structure arises from the highly curved bilayers due to wedge shaped molecular geometry of MO (Kulkarni et al. 2011). Incorporating lipids with differing molecular geometries such as DOPC, will alter the structure and properties of the cubosomes. The cryo-TEM image of the MO cubosomes in **Figure 3-2a** shows particles with particle size of around 200 nm and cubic inner structure of the *Im3m* phase as revealed in the Fast Fourier Transform (FFT) in the inset. Further confirmed using SAXS results (**Figure 3-2b**), the inner structure of the cubosomes displayed diffraction peaks associated with the *Im3m* cubic phase and a lattice structure of 15.71 nm aligning with previously reported results (Lakic et al. 2025). The particle size measurements in **Figure 3-2c** were consistent with the cryo-TEM images, where MO cubosomes with diameter of ~200 nm and uniform size distribution (PDI ~ 0.2) were observed. Well-stabilized and dispersed particles were formed according to the high zeta potential of the cubosomes ≈ -27 mV (**Figure 3-2d**). The cubosomes showed high optical density values in **Figure 3-2e**, which is characteristic of cubic phases (Fong et al. 2014).

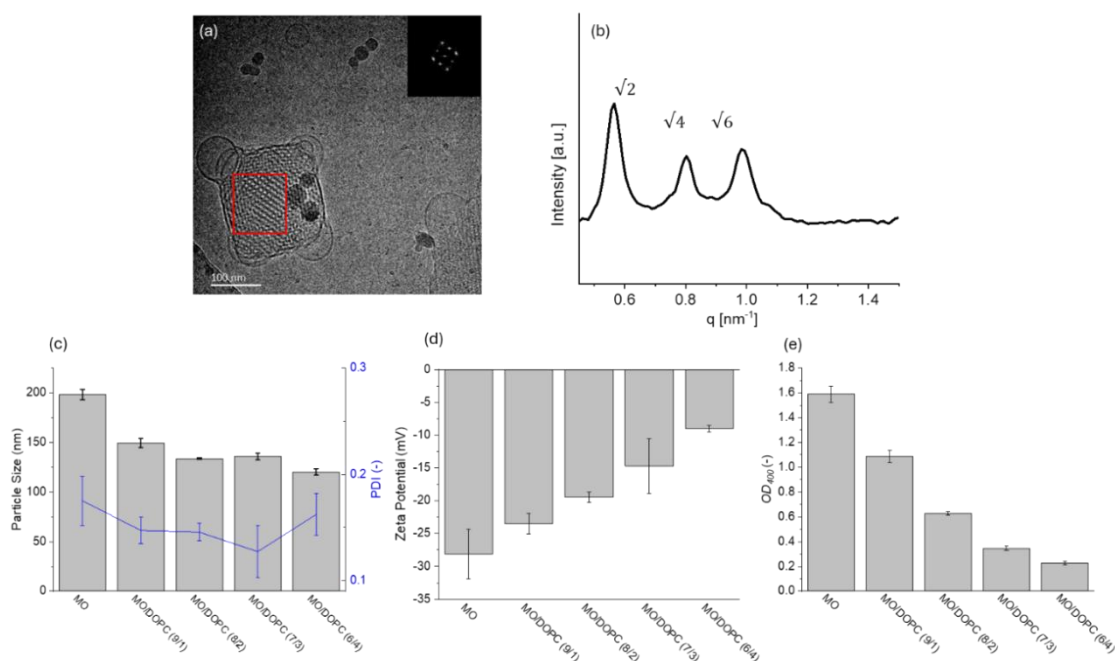


Figure 3-2 (a) Cryo-TEM image of MO cubosomes with the inset showing the corresponding Fast Fourier Transform (FFT) of the internal structure (red box) (b) SAXS profile of MO cubosomes; characterization of (c) Particle size and PDI (d) Zeta potential (e) OD_{400} of MO/DOPC particles. The concentration of particles is 50mM in the cryo-TEM and OD_{400} experiments is 50mM and 0.05mM in the size, PDI, and zeta potential experiments.

When DOPC is incorporated into the cubosomes, a transition from the cubic phase to the lamellar phase occurs. This is due to the opposite molecular geometries of MO and DOPC (**Figure 3-3**), where MO promotes the formation of highly curved bilayers and DOPC induces the transition towards membranes with lower negative curvature (Milogrodzka et al. 2023). In previous works, it was shown that higher fractions of PC lipids such as egg phosphatidylcholine (EPC) or 1-palmitoyl-2-oleoyl-*sn*-glycero-3-phosphocholine (POPC) triggered the complete transition from cubic phase to the lamellar phase around MO/PC molar ratio of $\approx (6/4)$ (Nakano et al. 2005). Another study revealed that even small amounts of DOPC (< 2 mol%) can drive the transition of the cubosomes to form lamellar vesicles over an extended period of time (Vandoolaeghe et al. 2009). The transition from lamellar vesicles to the bicontinuous phase could also be indicated by changes in particle size and turbidity (Rui, Watanabe, et al. 2024). This transition is observed in the obtained results, where increasing the DOPC ratio in the cubosomes has resulted in noticeable changes in such properties. The size and zeta potential values as well as the optical density of the cubosomes decreased upon increasing the DOPC content, indicating phase change from the cubic to the lamellar phase. It was reported previously that the transition from lamellar vesicles to the bicontinuous phase is accompanied by an increase in particle size and turbidity in DDAB/phytantriol systems (Muir et al. 2012). Thus, the reduction of the OD_{400} values observed at higher DOPC ratios (~ 30 -40 mol%) further confirms the transition from cubosomes to lamellar vesicles.

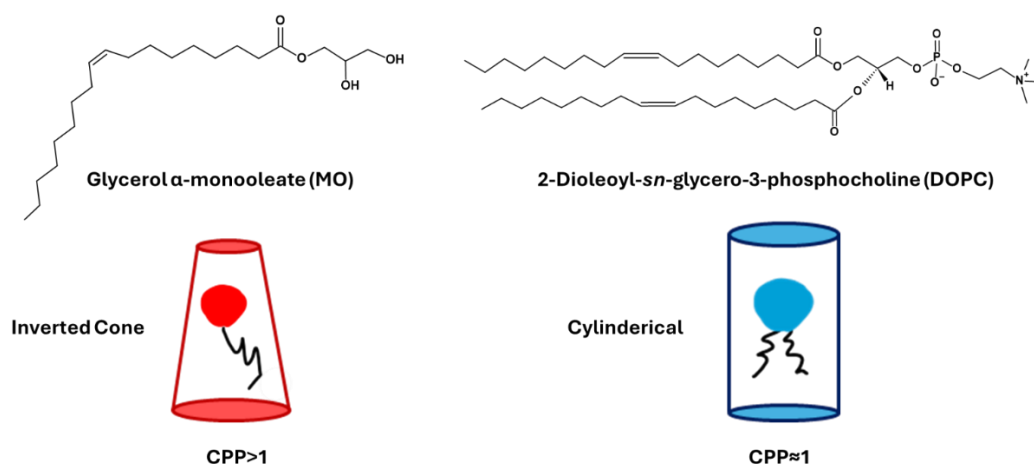


Figure 3-3 Structures and molecular geometries of MO and DOPC

3.2 Evaluation of the Membrane Properties of MO/DOPC Nanoparticles

Membrane bound fluorescence probes are effective in revealing the environment of their surrounding membrane. The properties of the inner membranes of the cubosomes have not been fully elucidated yet, especially in the context of phase transition when interacting with cell membrane lipids such as DOPC. Such an examination is vital for the assessment of the drug release pattern of the carrier as well as understanding the fusion kinetics. In addition, it is necessary to explore the effects of lipid mixing and examine how the cubic membrane is modified with increasing phospholipid amount. Laurdan and DPH probes were used to assess the cubosomes' membrane hydration and membrane fluidity, respectively employing both steady-state and time-resolved methods. In the case of Laurdan, depending on the polarity of the local environment of the membrane, the emission of Laurdan can shift with emissions at longer wavelengths corresponding to non-polar environments and shorter wavelengths corresponding to polar environments (Parasassi et al. 1998). In **Figure 3-4**, the steady-state Laurdan spectra of the different MO/DOPC compositions are denoted in the colormap from black to blue. The MO cubosomes displayed a spectrum with significant blue-shift, however with increasing DOPC concentration, the spectra show more pronounced emission at shorter wavelengths. These spectra were used to calculate the generalized polarization of Laurdan (GP_{340}), which is commonly used to assess the membrane hydration of lipid membranes.

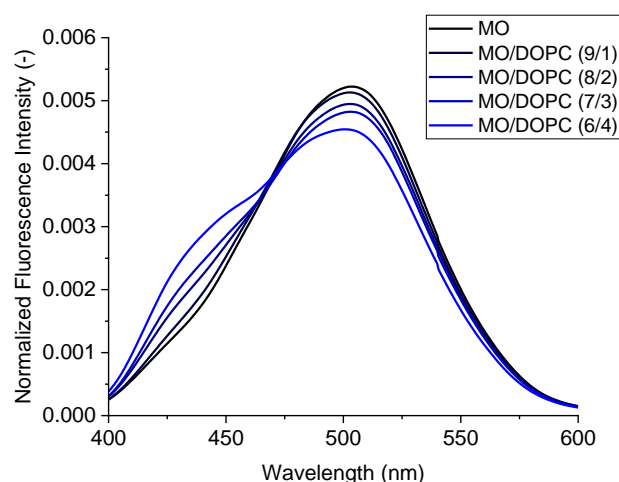


Figure 3-4 Steady-state spectra of Laurdan in (a) MO (b) MO/DOPC (9/1) (c) MO/DOPC (8/2) MO/DOPC (7/3) (e) MO/DOPC (6/4) cubosomes. The final concentration of cubosomes is 0.5 mM

The GP_{340} of the MO/DOPC compositions is shown in **Figure 3-5a**. A GP_{340} value of ≈ -0.35 was observed for MO cubosomes, reflecting a well-hydrated membrane environment. Increasing the DOPC in the particles yielded higher GP_{340} values, denoting a transition towards a less-hydrated bilayer. Similar trends were observed in the MO bulk cubic phases of $Pn3m$ symmetry in the literature, where GP values of MO dispersions increased at higher DOPC fractions (Mangiarotti et al. 2021a). This implies that the behavior of the membranes of the dispersed cubic phases does not differ greatly from the bulk cubic phases. The changes in membrane fluidity were examined using DPH, which can reveal the inner membrane properties of membrane, namely the acyl chain region (Watanabe et al. 2017). MO cubosomes displayed high membrane fluidity initially, which decreased upon with more DOPC concentration (**Figure 3-5b**). The high membrane hydration of the cubic membrane is attributed to its high membrane curvature which allows for more water relaxation around Laurdan (Mangiarotti et al. 2021a). In the same vein, the increased membrane curvature due MO molecules adopt enhanced wedge shape configuration, could explain the high membrane fluidity caused by lower membrane packing (Nakano et al. 2005). The reduction of the hydration and fluidity of the cubic membrane due to increasing DOPC content are in line with the results in the previous section in relation to the transition from cubic to lamellar phase. Due to the reduction of the negative bilayer curvature because of the molecular geometry of DOPC,

Laurdan is likely to experience less water relaxation around it. In the same vain, DPH would sense a more packed membrane condition.

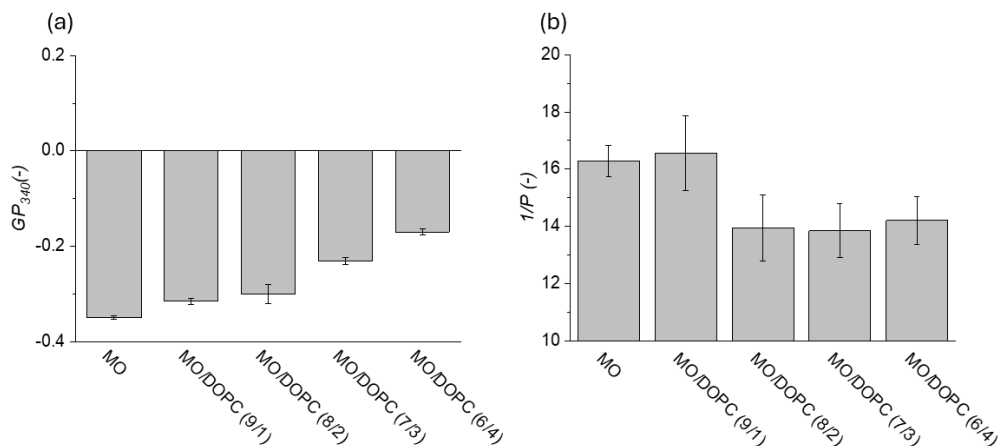
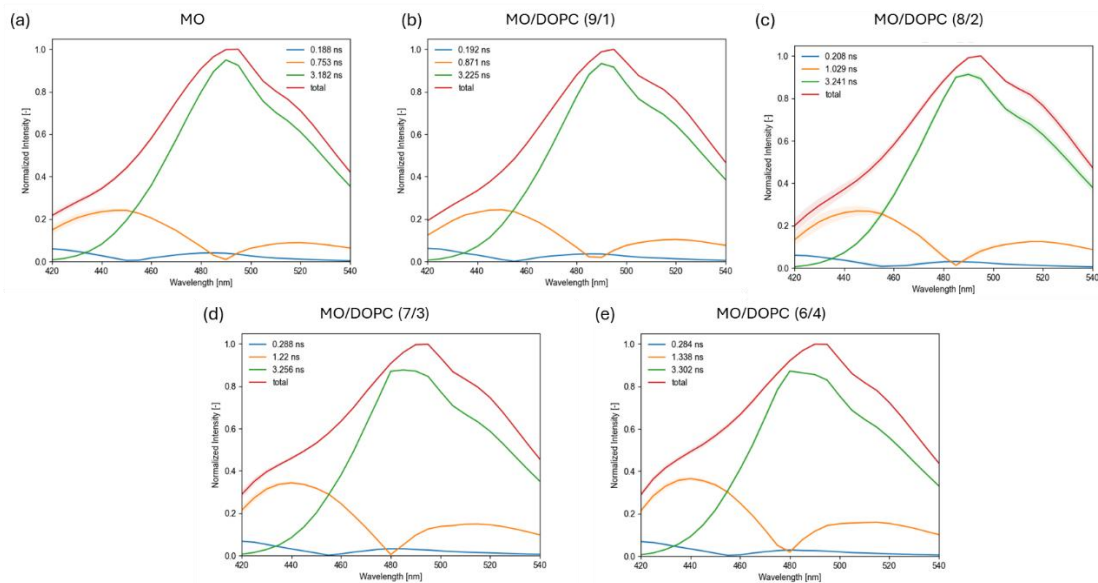


Figure 3-5 Results of (a) GP_{340} (b) $1/P$ values of MO/DOPC compositions. The final concentration of cubosomes is 0.5 mM.

While the steady-state GP analysis indicates the general membrane hydration environment, the deconvolution of the decay associated spectra (DAS) with the solvent modeling method allows for deeper understanding of the different regions of the membrane (Watanabe, Suga, et al. 2019; Ito et al. 2023). The fitting of the fluorescence decay curves of Laurdan in the MO/DOPC compositions which was done using equation (3) implies the presence of three lifetime components as shown in **Table 3-1**. Across the board, the increase of the DOPC content in the cubosomes resulted in an increase in lifetimes. This could be attributed to the reduction of water dipolar relaxation in the system due to the gradual transition from cubic to lamellar phase. The quenching effect of water molecules, that are much more abundant in the cubic membrane, results in shorter lifetimes in compositions with higher MO fractions. DAS of Laurdan in MO/DOPC compositions are shown in **Figure 3-6**. The changes observed in the total spectrum (shown in red) are consistent with the steady-state Laurdan results. Regarding the three lifetime components, the normalized intensity of τ_1 is much smaller compared to τ_2 and τ_3 , implying that its contribution to the overall spectrum is minimal. Increasing the DOPC content in the cubosomes, showed noticeable changes to the two emission peaks of component τ_2 , where significant shift of their peak centers towards lower wavelengths is observed.

Table 3-1. Results of fitting of the decay curves of Laurdan in MO/DOPC bilayers

	MO	MO/DOPC (9/1)	MO/DOPC (8/2)	MO/DOPC (7/3)	MO/DOPC (6/4)
τ_1 (ns)	0.188 ± 0.0110	0.192 ± 0.0029	0.208 ± 0.0270	0.288 ± 0.0092	0.284 ± 0.0309
τ_2 (ns)	0.753 ± 0.0064	0.871 ± 0.0153	1.029 ± 0.0110	1.220 ± 0.0130	1.338 ± 0.0107
τ_3 (ns)	3.182 ± 0.0055	3.225 ± 0.0166	3.241 ± 0.0082	3.256 ± 0.0045	3.302 ± 0.0051

**Figure 3-6** DAS of Laurdan in (a) MO (b) MO/DOPC (9/1) (c) MO/DOPC (8/2) (d) MO/DOPC (7/3) (e) MO/DOPC (6/4) cubosomes. The final concentration of cubosomes is 0.5 mM.

To visualize the changes occurring to all the components, the utilization of the τ vs λ plot is an effective approach. By assigning each emission component using solvent modeling. This is an approach that employs the representation of the complex nature of the lipid membrane in terms of the distribution of Laurdan in different solvents, in which the changes in specific membrane regions could be examined (Ito et al. 2023). The distributions of deconvolution components of the different MO/DOPC compositions are shown in the τ vs λ plots, and their contribution based on solvent modeling in **Figure 3-7a-f**. While the changes are subtle with increasing DOPC content, less contribution from the water region and more contribution from the high polar protic region is observed. This implies that the environment of the inner cubic membrane is becoming less hydrated due to the insertion of DOPC.

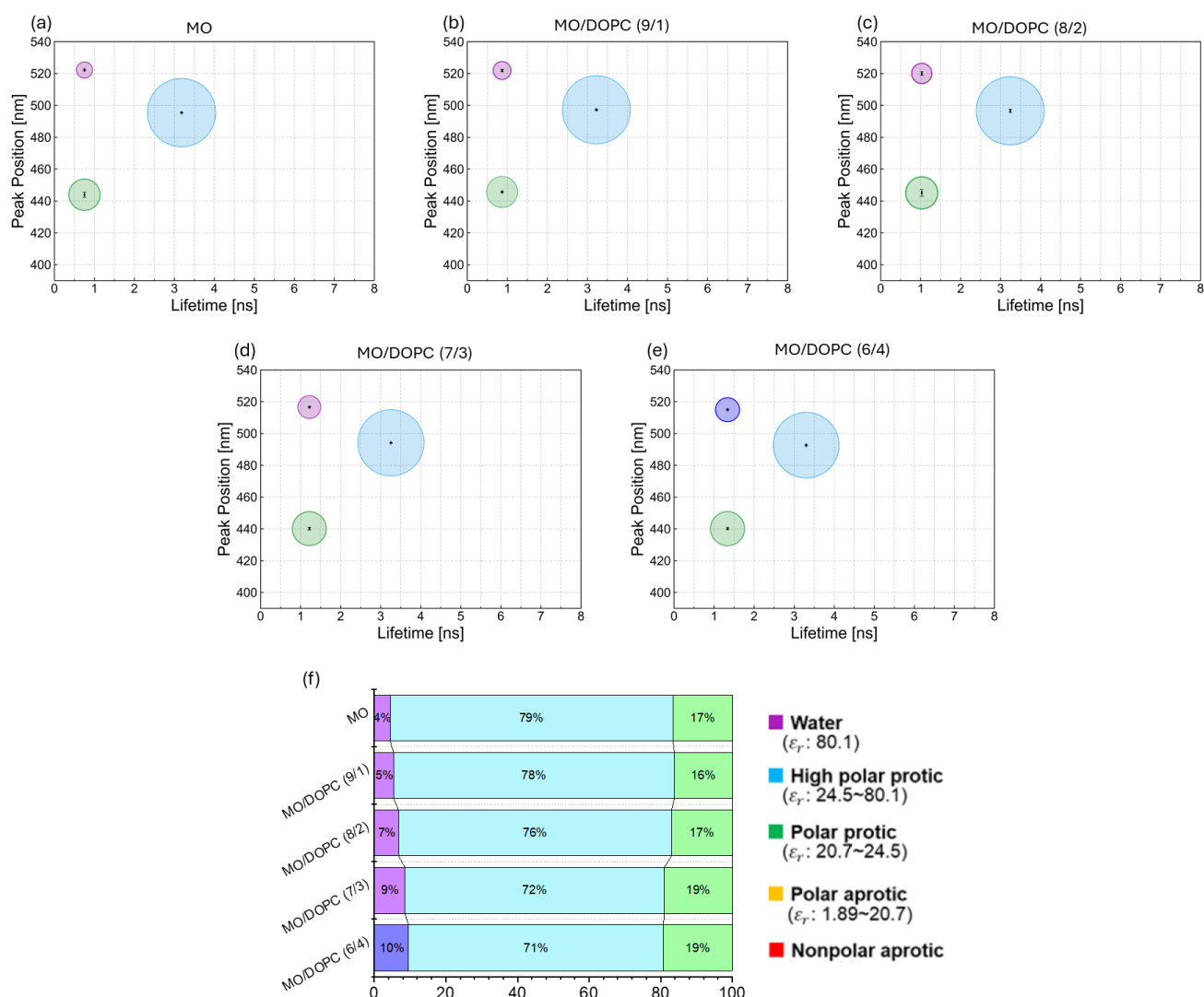


Figure 3-7 Distribution of deconvolution components in the τ vs λ plot of Laurdan in (a) MO (b) MO/DOPC (9/1) (c) MO/DOPC (8/2) (d) MO/DOPC (7/3) (e) MO/DOPC (6/4) cubosomes; (f) The contribution different fluorescence contributions based on solvent modeling for MO/DOPC compositions. The final concentration of cubosomes is 0.5 mM.

Interestingly, the two emission peaks of the shorter lifetime component (τ_2) showed noticeable change as shown in the overlap of the τ vs λ plots in **Figure 3-8a**. It was noted previously, also based on solvent modeling, there is a dependency of the fluorescence lifetime with the micro-viscosity of the membrane. By using time-resolved anisotropy of DPH, it was shown that the micro-viscosity of the membrane increases with increasing DOPC concentration (**Figure 3-8b**). Compared to the steady-state measurements of Laurdan and DPH, the time-resolved fluorescence measurements were

shown to better elucidate the subtle changes in the cubic membrane environment in relation to the transition to the lamellar phase. The application of such methods provides deeper understanding of the changes in the environment of different regions in the cubic membranes of the cubosomes such as the interfacial and inner cubic membrane.

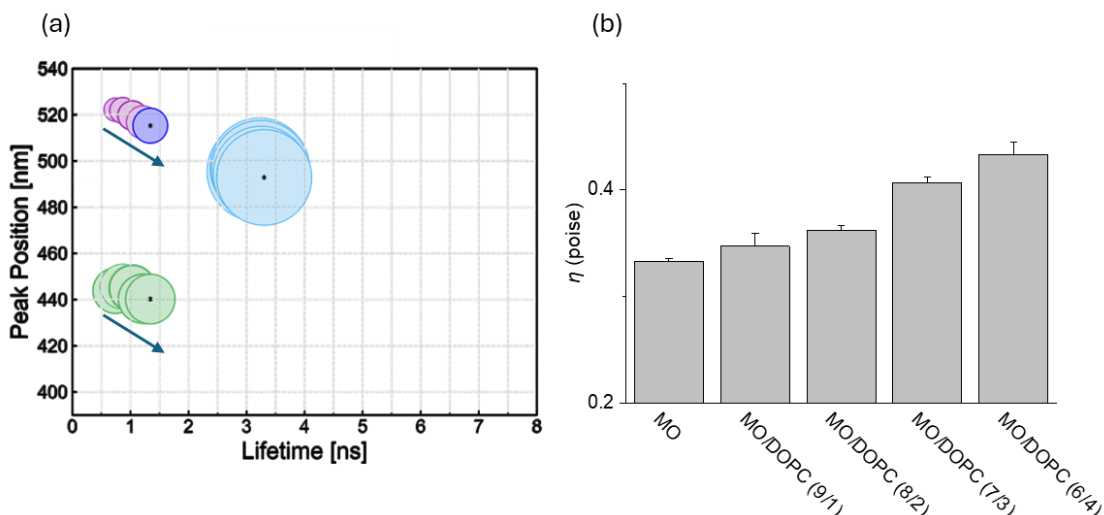


Figure 3-8 (a) Overlap of the distribution of deconvolution components in τ vs λ plot of Laurdan (b) η values of MO/DOPC compositions. The final concentration of cubosomes is 0.5 mM.

3.3 Structural and Membrane Property Changes of MO Cubosomes and DOPC Liposomes Upon Mixing

In the previous sections, the changes that occur to the properties of the cubosomes with increasing DOPC concentration were examined to demonstrate the alteration in the cubosome structure and membrane. To confirm the validity of the previous results, the changes to the structural and membrane properties of MO cubosomes with DOPC liposomes, as cell membrane model, using time-resolved SAXS and examination of membrane property changes were assessed. In **Figure 3-9a**, the time-resolved SAXS of MO cubosomes after being mixed with DOPC cubosomes is shown. At $t = 0$ s (top), the SAXS profile displays diffraction peaks associated with the $Im3m$ cubic phase like the cubosomes before mixing (**Figure 3-3b**). As time progresses, the peaks positions of the cubic phase increase to higher q values and the intensities decrease until they are no longer present (**Figure 3-9b**). Finally, a single diffraction peak at $q = 1.0 \text{ nm}^{-1}$ is observed that is attributed to the lamellar phase. This shift in the peak positions reflects a reduction in the

size of the cubic lattice and an increase in the fraction of vesicles over time due to the exchange of lipids between the cubosomes and liposomes.

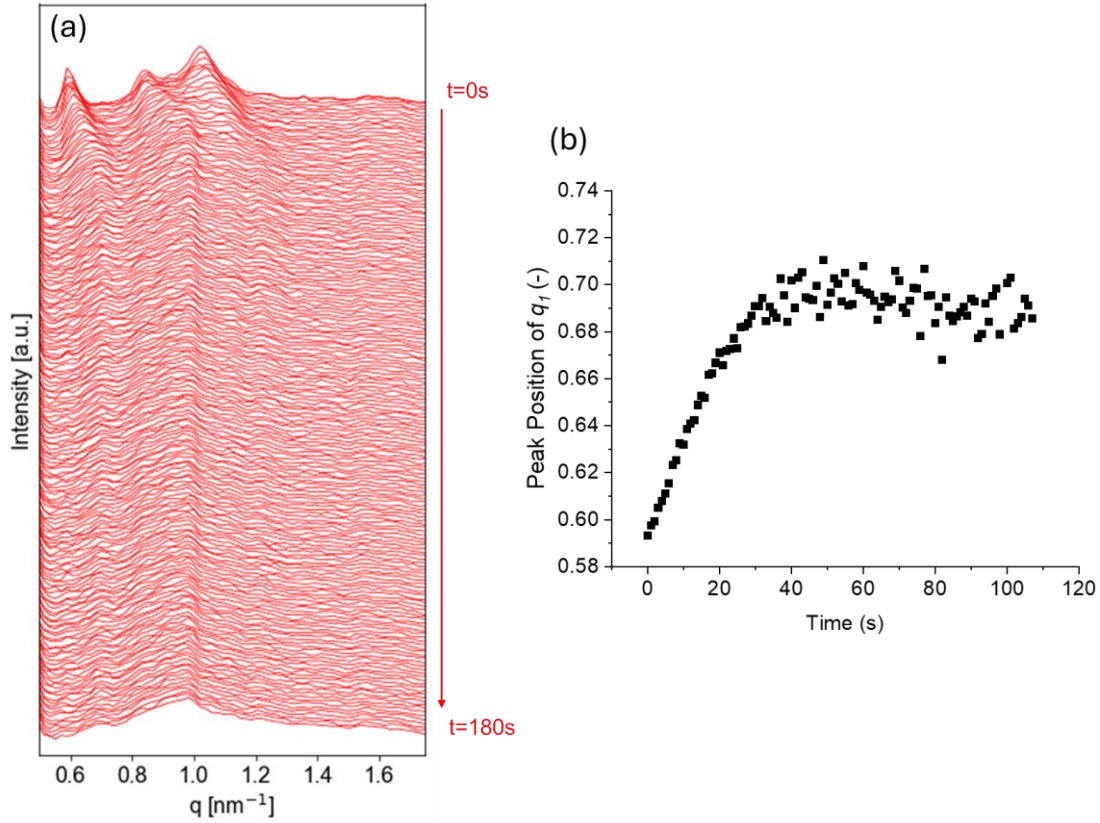


Figure 3-9 (a) TR-SAXS profiles MO cubosomes after mixing with DOPC liposomes each spectrum was taken at 1s interval across 180s. (b) Changes to the peak of position of the first diffraction peak (q_{110}) of the MO cubosomes after mixing with DOPC liposomes. The final concentration of cubosomes and liposomes are 25mM and 12.5mM.

In previous work, it was shown that the MO cubosomes are close to structural change that can be induced by even small amounts of DOPC concentration, implying that the cubosomes are close to structural transition (Vandoolaeghe et al. 2009). The particle size, zeta potential, OD_{400} were also examined 5 minutes after mixing (to ensure that the interaction between the cubosomes and liposomes has equilibrated). The results fit well with the trends from the previous sections (**Figure 3-10**).

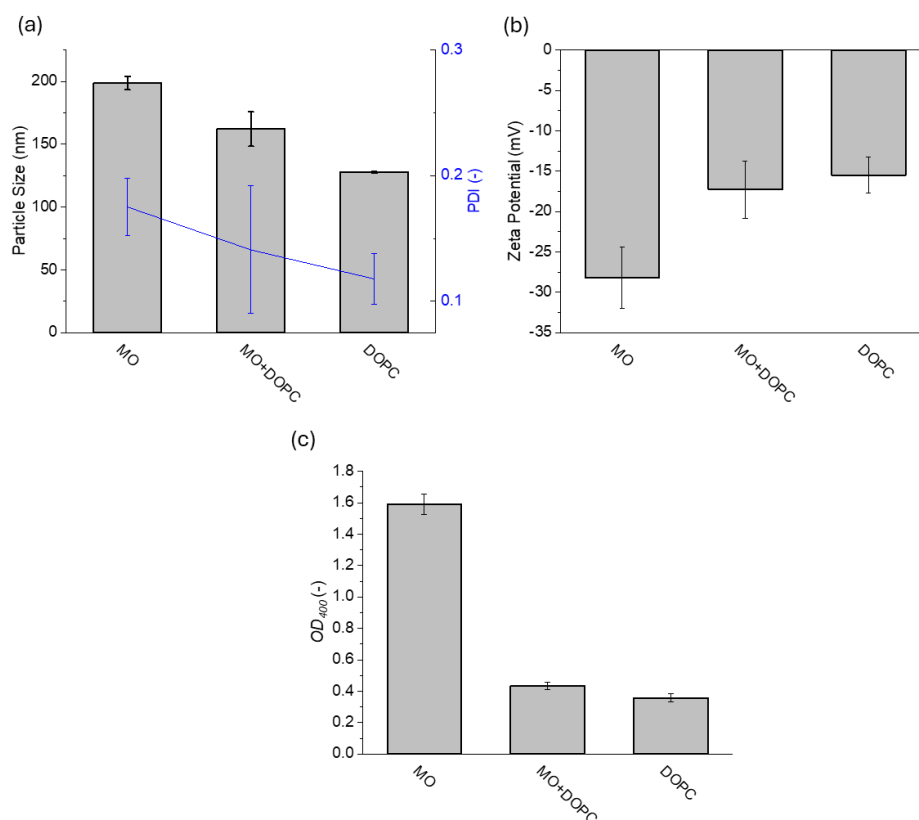


Figure 3-10 Examination of the properties of MO cubosomes 5 min after mixing with DOPC (a) Particle size and PDI (b) Zeta potential (c) Optical density

The changes to the membrane hydration state of the cubic membrane were conducted by probing the cubosomes with Laurdan prior to mixing and examining the evolution of the spectra over time shown in the colormap in **Figure 3-11a**. As expected, the intensity of the dominant peak in the longer wavelength region decreases, and the contribution from the component in the short wavelength region. The calculated GP_{340} values from the Laurdan spectra, shown in **Figure 3-11**, detail the time course of the membrane hydration of the cubosomes after mixing. Up to 300 s, a sharp increase in the GP_{340} values is observed followed by a slight steady decline. The behavior of the two regions could be explained as apparent lipid exchange region ($t = 0-300$ s) and lipid reorganization region ($t > 300$). From the results of the previous section (effect of increasing DOPC content in MO cubosomes on the GP_{340} values), and the time scale in which the cubic phase transitioned to the lamellar phase in the time-resolved SAXS results, it can be concluded that region in which the GP_{340} values increase corresponds to lipid exchange between the cubosomes and liposomes. For the purposes of this study, the following section will focus on the lipid exchange region.

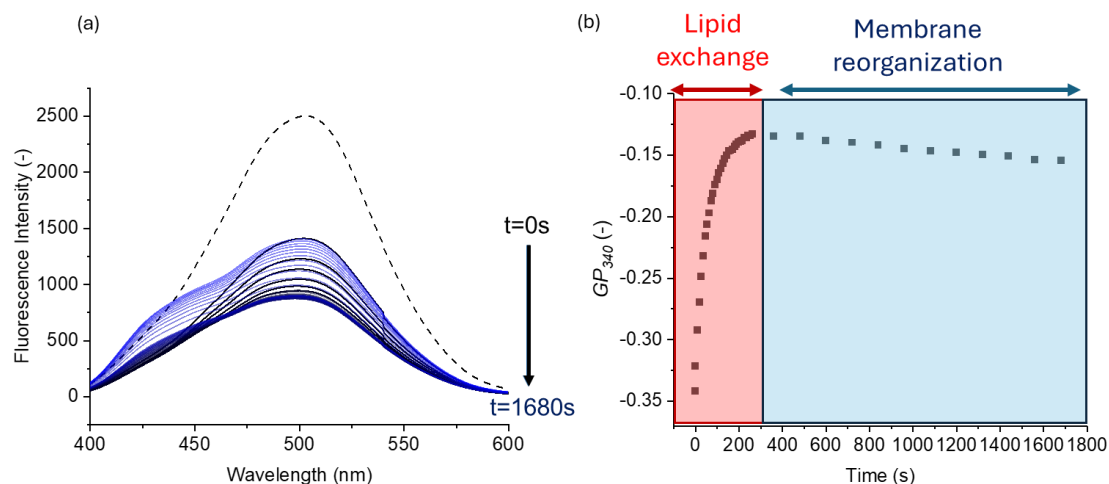


Figure 3-11 (a) Laurdan spectra of probed MO cubosomes before mixing (dashed line) and after mixing with DOPC liposomes represented in a colormap transitioning from black ($t=0$) to blue ($t=1680$) (b) changes of GP_{340} values of probed cubosomes over the course of 1680s after mixing with DOPC liposomes. The final concentration of cubosomes and liposomes are 0.25 mM and 0.125 mM.

3.4 Estimation of the Apparent Lipid Exchange between MO Cubosomes and DOPC Liposomes Using GP_{340} Values

The effectiveness of the application of the GP_{340} values of Laurdan in detailing the changes in the hydration states of the cubosomal membrane was elucidated in the previous section. Herein, an approach for the utilization of the GP_{340} for the estimation of the DOPC content in the Laurdan probed cubosomes after mixing with the DOPC liposomes is presented. Based on the GP_{340} values of the MO/DOPC compositions obtained in the first section, a calibration curve based on the percentage of DOPC in each composition (0-40 mol%) was constructed. The values were analyzed using polynomial regression, which resulted in curve represented by the quadratic equation shown in **Figure 3-12a**. The strong correlation of this model ($R^2=0.997$) made it possible to employ it to estimate DOPC content in the MO cubosomes after mixing with the liposomes. Using this model, the GP_{340} values of the lipid exchange region from **Figure 3-11b** GP_{340} were converted to DOPC mol% values, and a concentration vs time curve was obtained (**Figure 3-12b**). When fitting the curve using exponential regression, the fitted curve showed strong agreement with the results ($R^2=0.997$). From the resultant model, the amount of DOPC at different time points could be estimated and obtained the apparent rate constant can be considered as that of lipid exchange ($k_{app} \sim 0.022s^{-1}$). In a previous study, the rate constant of lipid exchange between methyl- β -cyclodextrin (M β CD) containing

vesicles and proteoliposomes was calculated to be around 0.04 s^{-1} (Vitrac et al. 2015). This suggests that the estimated k_{app} in this study is in line with previous findings. Such method can be an effective way to estimate the kinetics of the lipid exchange of the different types of cubosomes and liposomes.

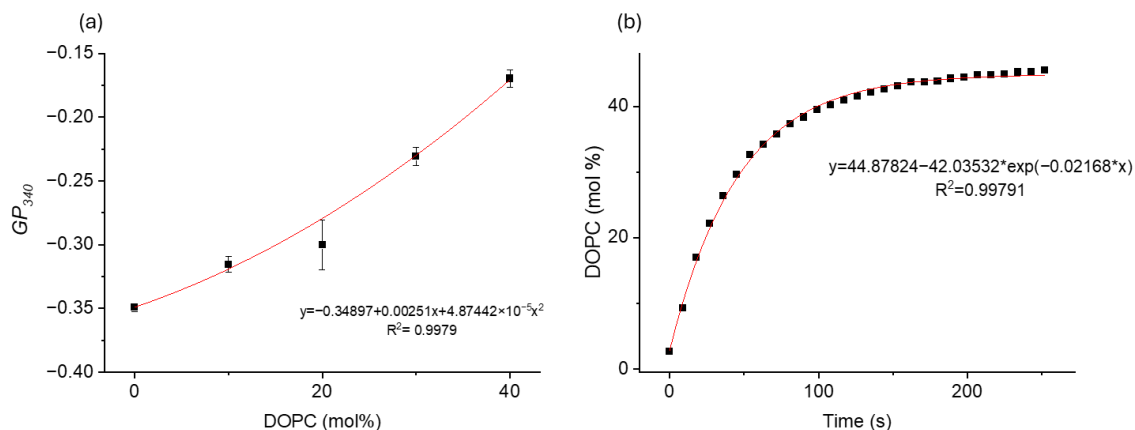


Figure 3-12 (a) Calibration curve of GP_{340} values of MO cubosomes based DOPC content (b) DOPC percentage as a function of time after mixing Laurdan probed cubosomes and DOPC liposomes.

Even though the approach above can be used to estimate the apparent DOPC content in the cubosomes, it was observed that this method tends to overestimate the amount of the lipid. The final molar ratio of MO and DOPC, after the mixing is complete, should be around (6.66/3.33). Following that assumption, the content of DOPC in the resultant vesicles should be no more than $\approx 33.3\%$. However, in the results of **Figure 3-12b**, the final DOPC content was estimated to be $\approx 45\%$. This over approximation could be due to different factors such the non-uniformity of mixing as well as possible compositional heterogeneity in the membrane of the lamellar vesicles where Laurdan allocates.

To examine the allocation of Laurdan in the resultant vesicles after mixing, the properties of either cubosomes or liposomes probed with Laurdan 5 minutes after mixing were assessed. Also, the membrane state of Laurdan in combination with DPPC liposomes in addition to DOPC liposomes were investigated. DPPC liposomes typically show higher GP_{340} values due to their highly ordered membranes that exhibit the gel phase (S_o) compared to DOPC membranes that exhibit the liquid disordered phase (L_d) at 25°C (Watanabe, Suga, et al. 2019; Davis et al. 2009). The GP_{340} of DOPC is closer in value to MO, therefore the comparison with DPPC would accentuate subtle differences

in compositional heterogeneity around Laurdan. **Figure 3-13a** shows the summary of the GP_{340} values of the cubosomes after mixing with the two types of liposomes. The final membrane state of (probed MO and DOPC) is very similar to (MO and probed DOPC). Interestingly, the values were very close to that of pure DOPC liposomes, possibly indicating the preference of Laurdan to DOPC more than MO. This is further demonstrated in the difference in the values of (probed MO and DPPC) and (MO and probed DPPC) where higher membrane hydration is observed in the former and lower membrane hydration in the latter. Also, the DAS spectra of the same combination were investigated (**Figure 3-14**). The distributions of the deconvolution of the fluorescence components shown in the τ vs λ plot of Laurdan in the different combinations are shown in **Figure 3-13b-g**. The results paint the same picture of the steady-state Laurdan, where the environment of Laurdan differed depending on whether MO or DPPC was probed. This does not seem to be the case for DPH where the results of both the steady-state and time-resolved measurements did not seem to show any preference for MO or the zwitterionic lipids. The approach presented to estimate the apparent rate constant (k_{app}) is a useful technique to study the kinetics of lipid exchange between cubosomes and cell membrane model (liposome). However, it is imperative to point out the potential over approximation due to possible Laurdan preference to zwitterionic lipids.

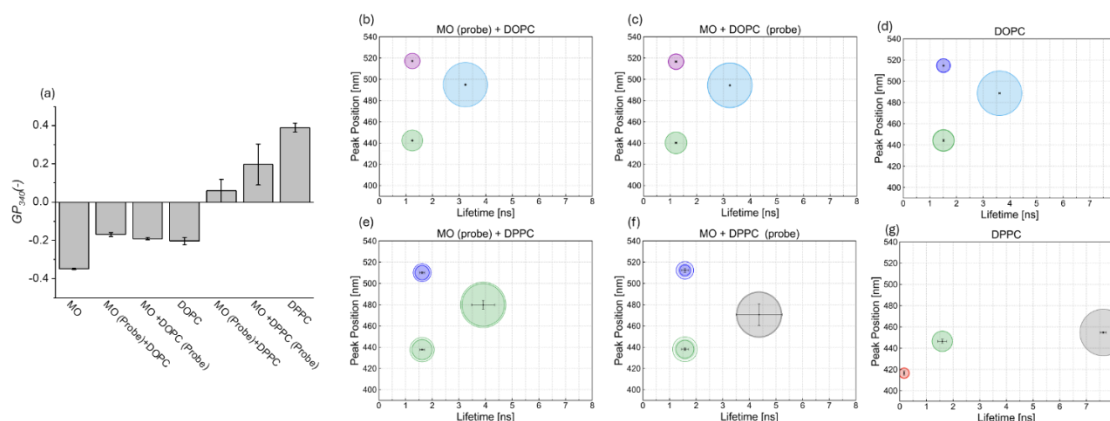


Figure 3-13 (a) GP_{340} values of mixing MO with DOPC and DPPC liposomes; distribution of deconvolution components in the τ vs λ plot of Laurdan in (b) MO (probe) and DOPC liposomes (c) MO and DOPC liposomes (probe) (d) DOPC liposomes (e) MO (probe) and DPPC liposomes (f) MO and DPPC liposomes (probe) (g) DPPC liposomes. The final concentration of cubosomes and liposomes are 0.25 mM and 0.125 mM.

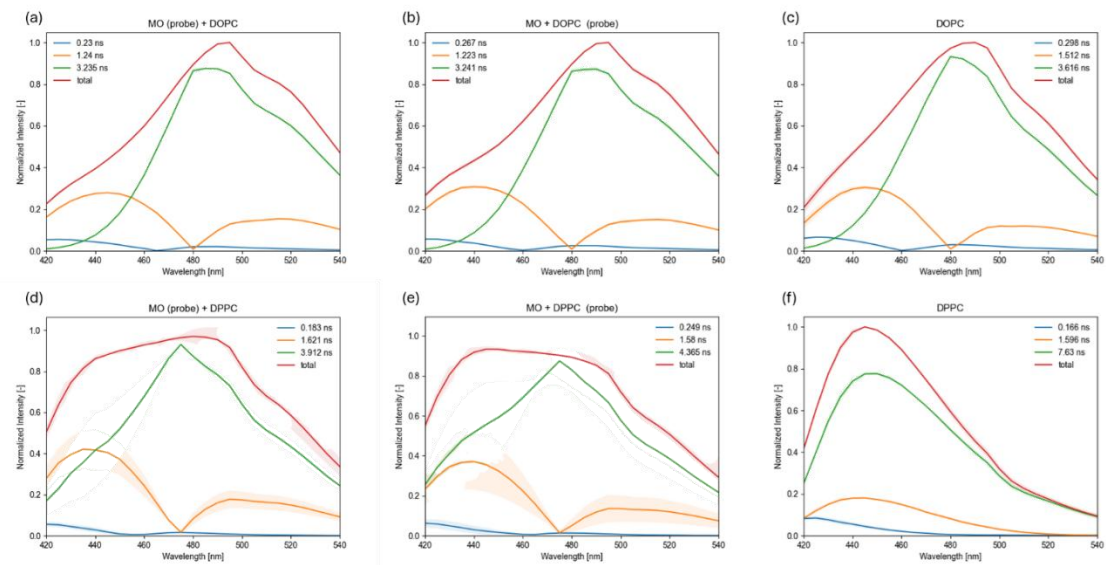


Figure 3-14 DAS of Laurdan in (a) MO (probe) and DOPC liposomes (b) MO and DOPC liposomes (probe) (c) DOPC liposomes (d) MO (probe) and DPPC liposomes (e) MO and DPPC liposomes (probe) (f) DPPC liposomes. The final concentration of cubosomes and liposomes are 0.25 mM and 0.125 mM.

4. Summary

The multitude of applications of membrane bound fluorescence probes in the study of the dispersed liquid lyotropic crystalline nanoparticles were demonstrated in this chapter. In the first part, the changes in the structural and membrane properties of MO cubosomes with increasing DOPC concentrations were indicated. Due to the molecular geometry of DOPC, the negative mean curvature of the cubic membrane decreases manifesting in decrease in the particle size, zeta potential, and OD_{400} indicating phase change from the cubic to the lamellar phase. The changes in the membrane environment which were examined by different fluorescence probes, primarily Laurdan, confirmed the structural alterations. Typically, the cubic membrane is well-hydrated and highly fluidic, however, as DOPC content increases, the membrane environment shifts to a less hydrated and viscous membrane state. The application of DAS to highlight the subtle changes in specific regions of the membrane were elucidated and visualized using τ vs λ plots. In the latter part of this work, the changes in the cubosome structure and membrane properties when mixing with DOPC liposomes as cell membrane model through time-resolved SAXS and GP_{340} value changes. The transition in the SAXS profiles were consistent with the results in the preceding part, where the transition from the $Im3m$ cubic phase to the lamellar phase was confirmed. When examining the GP_{340} values of Laurdan probed cubosomes after mixing with DOPC liposome, two distinct regions were observed: a lipid exchange region ($t < 300$ s) and a membrane reorganization region ($t = 300$ s). Utilizing the GP_{340} values of the MO/DOPC compositions in the former part of the study made it possible to construct a calibration curve with a strong based on the DOPC content, which in turn was converted to a DOPC mol% vs time curve. Exponential regression was applied to fit the curve, and it exhibited a good fit that allowed for the estimation of DOPC content any given time point as well as the apparent rate constant k_{app} which can be used to study the kinetics of the lipid exchange.

Chapter 4: Investigation of Cubosome Interactions with Liposomal Membranes Based on Time-Resolved Small-Angle X-ray Scattering (TR-SAXS) and Membrane Hydration State Analysis

1. Introduction

Although the examination of the structural properties of cubosomes when fusing with the cell membranes/cell membrane models is vital to clarify their behavior, the elucidation of the changes occurring to the cubic and cell membranes is equally important. This can be realized through the examination of membrane fluidity and polarity. Alterations to the cubic membranes of cubosomes can induce structural changes in them (Rui, Watanabe, et al. 2024; Rui, Okamoto, et al. 2024). Such changes can manifest in changes to their drug release and selectivity (Bompard et al. 2020). Membrane polarity and hydration play a major role even in many regulatory cell processes (Quinn 1981). Therefore, it is important to investigate the changes occurring in membrane of self-assemblies as well as the target cell membranes during fusion process. Additionally, the changes induced by the carrier on the cell membranes are vital factors to consider in the design process of drug delivery carriers, thus the state of the host membrane must be also examined.

In this chapter, the interactions of monoolein based cubosomes with cell membrane model (liposomes) were investigated through the utilization of stopped-flow setup in conjunction with TR-SAXS to capture the structural transition in cubosome structure at high-time resolution. The structural investigation was complemented with analysis of the cubic using membrane bound fluorescence probes. Since lipid compositions vary across different regions in cells, the interaction changes of cubosomes when interacting with different membrane compositions in terms of membrane phase state, charge, etc. were examined. Also, the alterations to the host membrane (liposomal membrane), induced by the fusion with the cubosomal carriers, were also investigated. The aim of this study is to provide further understanding of the changes in the structure and membrane and highlight the influence of membrane hydration state on the cubosome structure as well as the host membrane changes after the fusion process.

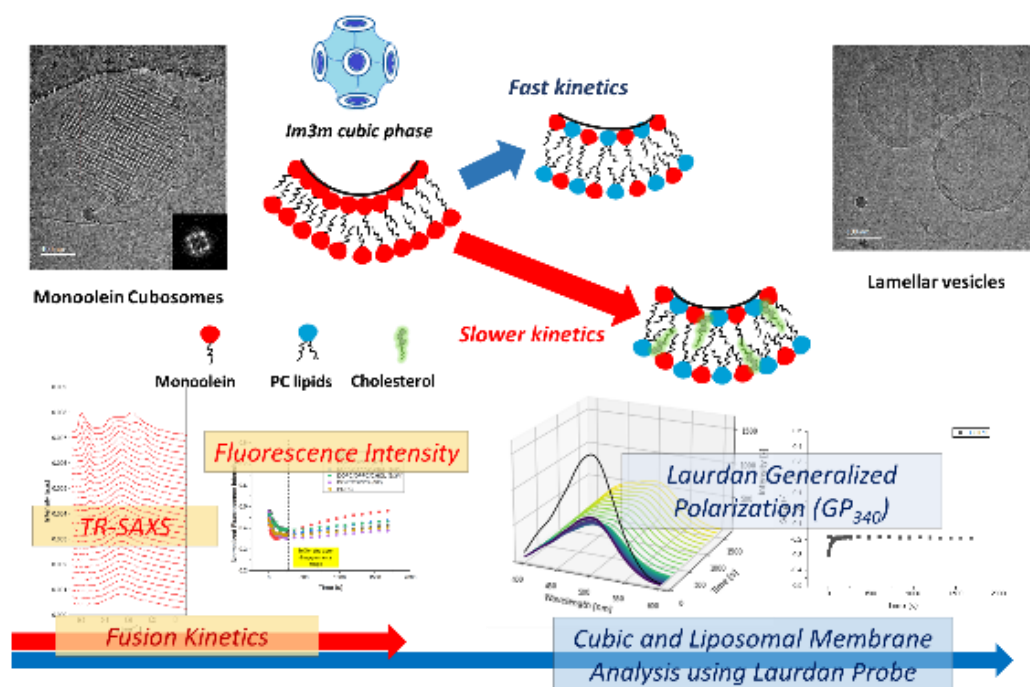


Figure 4-1 Schematic illustration of this work.

2. Materials and Methods

2.1 Materials

MO (glycerol α -monooleate) (purity > 99 %), Pluronic F127 (F127), Pluronic F108 (F108), and cholesterol (CHOL) were purchased from Sigma-Aldrich (St. Louis, MO). 2-Dioleoyl-*sn*-glycero-3-phosphocholine (DOPC), 1,2-dipalmitoyl-*sn*-glycero-3-phosphocholine (DPPC), 1,2-Dipalmitoyl-*sn*-glycero-3-phospho-L-serine, sodium salt (DPPS), and 1-Palmitoyl-2-oleoyl-*sn*-glycero-3-phosphocholine (POPC) were purchased from (Nippon Oil & Fats Corporation, Tokyo, Japan).

2.2 Preparation of Monoolein Cubosomes

The cubosomes were prepared by dissolving monoolein powder in chloroform, followed by removing the chloroform under vacuum conditions for 48 hours to create a lipid film. Lipid films were hydrated with preheated solutions of different concentrations of F127 or F108 to reach a total lipid concentration of 50 mM. The lipid to F127 weight ratio was 100:0.5 unless stated otherwise. The samples, then, were homogenized in an ice bath using a probe sonicator (TOMY Ultrasonic Disruptor UD-200) for 3 minutes at 100W. Finally, the samples were heated for 3 minutes at 70°C. The cubosomes were stored in the dark at room temperature.

2.3 Preparation of the Liposomes

The liposomes were prepared by dissolving lipids at different molar ratios in chloroform or chloroform/methanol 1 to 1 mixture for DPPS containing samples. After evaporating the solvent, a thin lipid film was obtained and kept under vacuum for at least 24 hours. The film was hydrated with ultrapure water and the suspension was agitated in a water bath for 15 minutes at 60°C. Finally, the liposome suspension was extruded 11 times through a polycarbonate 100 nm membrane filter (Liposofast; Avestin Inc., Ottawa, ON, Canada). The liposomes were stored at 4°C. The total concentration of the lipids of the liposomes was 25 mM.

2.4 TR-SAXS Measurements

SAXS measurements were conducted at the high flux beamline, BL40XU at SPring-8 synchrotron facility, Japan. The X-ray wavelength and sample to-detector distance were 0.0827 nm and 1.0 m, respectively, corresponding to an accessible q -range of 0.24 to 3.2 nm⁻¹. The detector used is an X-ray Image Intensifier (V7339P, Hamamatsu photonics,

Japan) with a high-speed CMOS camera (FASTCAM Nova S16, Photron, Japan), max 10 kHz, active area 100 mm in diameter. 75 μ l of each the cubosome and liposome solutions were mixed at a flow rate of 8 ml/s using multi-reserve syringe stopped-flow apparatus (SFM-4000/S stopped flow mixing system, BioLogic, France). The setup was attached to the X-ray environment with a scattering cell consisting of a quartz capillary (1.5 mm diameter, wall thickness 10 μ m). The flow time and deadtime of the rapid mixing of the cubosome and liposome solutions was 50 and 2.3 ms, respectively. The size of the X-ray beam at the sample position was around 50 μ m (vertical) by 150 μ m (horizontal) (full width at half maximum) with photon flux of 10^{14} photons/sec. An in-house developed X-ray shutter (Galvanometric type) limits the X-ray exposure to approximately 1 ms, and scattering measurements were taken 30 times, with 1 ms measurements every 10 seconds after mixing. The background signals were subtracted and the SAXS diffractograms were normalized. Three measurements were conducted for each sample. The lattice parameter of the *Im3m* cubic phase (a) was calculated from the scattering vector (q) and the inter-planar spacing (d) of each unit cell according to the following equation: $a = d\sqrt{h^2 + k^2 + l^2}$, where $d = 2\pi/q$, and the values h , k , and l are the Miller indices of the Bragg peaks (Kulkarni et al. 2011). All measurements were performed at a temperature of 25 °C unless otherwise mentioned.

2.5 Cryo-TEM Imaging

2.4 μ l of either the cubosomes or cubosomes and liposomes (volume ratio 1:1) at $t \approx 90$ s and $t \approx 300$ s after mixing were deposited immediately on to glow-discharged Quantifoil R2/2 in semi-automated vitrification device (Vitrobot Mark IV, Thermo Fisher Scientific) at 100% humidity. The samples were blotted for 4 s from both sides and submerged in liquid ethane immediately. The cryo-TEM images were captured under cryogenic conditions at a magnification of 59,000 \times using a Titan Krios (Thermo Fisher Scientific, MA) and operating at 300 kV and a Falcon2 CMOS camera. The temperature of the samples before the cryo-TEM measurements was 25°C.

2.6 Laurdan Spectra Measurements

The fluorescence measurements were conducted using FP-8500 spectrofluorometer (JASCO, Tokyo, Japan). The cubosome and liposome solutions were diluted with ultrapure water 100-fold to reach a volume of 1.5 ml, then 15 μ L of Laurdan

solution (1 mM, in ethanol) was added to either of them (total volume of each sample is 1.5 ml). After mixing the samples well, the probed sample was incubated for 30 minutes in the dark. Data collection was immediately started after mixing the cubosomes and liposomes. The Laurdan spectra were obtained by exciting the samples at 340 nm and measuring the intensities in the wavelength range of 400 nm to 600 nm over the time span of 1680s. The generalized polarization (GP_{340}) was calculated according to the following equation:

$$GP_{340} = \frac{I_{440} - I_{490}}{I_{440} + I_{490}} \quad \text{Eq. 4-1}$$

where I_{440} and I_{490} are the fluorescence intensities at 440 and 490 nm, respectively.

3.Results and Discussion

The interactions of MO cubosomes were examined with the following compositions of liposomes: DOPC, DOPC/DPPC (1/1), DOPC/DPPC/CHOL (4/4/2), DOPC/DPPC/CHOL (3/3/4), DOPC/DPPS (8/2), and POPC. Phosphatidylcholines (PCs) such as DOPC, DPPC, and POPC make up around 40-60% of total lipids of the cell membranes. CHOL, another major constituent of cell membranes, impacts the partition of molecules into the membrane (McMullen et al. 2004). DPPS is a charged lipid which is found in the inner leaflet of the cell membrane. DOPC, which contains two unsaturated acyl chains, and POPC, which contains one saturated and one unsaturated acyl chain, exhibit liquid disordered (L_d) phase while DPPC membranes exhibit gel (S_o) phase at the same temperature. Both DPPC and CHOL increase the packing of the membrane in respect to the (L_d) phase, therefore, DOPC/DPPC/CHOL ratio dictates the phase state of the liposome. DOPC/DPPC (1/1), DOPC/DPPC/CHOL (4/4/2), and DOPC/DPPC/CHOL (3/3/4) liposomes exhibit L_d/S_o phase coexistence, L_d/L_o phase coexistence, and L_o phase, respectively (Davis et al. 2009; Zaytseva et al. 2022). The above compositions were selected to examine the effects of factors such as membrane phase state, acyl chain, and charge in altering the cubic structure and cubic and liposomal membrane hydration states.

3.1 Examination of Structural Changes in MO Cubosomes Using TR-SAXS

The TR-SAXS profiles of MO cubosomes before mixing with liposomes showed Bragg peaks with relative positions at spacing ratios of $\sqrt{2}$: $\sqrt{4}$: $\sqrt{6}$ (**Figure 4-2**). These peaks correspond to the [110], [200], and [211] reflections of the $Im3m$ cubic phase (Kulkarni et al. 2011). The intensities and peak positions remained unchanged over the course of 300 s, indicating that effects of X-ray damage are minimal on the cubosome internal structure.

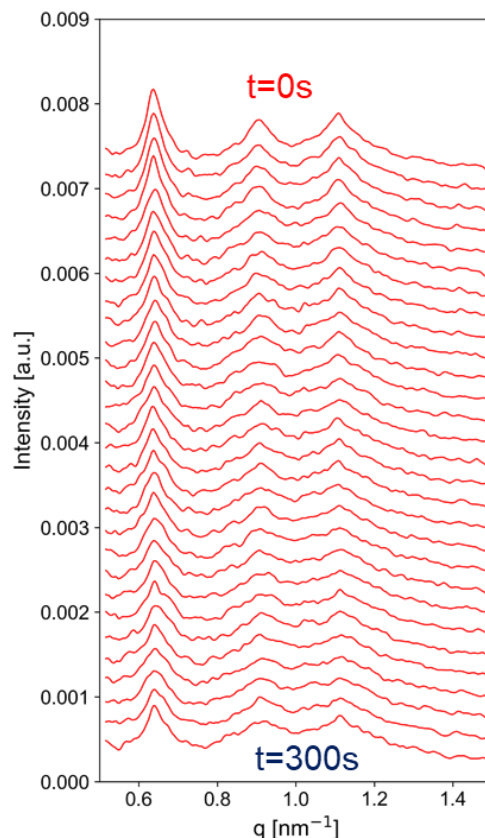


Figure 4-2 (a) TR-SAXS profiles of MO cubosomes after being diluted with equal volume of water.

Figure 4-3 depicts the changes to the diffractograms of the cubosomes after being mixed with liposomes of different compositions (red spectra). The SAXS profile of MO cubosomes (top) and liposomes (bottom) before mixing denoted in black. The profiles of MO showed peaks associated with the cubic $Im\bar{3}m$ phase overlapping with the lamellar peaks. In the case of the SAXS profiles of the liposomes, a diffraction peak corresponding to the lamellar peak around $q \approx 0.94\text{--}1.0\text{ nm}^{-1}$ was observed except for DOPC/DPPS (8/2) liposomes **Figure 4-3e**. The peak arises from the presence of small amounts of multi-lamellar vesicles along with the liposomes (Vandoolaeghe et al. 2009). For DPPS containing liposomes, the peak was not as pronounced as the addition of the charged lipids can reduce the Bragg reflections by enhancing unilamellarity (Scott et al. 2019). Note that the SAXS profile mixing with DPPC was unable to obtain due to the rapid sedimentation of DPPC liposomes. As time progresses, the cubic peaks lose intensity and shift to higher q values leaving behind the lamellar peak. DOPC has a relatively large headgroup with a critical packing parameter (CPP) < 1 , which promotes the transition towards less negatively curved phases. This results in the shift from cubic membranes with high

negative curvature into planar lamellar membranes (Van'T Hag et al. 2017). These results were in line with previous TR-SAXS study, where after mixing monoolein cubosomes and DOPC unilamellar vesicles, the cubic $Im3m$ peaks increased in q values over time until the lamellar phase was observed (Vandoolaeghe et al. 2009). It is worth noting that depending on the composition of the liposomes, the time for transition from the cubic phase to the lamellar phase was different. For example, the profiles of the cubosomes mixed with L_d phase membranes like DOPC, DOPC/DPPS (8/2), and POPC liposomes did not retain the cubic peaks (160~200 s) as long as DOPC/DPPC (1/1) (L_d/S_o), DOPC/DPPC/CHOL (4/4/2) (L_d/L_o), DOPC/DPPC/CHOL (3/3/4) liposomes (L_o) (250~300 s) as shown in the normalized SAXS intensities of the cubic peak in **Figure 4-4**. DOPC-rich liposomes and POPC liposomes exhibit high membrane fluidity, causing faster lipid exchange with the cubosome, altering its structure. Also, the introduction of DPPS in DOPC/DPPS (8/2) liposomes did not seem to significantly alter the disappearance time of the cubic phase. This could indicate that the cubosomes interact in similar kinetics with zwitterionic and anionic membranes.

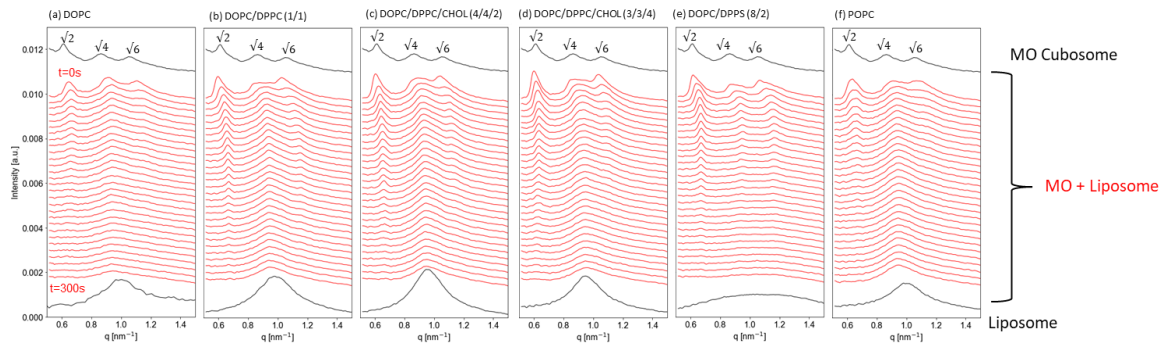


Figure 4-3 SAXS profiles of MO (top) and liposomes (bottom) before mixing denoted in black color.

TR-SAXS profiles of MO at 25°C after mixing with (a) DOPC (L_d) (b) DOPC/DPPC (1/1) (L_d/S_o) (c) DOPC/DPPC/CHOL (4/4/2) (L_d/L_o) (d) DOPC/DPPC/CHOL (3/3/4) (L_o) (e) DOPC/DPPS (8/2) (L_d) (f) POPC (L_d) liposomes denoted in red color. Each spectrum was taken at 10s interval and the final total lipid concentration of cubosomes, and liposomes are 25mM and 12.5mM. The cubosome to liposome volume ratio is (1/1).

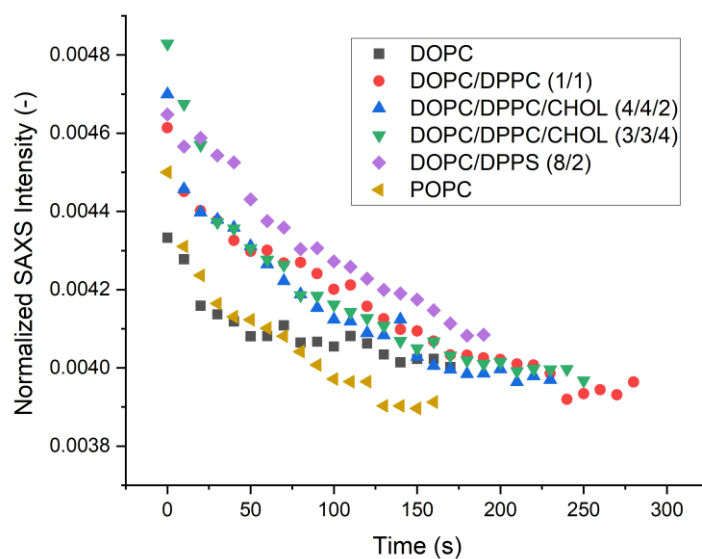


Figure 4-4 Normalized SAXS intensity of diffraction peak of the scattering vector ($q_{110} = \sqrt{2}$) of MO after mixing with DOPC (L_d) (black squares), DOPC/DPPC (1/1) (L_d/S_o) (red circles), DOPC/DPPC/CHOL (4/4/2) (L_d/L_o) (blue triangles), DOPC/DPPC/CHOL (3/3/4) (L_o) (green triangles), DOPC/DPPS (8/2) (L_d), (purple diamonds), and POPC (L_d) (yellow triangles) liposomes. The final total lipid concentration of cubosomes and liposomes are 25mM and 12.5mM. The volume ratio of cubosome and liposome solutions is (1/1).

Similar trends were observed when cubosomes were prepared with higher MO to non-ionic surfactant weight ratios (10:1), where the lipid composition of the liposomes dictated the transition time from the cubosome phase to the lamellar phase (**Figure 4-5**). The increased surfactant concentrations resulted in lower q values, possibly to F127 interacting with the cubic membrane (Nakano et al. 2001), however, the concentration of F127 did not seem to significantly affect the structural transition to the lamellar phase.

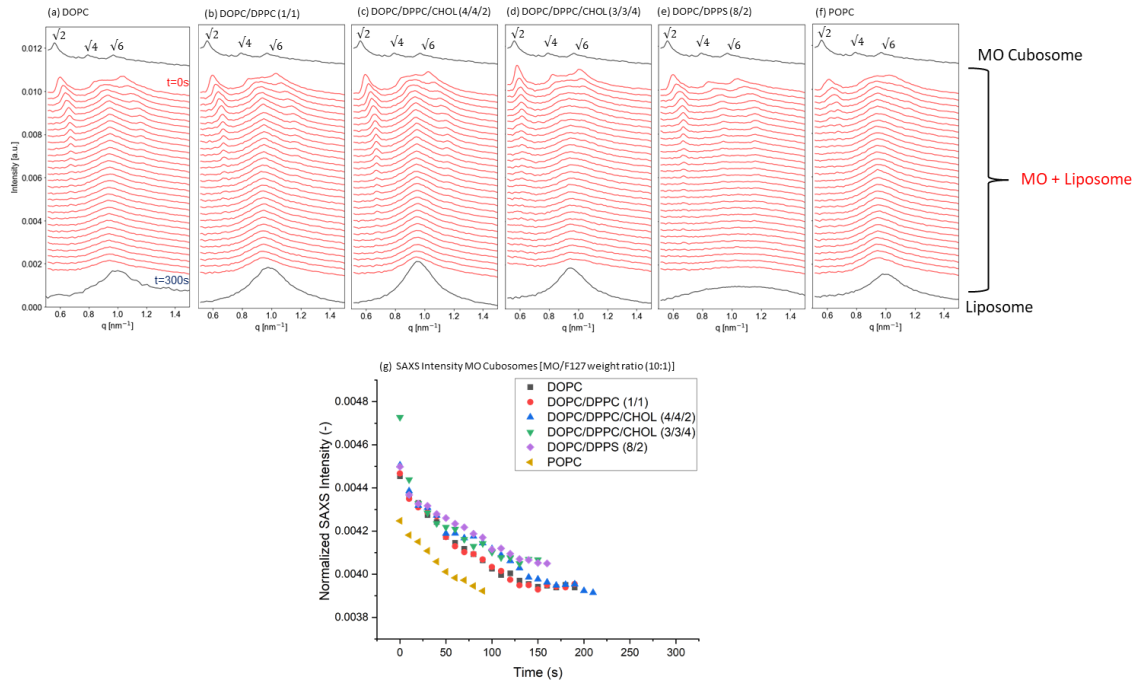
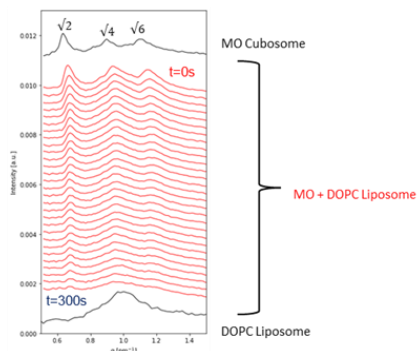


Figure 4-5 SAXS profiles of MO cubosomes [Lipid to F127 weight ratio (10:1)] (top) and liposomes (bottom) before mixing denoted in black color. TR-SAXS profiles of MO cubosomes after mixing with (a) DOPC (L_d) (b) DOPC/DPPC (1/1) (L_d/S_o) (c) DOPC/DPPC/CHOL (4/4/2) (L_d/L_o) (d) DOPC/DPPC/CHOL (3/3/4) (L_o) (e) DOPC/DPPS (8/2) (L_d) (f) POPC (L_d) liposomes denoted in red color. (g) Normalized SAXS intensity of diffraction peak of the scattering vector ($q_{110}=\sqrt{2}$) of MO after mixing with different liposome compositions. The final total lipid concentration of cubosomes and liposomes are 25mM and 12.5mM. The volume ratio of cubosome and liposome solutions is (1/1).

On the other hand, by changing the type of surfactant used from Pluronic F127 to F108, the transition time to the lamellar phase was much longer. Cubosomes prepared with F108 were shown to retain the cubic phase almost double the time that of the ones prepared with F127 (**Figure 4-6**). This is because F108 is better at stabilizing the cubosomes and retaining the $Im3m$ phase (Chong et al. 2011). This indicates that the structural changes could be also affected by the type of surfactant.

(a) TR-SAXS MO cubosomes with DOPC liposome of [MO/F108 weight ratio (10:1)]



(b) SAXS Intensity of MO Cubosomes with DOPC liposomes

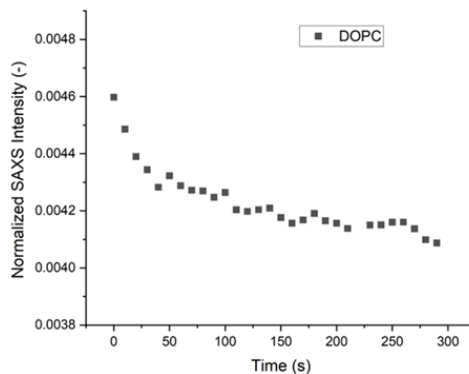


Figure 4-6 (a) TR-SAXS profiles of MO cubosomes [Lipid to F108 weight ratio (10:1)] at 25°C after mixing with DOPC (L_d) liposomes. (b) Normalized SAXS intensity of diffraction peak of the scattering vector ($q_{110} = \sqrt{2}$) of MO after mixing with DOPC (L_d) liposomes. The final total lipid concentration of cubosomes and liposomes are 25mM and 12.5mM. The volume ratio of cubosome and liposome solutions is (1/1).

3.2 Changes to the Cubic Lattice After Mixing

The changes to the cubosome lattice when mixed with the liposomes are shown in **Figure 4-2**. Before mixing, the lattice parameter of MO cubosomes was 14.4 nm, which is typical of $Im3m$ phase cubosomes (Mathews et al. 2022). In all combinations, a decrease in lattice parameters was observed due to the exchange of lipids from the cubosomes to the liposomes and vice-versa. Since the composition of lipids (DOPC, DPPC, and POPC) that reduce negative curvature is relatively high in the liposomes, such exchange of lipids with MO can cause the decrease in number of cubosomes, as well as the reduction in the volume fraction of the cubic phase of the cubosomes (Vandoolaeghe et al. 2009). The changes to the cubic lattice did not seem to be influenced greatly by the type of liposomal membrane besides DOPC/DPPC/CHOL (3/3/4), L_o phase liposomes. CHOL concentration was shown to be a crucial factor in determining the changes in the cubic lattice. The increased concentration of CHOL of DOPC/DPPC/CHOL (3/3/4) liposomes caused the decrease in lattice to be much smaller than it of other combinations. This could be attributed to the membrane stiffening properties of CHOL that could hinder the lipid exchange between the cubosomes and liposomes, causing cubosome to retain a bigger lattice over time compared to less stiff membranes including L_d phase. In all

combinations, following the decrease, a complete transition to the lamellar phase was observed.

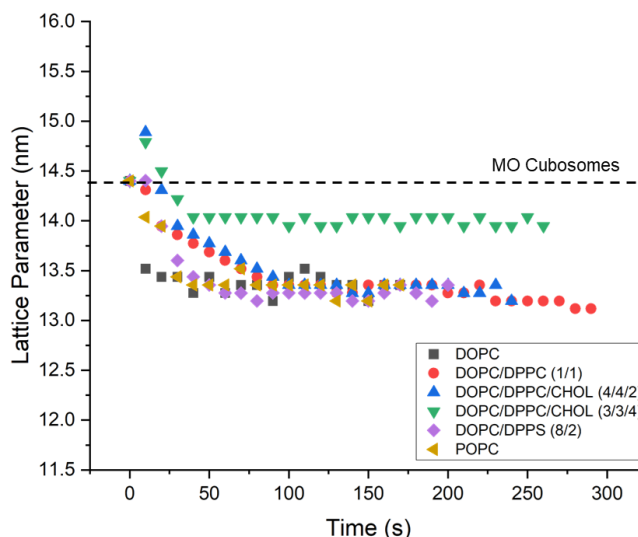


Figure 4-3 Lattice parameters of MO at 25°C after mixing with DOPC (L_d) (black squares), DOPC/DPPC (1/1) (L_d/S_o) (red circles), DOPC/DPPC/CHOL (4/4/2) (L_d/L_o) (blue triangles), DOPC/DPPC/CHOL (3/3/4) (L_o) (green triangles), DOPC/DPPS (8/2) (L_d), (purple diamonds), and POPC (L_d) (yellow triangles) liposomes. The dashed line represents the lattice parameter of MO after being diluted with equal volume of water. The final total lipid concentration of cubosomes and liposomes are 25mM and 12.5mM. The volume ratio of cubosome and liposome solutions is (1/1).

The changes of the cubic lattice of the MO cubosomes prepared with higher F127 concentration (MO:F127, 10:1) also displayed similar results (**Figure 4-4**). The transition was uniform across all combinations except DOPC/DPPC/CHOL (3/3/4), which retained a larger lattice parameters, before transitioning to the lamellar phase, confirming the effect of CHOL concentration in influencing the changes in the lattice size. Interestingly, the time scale the cubic lattice was present was shorter compared to the cubosomes prepared with a lower concentration of F127. In a previous report, it was shown that increased F127 concentrations could increase the rates of lipid exchange in and out of the cubosomes (Tilley et al. 2012), which in turn could cause the cubic lattice to be disappeared faster at higher concentration of F127.

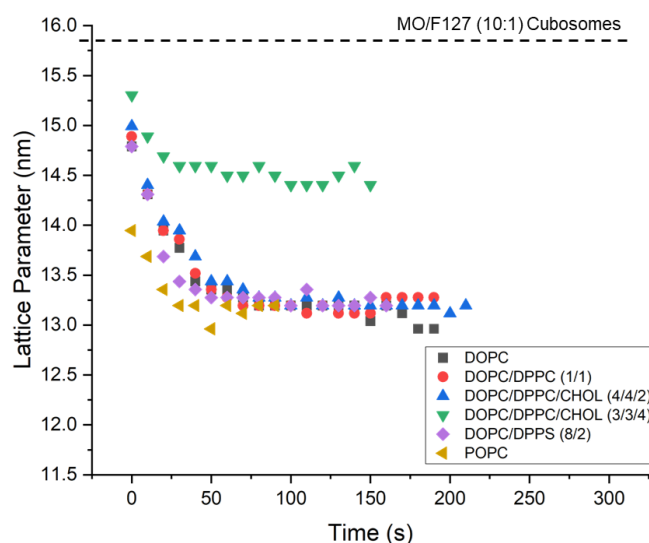


Figure 4-5 Lattice parameters of MO cubosomes [Lipid to F127 weight ratio (10:1)] at 25°C after mixing with DOPC (L_d) (black squares), DOPC/DPPC (1/1) (L_d/S_o) (red circles), DOPC/DPPC/CHOL (4/4/2) (L_d/L_o) (blue triangles), DOPC/DPPC/CHOL (3/3/4) (L_o) (green triangles), DOPC/DPPS (8/2) (L_d), (purple diamonds), and POPC (L_d) (yellow triangles) liposomes. The dashed line represents the lattice parameter of MO after mixing with water. The final total lipid concentration of cubosomes and liposomes are 25mM and 12.5mM. The volume ratio of cubosome and liposome solutions is (1/1).

3.3 Cryo-TEM Imaging

The changes to the cubosome structure were further investigated using cryo-TEM. Before mixing, the particle size of the cubosomes ranged between 150-300 nm. The cubosomes showed well-defined internal structure, characteristic of the cubic phase, and the fast Fourier transform (FFT) revealed reflections of the $Im3m$ cubic phase (Demurtas et al. 2015) (**Figure 4-9a**). Around 300 s, after being mixed with DOPC liposomes, the lattice patterns of the internal structure observed in MO cubosomes completely disappeared, and particles with lamellar structures were observed (**Figure 4-9b**).

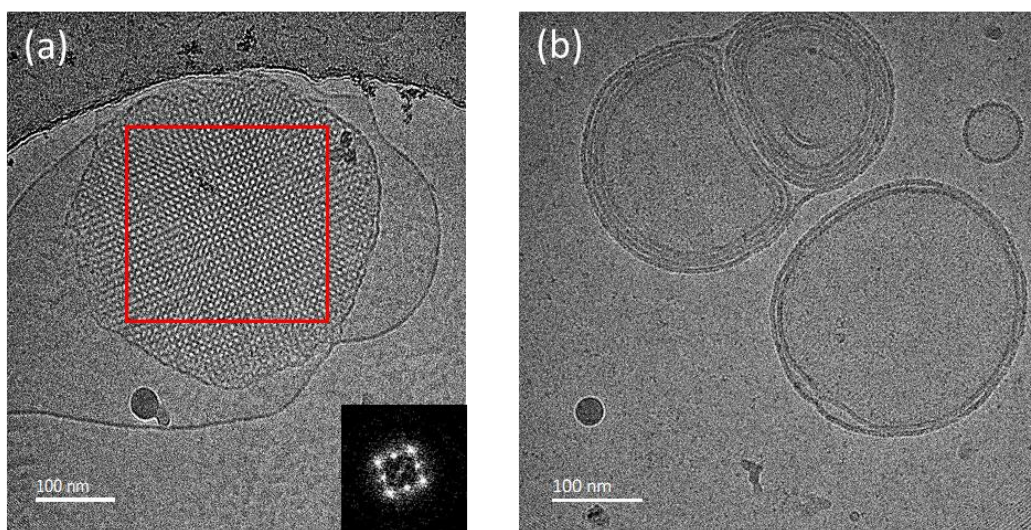


Figure 4-6 Cryo-TEM image of (a) MO with corresponding fast Fourier-transform (FFT) of the inset (red box) (b) MO after mixing with DOPC (Ld) liposomes ($t \approx 300$ s). The total lipid concentration of the cubosomes and liposomes before mixing are 50mM and 25mM, respectively. The volume ratio of cubosome and liposome solutions is (1/1).

More investigation was also conducted with cubosomes prepared with higher MO to F127 weight ratio (10:1), shown in **Figure 4-10**, at different timepoints after mixing with DOPC liposomes. Initially, only cubosomes with well-defined internal structures are observed (**Figure 4-10a**). However, at $t \approx 30$ s, coexistence of both the cubosomes and lamellar vesicles can be observed with higher fraction of lamellar vesicles being present (**Figure 4-10b**). Finally, images taken around $t \approx 300$ s show lamellar vesicles only, with complete disappearance of the cubic nanoparticles (**Figure 4-10c**). These results confirm the conclusions from the TR-SAXS transition in the cubosome structure from $Im3m$ phase to lamellar phase, when interacting with the liposomes. In addition, the decrease of the intensity and the shift to higher q values in the SAXS diffractograms can be visually confirmed with the cubosome internal structure getting smaller and higher fractions of vesicles appearing in the cryo-TEM images. (**Figure 4-10d**) details the information presented in the preceding sections.

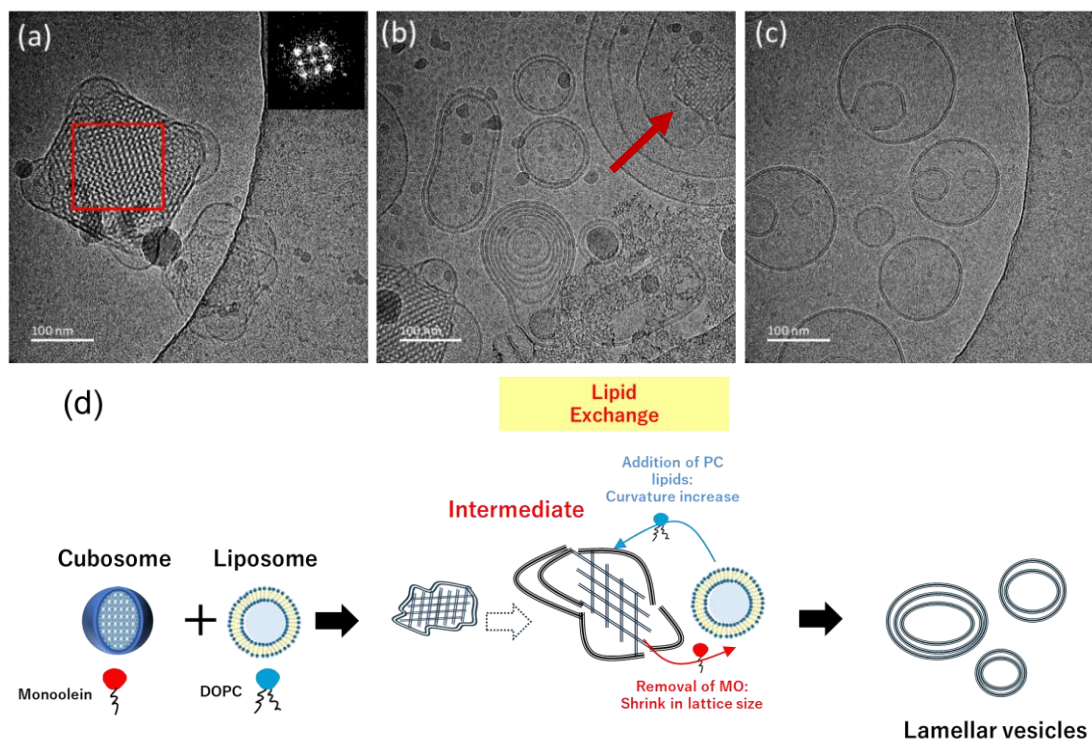


Figure 4-7. Cryo-TEM image of (a) MO cubosomes [Lipid to F127 weight ratio (10:1)] with corresponding fast Fourier-transform (FFT) of the inset (red box) (b) MO cubosomes after mixing with DOPC (Ld) liposomes ($t \approx 30s$) (c) MO cubosomes after mixing with DOPC (Ld) liposomes ($t \approx 300s$). (d) Illustration of the effects of the lipid exchange process between cubosomes and liposomes on cubosome structure. The total lipid concentration of the cubosomes and liposomes before mixing are 50mM and 25mM, respectively. The volume ratio of cubosome and liposome solutions is (1/1).

3.4 Fluorescence Intensity of Laurdan Probed MO cubosomes

Laurdan probe is a useful tool for indicating the membrane polarity and its hydration state. It exhibits fluorescence in hydrophobic environments such as in the lipid membrane. Examination of the fluorescence of Laurdan probed cubosomes can provide further information on their membrane condition after interacting with the liposomes. Any changes to their intensity could indicate instability of the membranes in vicinity to Laurdan. **Figure 4-11** shows the changes to the Laurdan spectra of the probed cubosomes after being mixed with liposomes.

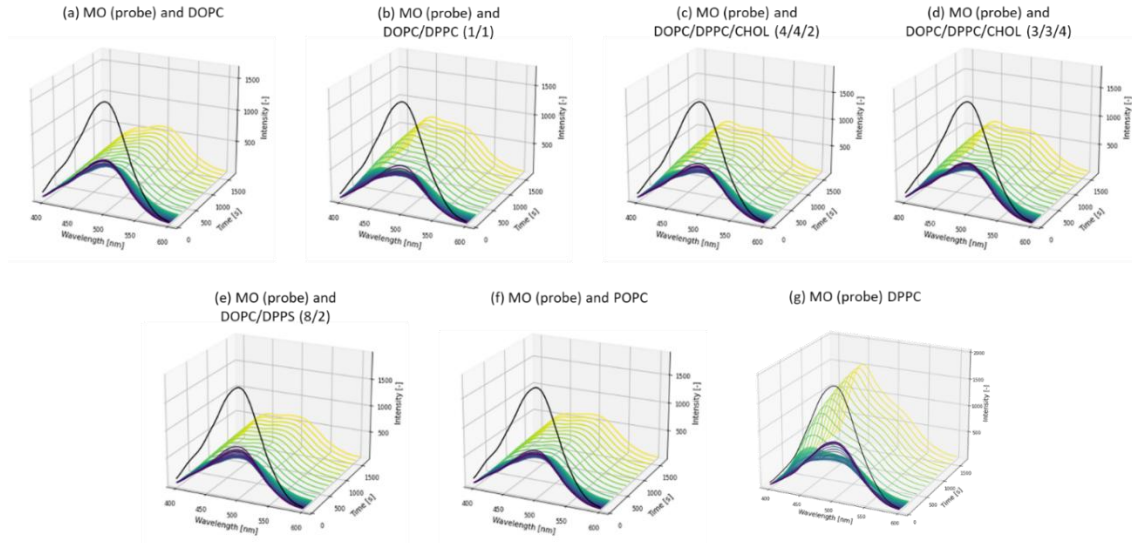


Figure 4-8 Laurdan spectra of MO cubosomes and different compositions of liposomes over time (Purple to yellow). The spectra in black are the Laurdan spectrum of the cubosome before mixing. The final total lipid concentration of cubosomes and liposomes are 0.25 mM and 0.125 mM. The volume ratio of cubosome and liposome solutions is (1/1).

In **Figure 4-12**, the sum of the emission intensities of the probed MO cubosomes from 400nm to 600nm are adjusted relative to the sum of the fluorescence intensities of the cubosomes before mixing, ensuring normalization. Across all combinations, the normalized fluorescence intensities gradually decreased over time reaching minimum values at $t \approx 100\text{-}300$ s, followed by steady intensity recovery after that. The intensity decline can be explained as the collapse of the cubic membrane during contact with liposomes. The decrease in the fluorescence intensity over time is in line with the decrease in the SAXS intensity of the scattering vector ($q_{110}=\sqrt{2}$) of MO cubosomes after mixing with the liposomes (**Figure 4-4**) in the time span of around 150-300 s (**Figure 4-12**, dotted line). The intensity recovery of Laurdan, on the other hand, indicates the reorganization (realignment) of lipids, and the formation of the vesicular membrane. It should be noted that there was no significant effect of the composition of the liposomes on the fluorescence intensity of Laurdan, which indicates that the kinetics of the reorganization of the lipids and the disappearance of the cubic phase are similar regardless of composition.

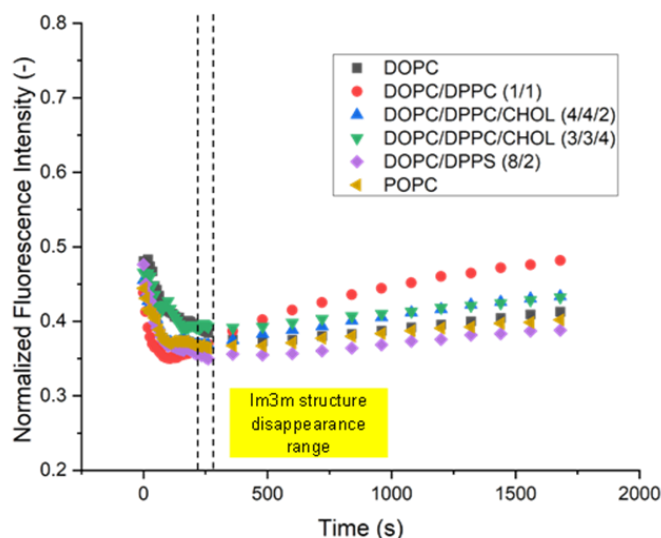


Figure 4-9 Normalized fluorescence intensity of Laurdan probed MO after mixing with DOPC (L_d) (black squares), DOPC/DPPC (1/1) (L_d/S_o) (red circles), DOPC/DPPC/CHOL (4/4/2) (L_d/L_o) (blue triangles), DOPC/DPPC/CHOL (3/3/4) (L_o) (green triangles), DOPC/DPPS (8/2) (L_d) (purple diamonds), and POPC (L_d) (yellow triangles) liposomes. The final total lipid concentration of cubosomes after mixing is 0.25 mM. The volume ratio of cubosome and liposome solutions is (1/1).

3.5 Generalized polarization GP_{340} of the cubic and liposomal membranes

To examine the individual changes to the membranes of the cubosomes and liposomes upon mixing, two independent experiments were done, one where the Laurdan was present only in the cubosomes and other only in the liposomes. Laurdan emission peaks appear at 440 nm and 490 nm, corresponding to hydrophobic and hydrophilic membrane environments, respectively (Parasassi et al. 1998). The changes to the Laurdan spectra of the probed liposomes over time are also shown in **Figure 4-13**. The membrane polarity spectra of the cubosomes before mixing revealed a hydrophilic membrane, with a dominant peak around 490 nm. The spectra of the liposomal membranes, on the other hand, showed more contribution from the hydrophobic peak at 440 nm, and their hydration state depended on their composition. After mixing the nanoparticles, the Laurdan spectra of the probed cubic/liposomal membranes showed noticeable changes over time (denoted in the colormaps from purple to yellow). For the cubosomes, the intensities of the peak at 490 nm decreased over time with an increase in the peak around 440 nm, indicating that the membrane is becoming more hydrophobic (**Figure 4-11**). On

the contrary, the liposomal membranes became more hydrophilic, as a decrease in the 440 nm peak and an increase in the 490 nm peak were observed (**Figure 4-13**). This shows that the interaction of both cubosomes and liposomes results in alteration in their membrane polarity to closer resemble the polarity of its counterpart.

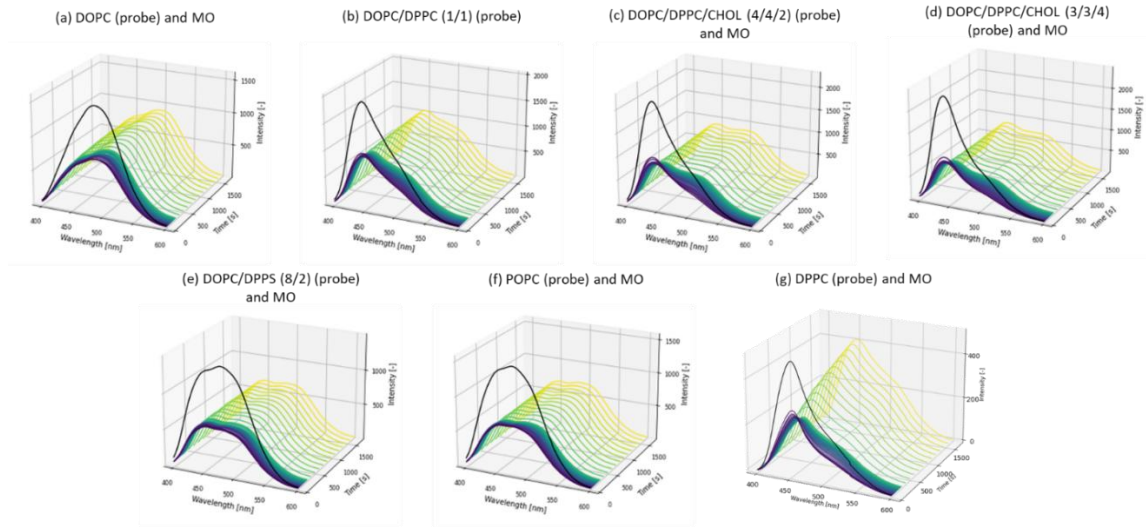


Figure 4-13 Laurdan spectra of different compositions of liposomes and MO cubosomes over time (Purple to yellow). The spectra in black are the Laurdan spectrum of the liposomes before mixing. The final total lipid concentration of cubosomes and liposomes are 0.25 mM and 0.125 mM. The volume ratio of cubosome and liposome solutions is (1/1).

The GP_{340} values are an indication of the membrane polarity and fluidity which are important factors when examining cubosome-liposome interaction. The GP_{340} values of the cubosomes and liposomes before mixing are shown in **Table 4-1**. In addition to the previous liposome compositions, the GP_{340} of MO cubosomes after being mixed with DPPC liposomes were examined. The GP_{340} value of the MO cubosomes originally were -0.31, which reflects a hydrophilic nature, caused by the highly curved cubic membranes (Fracassi et al. 2023). The probed liposomes on the other hand displayed different GP_{340} values, initially, depending on their composition (**Table 4-1**). Liposomes composed of higher compositions of DOPC (L_d phase) displayed lower GP_{340} values, due to membranes exhibiting higher fluidity and polarity. Meanwhile, DPPC and CHOL containing liposomes (L_o or S_o phase) displayed higher GP_{340} values due to increase in membrane packing (Bui et al. 2016). In **Figure 4-14**, the GP_{340} value changes for the Laurdan probed cubosomes and liposomes are shown. After mixing, the GP_{340} values of the cubosomes increased in all combinations. Previously, it was reported that the water

relaxation of Laurdan in the $Pn3m$ cubic phase is much higher than that in the lamellar phase (Mangiarotti et al. 2021b). Therefore, the increase in the GP_{340} values could be due to Laurdan experiencing less water relaxation around it due to the transition from cubic to lamellar phase, as seen in the TR-SAXS results. For the probed liposomes, two trends in the GP_{340} value changes were observed. For liposomes with fluid membranes such as DOPC, DOPC/DPPS (8/2), POPC systems (L_d phase), almost no change occurred in the GP_{340} values. Similar trend was shown in the literature where DOPC/MO self-assemblies with higher DOPC ratios would show Laurdan behavior similar to DOPC only (Mangiarotti et al. 2021b). As for DOPC/DPPC (1/1) (L_d/S_o), DOPC/DPPC/CHOL (4/4/2) (L_d/L_o), DOPC/DPPC/CHOL (3/3/4) (L_o), and DPPC liposomes (S_o), a decrease in the GP_{340} values for these systems, due to the incorporation of MO into the membranes of the liposomes, increasing their polarity. By comparing the changes in the POPC (L_d) and DOPC/DPPC (1/1) (L_d/S_o) systems, which contain similar acyl chain region, it can be noted that the influence of the acyl chain region is not as dominant as the membrane hydration and membrane phase state in determining the GP_{340} value changes after mixing.

Table 4-1 GP_{340} values of cubosomes and liposomes at different compositions and temperatures

		MO Cubosomes 25°C	MO Cubosomes 37°C			
		-0.311	-0.335			
Liposomes 25°C						
DOPC	DOPC/DPPC (1:1)	DOPC/DPPC/CHOL (4:4:2)	DOPC/DPPC/CHOL (3:3:4)	DOPC/DPPS (8:2)	POPC	DPPC
-0.148	0.236	0.314	0.354	-0.026	-0.031	0.52551
Liposomes 37°C						
DOPC	DOPC/DPPC (1:1)	DOPC/DPPC/CHOL (4:4:2)	DOPC/DPPC/CHOL (3:3:4)	DOPC/DPPS (8:2)	POPC	DPPC
-0.225	-0.066	0.186	0.269	-0.111	-0.136	0.43378

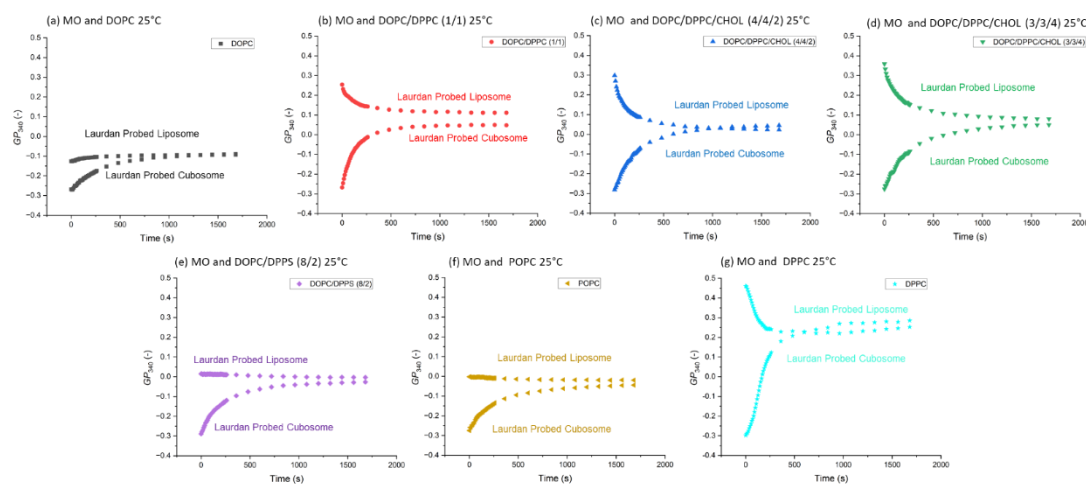


Figure 4-14 Changes to the GP_{340} values over time at 25°C of Laurdan probed MO cubosomes and Laurdan probed (a) DOPC (L_d) (black squares), (b) DOPC/DPPC (1/1) (L_d/S_o) (red circles), (c) DOPC/DPPC/CHOL (4/4/2) (L_d/L_o) (blue triangles), (d) DOPC/DPPC/CHOL (3/3/4) (L_o) (green triangles), (e) DOPC/DPPS (8/2) (L_d), (purple diamonds), (f) POPC (L_d) (yellow triangles) and (g) DPPC (S_o) (Cyan stars) liposomes. The final total lipid concentration of cubosomes and liposomes are 0.25 mM and 0.125 mM. The volume ratio of cubosome and liposome solutions is (1/1).

Over time, the membrane hydration states of the cubosomal and liposomal membrane slowly changed towards the hydration states of their counterpart. The GP_{340} values of the (Laurdan probed cubosomes and liposomes) and (Laurdan probed liposomes and cubosomes) of all combinations were reached the same GP_{340} values for each respective combination. This further confirms the lipid exchange and the interaction between the cubosomes and liposomes. More importantly, the original hydration state of the liposomes dictated the speed of the convergence of the GP_{340} values. In **Table 4-2**, the summary of the difference in the initial GP_{340} of the probed cubosomes and liposomes and the time of convergence (t_c) where GP_{340} of cubosomes is equal to that of liposomes.

Table 4-2 Difference in GP_{340} and time of convergence for GP_{340} values of the probed cubosomes and liposomes

Combination	MO Cubosomes 25°C						
	DOPC	DOPC/DPPC (1/1)	DOPC/DPPC/CHOL (4/4/2)	DOPC/DPPC/CHOL (3/3/4)	DOPC/DPPS (8/2)	POPC	DPPC
Initial Difference in GP_{340}	0.14	0.52	0.58	0.63	0.30	0.27	0.84
Time of convergence (s)	≈900	>1680	>1680	>1680	>1680	>1680	>1680
Combination	MO Cubosomes % 37°C						
	DOPC	DOPC/DPPC (1/1)	DOPC/DPPC/CHOL (4/4/2)	DOPC/DPPC/CHOL (3/3/4)	DOPC/DPPS (8/2)	POPC	DPPC
Initial Difference in GP_{340}	0.12	0.25	0.46	0.55	0.23	0.20	0.74
Time of convergence (s)	≈200	≈700	≈1680	>1680	≈1250	≈700	≈1680

The time scale in which that occurs was shown to be relatively long (**Table 4-2**) compared to the time needed for the cubic phase to disintegrate due to fusion (**Figure 4-7**). Therefore, the convergence time would include the duration of the fusion phenomenon as well as time for the reorganization of newly formed lamellar membranes. It can be noted that in the combinations of the cubosomes with more fluid membrane liposomes (L_d phase), the GP_{340} values converged to the same membrane state much faster than liposomes with more packed and ordered membranes. Even within the L_d phase liposomes, the convergence of the membrane hydration was different depending on the initial difference of the GP_{340} values between the cubosomes and liposomes. For example, the combination with DOPC liposomes (GP_{340} value difference = 0.14) converged much faster ($t_c \approx 900$ s) compared to DOPC/DPPS (8/2) (GP_{340} value difference = 0.14) which converged at and $t_c > 1680$ s. This could be attributed to the negative charge of DPPS

whose repulsive forces might inhibit lipids partitioning. The time needed for the membrane states to converge seems to be longer with liposomes that exhibit the more ordered membranes such DOPC/DPPC/CHOL (4/4/2) (L_d/L_o phase), DOPC/DPPC/CHOL (3/3/4) (L_o phase), and DPPC (S_o). The GP_{340} values MO cubosomes interacting with DOPC/DPPC/CHOL (3/3/4) liposomes (GP_{340} value difference = 0.63) converged at a later time ($t_c > 1680s$) compared to DOPC/DPPC/CHOL (4/4/2) (GP_{340} value difference = 0.58) which converged around ($t_c \approx 1000s$) due to higher membrane order. The combination with DPPC liposomes displayed similar behavior to other combinations at first, where the hydration states of the MO and DPPC start to approach the same value. However, unlike other combinations, they intersect with each other around $t \approx 600$ s with a difference in their GP_{340} values that seemed to get smaller over time. The large initial difference in the GP_{340} values in this combination (0.84) could have caused the partitioning or relocation of Laurdan to progress faster at first. However, over time with the slow progression of the fusion of MO, some partitioning of Laurdan into the DPPC membranes could have occurred and much more time might be needed for the complete convergence of the membrane hydration states of MO and DPPC. Thus, it can be concluded that the kinetics of the membrane hydration changes are influenced primarily by the phase state and hydration state of the guest membrane (liposomal membrane).

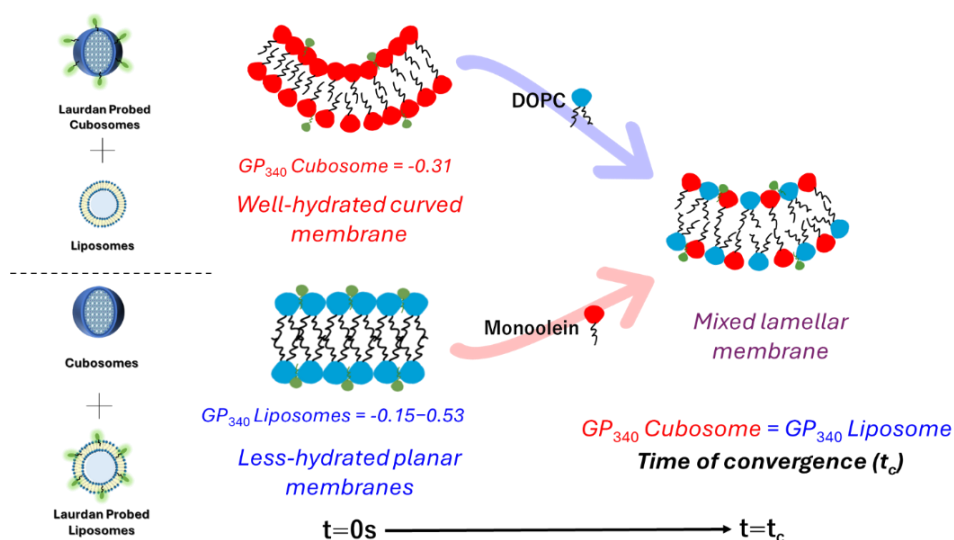


Figure 4-15 Illustration of the time of convergence (t_c) of the Laurdan probed cubosomes and liposomes.

To further confirm the influence of hydration state difference and liposomes' phase state on the kinetics of the GP_{340} values, the same experiment was conducted at 37°C (**Figure 4-16**). The GP_{340} values of the cubosomes did not seem to change drastically with the temperature increase. However, the GP_{340} values of the liposomes decreased indicating more disordered and hydrophilic membranes. Especially for systems exhibiting phase separation at 25°C (heterogeneous membranes), the increase in temperature is likely to transition them into a more homogeneous disordered state as seen in the ternary DOPC/DPPC/CHOL phase diagram (Davis et al. 2009; Veatch et al. 2003). For example, DOPC/DPPC (1:1) system transition from L_d / S_o phase coexistence to homogeneous L_d phase at elevated temperatures. This transition can be observed in the GP_{340} value changes of MO with DOPC/DPPC (1:1) in **Figure 4-16b**, where the changes closer resemble the interactions with more homogeneous L_d phase DOPC liposomes shown in **Figure 4-16a**. As temperature gets closer to the phase transition of DPPC ($T_m=41.0^\circ\text{C}$) from S_o phase to L_d phase, the behavior of the DOPC/DPPC (1:1) liposomes with L_d / S_o phase coexistence and DPPC S_o phase will resemble that of DOPC L_d phase liposomes, and converging faster. As for the DOPC/DPPC/CHOL (4/4/2) and DOPC/DPPC/CHOL (3/3/4) combinations, according to the phase diagram, they are still likely to exhibit L_o phase (Davis et al. 2009). Such phase ordered membrane state of the liposomes could explain the slower kinetics reminiscent of heterogeneous systems at 25°C in **Figure 4-14**. In comparison with the results at 25°C, the combinations converged to the same membrane state much faster due to smaller difference in membrane hydration state due to the increase in membrane disorder in the liposomal membranes.

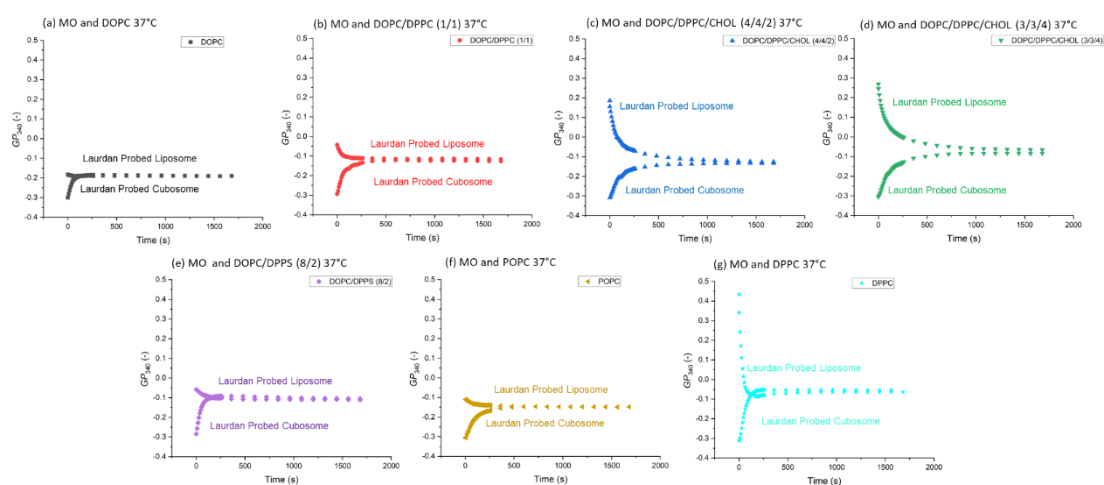


Figure 4-15 Changes to the GP_{340} values over time at 37°C of Laurdan probed MO F127 5 wt% cubosomes

and Laurdan probed (a) DOPC (L_d) (black squares), (b) DOPC/DPPC (1/1) (L_d) (red circles), (c) DOPC/DPPC/CHOL (4/4/2) (L_o) (blue triangles), (d) DOPC/DPPC/CHOL (3/3/4) (L_o) (green triangles), (e) DOPC/DPPS (8/2) (L_d), (purple diamonds), (f) POPC (L_d) (yellow triangles) and (g) DPPC (S_o) (Cyan stars) liposomes. The final total lipid concentration of cubosomes and liposomes are 0.25 mM and 0.125 mM. The volume ratio of cubosome and liposome solutions is (1/1).

4.Summary

In this chapter, the changes to the cubosomal structure and cubic membrane after interacting with model cell membranes were investigated. The TR-SAXS results showed a transition in the cubosome structure from the *Im3m* phase to the lamellar phase. The composition of the liposomes were shown to affect the phase transition time from the cubic to the lamellar phase. When probing the cubic and liposomal membranes with Laurdan, it was shown that membrane hydration states of the cubosomes and liposomes shift to resemble their counterpart. The lipid exchange between the particles resulted in decreasing the negative membrane curvature of the cubosomes over time, resulting in decreasing lattice parameters. The duration of the fluorescence intensity decrease in the probed cubosomes closely matched the time required for the cubic phase to transition to the lamellar phase in the SAXS diffractograms. Also, both the fluorescence and SAXS intensity showed that the lipid composition of the liposomes did not greatly affect the kinetics of the disintegration of the cubic phase upon fusing. Cryo-TEM data further confirmed the transition to lamellar vesicles and the loss of the well-defined internal structure characteristic of the cubosomes. Through the examination of the membrane polarity from GP_{340} values, it was shown that the kinetics of the membrane hydration state changes were influenced primarily by the phase state and membrane hydration of the guest membrane. This implies that this method could be used to not only examine the membrane hydration states, but to also get an indication of the time required for the fragmentation of the cubic phase and reorganization of the lipids forming the new lipid membrane.

Chapter 5: Examination of Effects of Hydrophobic Drug Incorporation on Cubosome-Cell membrane Model Interactions.

1. Introduction

The properties of the membranes of drug carriers were shown previously to be instrumental in determining their targeting (Bompard et al. 2020) as well as their drug release (Zhao et al. 2020). Therefore, thorough assessment of the cubic membrane is necessary to maximize the therapeutic effects of the cubosome carriers. For example, the incorporation of hydrophobic drugs into lipidic carriers can induce changes to their structure, stability, and membrane. Examination of the changes in cubic membrane when interacting with cell membrane lipids in the context of hydrophobic drug loading could further improve the design of these carriers.

In this chapter, the influence of loading MO cubosomes with the hydrophobic drug, HC on their interactions with POPC liposomes as cell membrane model through the usage of TR-SAXS and Laurdan probe. Cubosomes could be utilized to increase HC's therapeutic effects and reduce its side effects (Mulet et al. 2010). The aim of this work is to reveal the effects of drug loading on the interactions of MO cubosomes with POPC liposomes through the examination of the cubosome structure as well as cubic membrane.

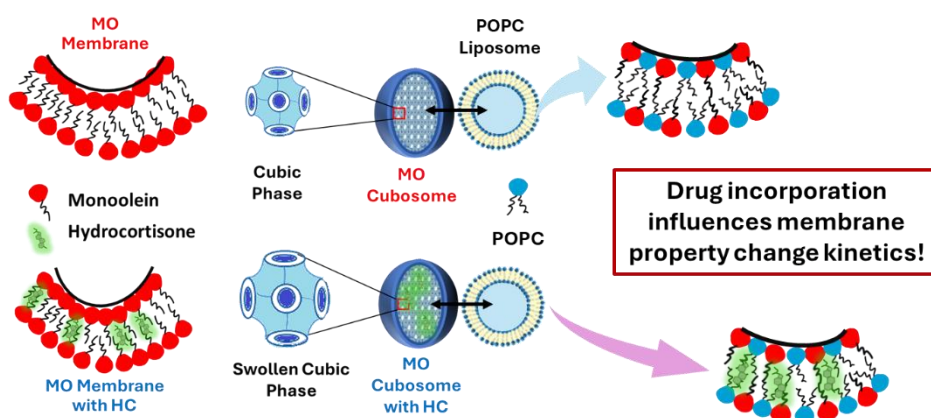


Figure 5-10 Schematic illustration of this work.

2. Materials and Methods

2.1 Materials

MO (glycerol α -monooleate) (purity > 99 %) and Pluronic F127 (F127) were purchased from Sigma-Aldrich (St. Louis, MO). Hydrocortisone (HC) was purchased from Wako Pure Chemical Industries (Osaka, Japan). 1-Palmitoyl-2-oleoyl-sn-glycero-3-phosphocholine (POPC) was purchased from (Nippon Oil & Fats Corporation, Tokyo, Japan).

2.2 Preparation of Monoolein Cubosomes

The cubosomes were prepared by dissolving MO or MO and HC (mol ratio = 9.5/0.5) in chloroform, followed by removing the chloroform under vacuum conditions for 48 hours. The lipid films were hydrated with preheated solution of F127 to reach a final concentration of 50 mM. The lipid to F127 weight ratio was 100:1. The cubosomes were homogenized in an ice bath using a probe sonicator (TOMY Ultrasonic Disruptor UD-200) for 3 minutes. Finally, the samples were heated for 3 minutes at 70°C.

2.3 Preparation of the Liposomes

The liposomes were prepared by dissolving POPC in chloroform. After evaporating the solvent, a thin lipid film was obtained and kept under vacuum for at least 24 hours. The film was hydrated with ultrapure water and the suspension was agitated in a water bath for 15 minutes at 60°C. The liposome suspension was extruded 11 times through a polycarbonate 100 nm membrane filter. The liposomes were stored at 4°C. The concentration of the liposomes was 25 mM.

2.4 TR-SAXS Measurements

SAXS measurements were conducted at the high flux beamline, BL40XU at SPring-8 synchrotron facility, Japan. The X-ray wavelength and sample to-detector distance were 0.0827 nm and 1.0 m, respectively, corresponding to an accessible q -range of 0.24 to 3.2 nm⁻¹. 75 μ l of each the cubosome and liposome solutions were mixed using stopped-flow apparatus. The scattering patterns were taken with 1 ms measurements every 10 seconds after mixing. The lattice parameter (a) of the $Im\bar{3}m$ cubic phase was calculated from the scattering vector (q) and the inter-planar spacing (d) of each unit cell according to the following equation: $a = d\sqrt{(h^2+k^2+l^2)}$, where $d = 2\pi/q$, and the values h , k , and l are the Miller indices of the Bragg peaks (Nakano et al. 2002).

2.5 Laurdan Spectra Measurements

The fluorescence measurements were conducted using FP-8500 spectrofluorometer (JASCO, Tokyo, Japan). The cubosome and liposome solutions were diluted with ultrapure water 100-fold then 15 μ L of Laurdan solution (1 mM, in ethanol) was added to either of them. The probed sample was incubated for 30 minutes. After mixing the cubosomes and liposomes, the Laurdan spectra were obtained by exciting samples at 340 nm and measuring the intensities in the wavelength range of 400 nm to 600 nm over the time span of 250s. The generalized polarization (GP_{340}) was calculated according to the following equation:

$$GP_{340} = \frac{I_{440} - I_{490}}{I_{440} + I_{490}} \quad \text{Eq. 5-1}$$

where I_{440} and I_{490} are the fluorescence intensities at 440 and 490 nm, respectively.

3.Result and Discussion

3.1 Effects of Drug Incorporation on Cubosome Structure

The SAXS profiles of MO and MO/HC cubosomes are shown in (Figure 5-2). Both cubosomes showed Bragg peaks with relative positions at spacing ratios of $\sqrt{2}$: $\sqrt{4}$: $\sqrt{6}$ corresponding to the [110], [200], and [211] reflections of the $Im3m$ cubic phase (Driever et al. 2011). A shift to lower peak positions in the HC-loaded cubosomes was observed, indicating the formation of larger cubic lattice. Upon drug incorporation, the lattice structure of MO increased from 15.76 nm to 16.48 nm. It was reported previously corticoid drugs such as HC can increase the lattice size of cubosomes by increasing the membrane curvature (Mulet et al. 2010). Also, cholesterol which structurally resembles HC was shown to induce swollen cubic lattices (Barriga, Ces, et al. 2019; Tyler et al. 2015).

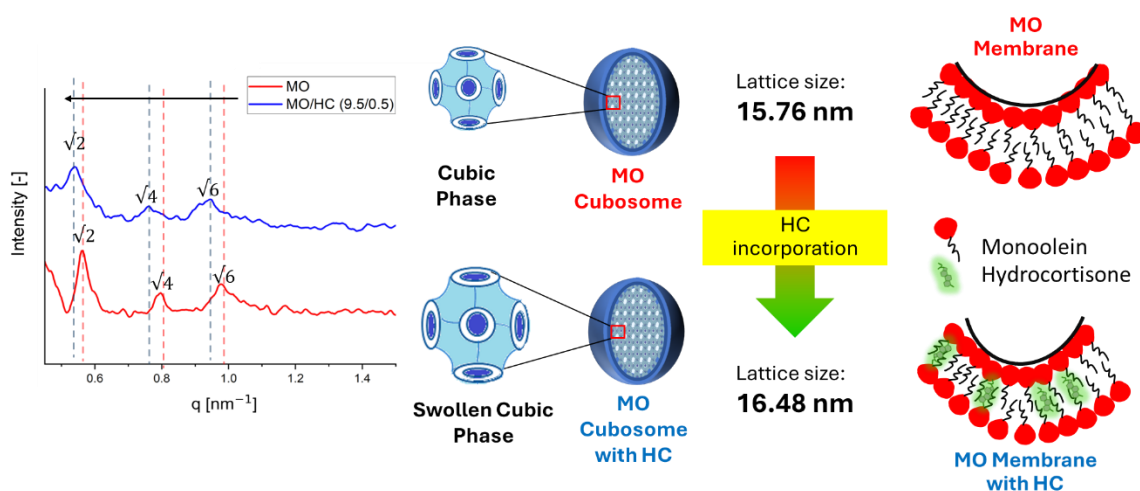


Figure 5-2 SAXS profiles and lattice parameters of MO and MO/HC cubosomes.

3.2 Examination of Structural Changes in MO Cubosomes Using TR-SAXS

Figure 5-3a shows the TR-SAXS profiles of MO and MO/HC cubosomes after being mixed with POPC liposomes. The profiles on top ($t=0s$) also showed peaks associated with the cubic $Im3m$ phase overlapping with the lamellar peak around $q \approx 0.95 \text{ nm}^{-1}$, which arises from the presence of small amounts of multi-lamellar vesicles along with the liposomes (Scott et al. 2019). For both cubosomes, as time progresses, the cubic peaks lose intensity and shift to higher q values leaving behind a peak associated with the lamellar phase. The cubic to lamellar phase transition occurs due to the lipid exchange with POPC, which has a critical packing parameter (CPP) < 1 . This reduces the curvature

of the cubic membrane and transitions them into planar lamellar membranes (Vandoolaeghe et al. 2009; Milogrodzka et al. 2023). Compared to MO cubosomes, the time needed for the cubic structure to disintegrate is closely similar ($t \approx 120$ s), which indicated that the incorporation of HC does not influence the structural transition of the cubosomes drastically. The changes to the SAXS intensity of the scattering vector q_{110} of the cubic phase were investigated. This peak was selected because it can be distinguished from the lamellar peak, and it is the highest in intensity (Figure 5-3b). The results showed that the incorporation of the drug into the cubosomes did not seem to alter the cubic to lamellar phase transition as well.

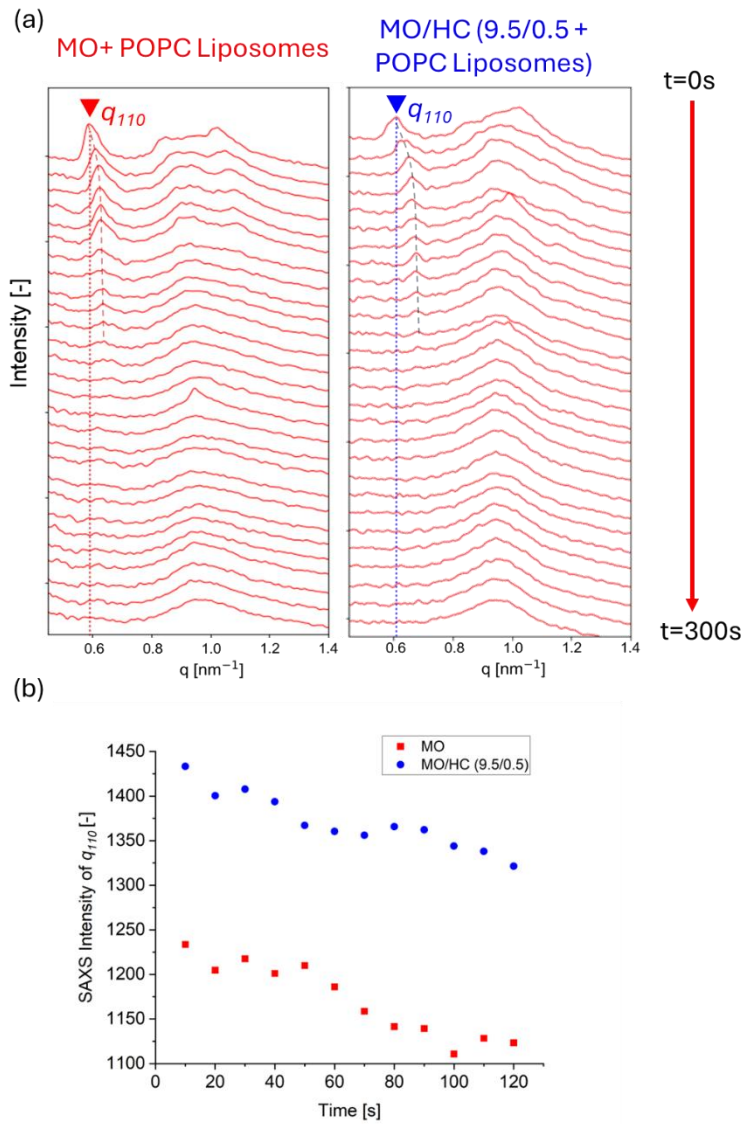


Figure 5-3 (a) TR-SAXS profiles of MO and MO/HC cubosomes after mixing with POPC liposomes, (b) intensity of diffraction peak of the scattering vector of ($q_{110} = \sqrt{2}$) of MO and MO/HC cubosomes after mixing with POPC liposomes.

3.3 Fluorescence Intensity of Laurdan Probed Drug Loaded Cubosomes and Liposomes

To further clarify the effect of HC on the interaction between cubosomes and lipid membranes, the changes in membrane property were explored by using Laurdan probe, which is effective in indicating hydration state of its surrounding membrane (Ito et al. 2023). The emission peaks of this probe appear at 440 nm and 490 nm, corresponding to hydrophobic and hydrophilic membrane environments, respectively (Parasassi et al. 1998). The changes in both the cubic and liposomal membranes upon mixing by probing either the cubosomes or liposomes were examined with Laurdan. **Figure 5-3** shows the evolution of the Laurdan spectra of the probed cubosomes/liposomes after being mixed with their counterpart. The spectra of both MO and MO/HC cubosomes revealed a hydrophilic membrane, with a dominant peak around 490 nm. On the other hand, the spectra of the POPC reflected a more hydrophobic environment with influence from the peak at 440 nm. After mixing, the spectra of the probed MO and MO/HC cubosomes the intensities of the peak at 490 nm decreased over time with an increase in the peak around 440 nm, a shift to a hydrophobic membrane state. As for the POPC liposomes, their membranes became more hydrophilic, as observed with the decrease in the 440 nm peak and an increase in the 490 nm peak. These results reveal that mixing the cubosomes and liposomes results in transition of their hydration state to become closer to that of its counterpart.

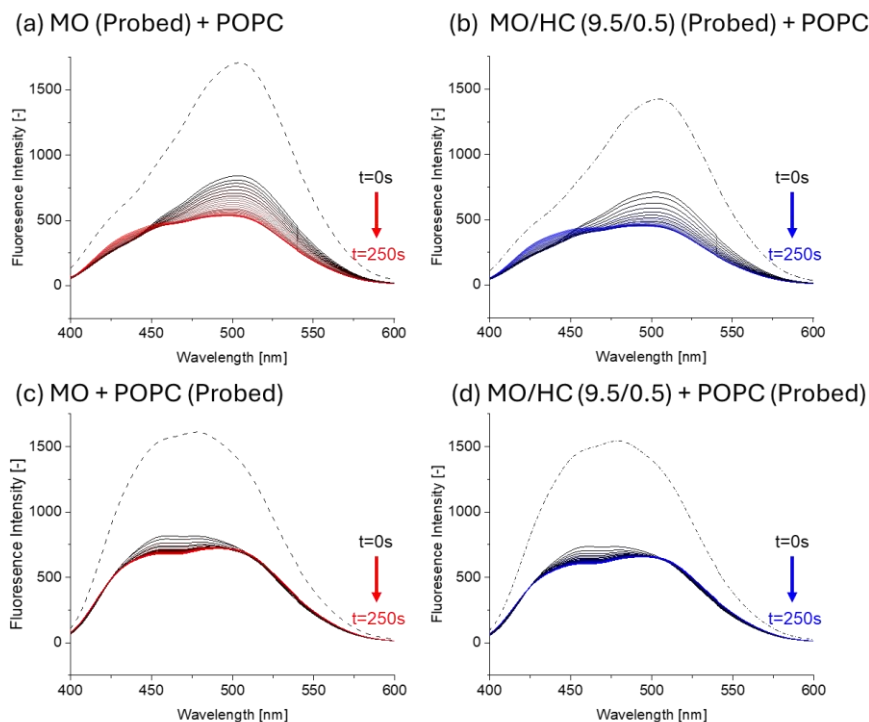


Figure 5-3 Laurdan spectra of different combinations of probed cubosomes and liposomes over time. The dashed spectra in black are the Laurdan spectrum of the cubosomes/liposome before mixing.

The changes in the fluorescence intensity of Laurdan can be also used to indicate instabilities or changes in the membranes close to Laurdan. The emission intensities from 400 nm to 600 nm, normalized to the spectra before mixing, of the probed MO and MO/HC cubosomes (**Figure 5-4a**) and probed POPC (**Figure 5-4b**) are shown. For the cubosomes, the normalized fluorescence intensities decreased over time to reach minimum values at $t \approx 100$ -200 s. Considering that the time scale of the cubic to lamellar phase transition in **Figure 5-3** of the MO and MO/HC cubosomes was around 120s, the decrease in intensity can be an indication of the disintegration of the cubic membrane while exchanging lipids with POPC liposomes. The drug loaded cubosomes showed slightly slower disintegration compared to blank cubosomes, which could be caused by HC enhancing the lateral interactions between the hydrocarbon chains of the lipids as shown in chapter 2, resulting in slowed exchange of POPC into the cubosomes. Unlike the cubosomes, the intensities of POPC liposomes after mixing with both types of cubosomes showed minimal changes, which indicates that interaction with cubosomes does not induce any instabilities to the liposomal membranes.

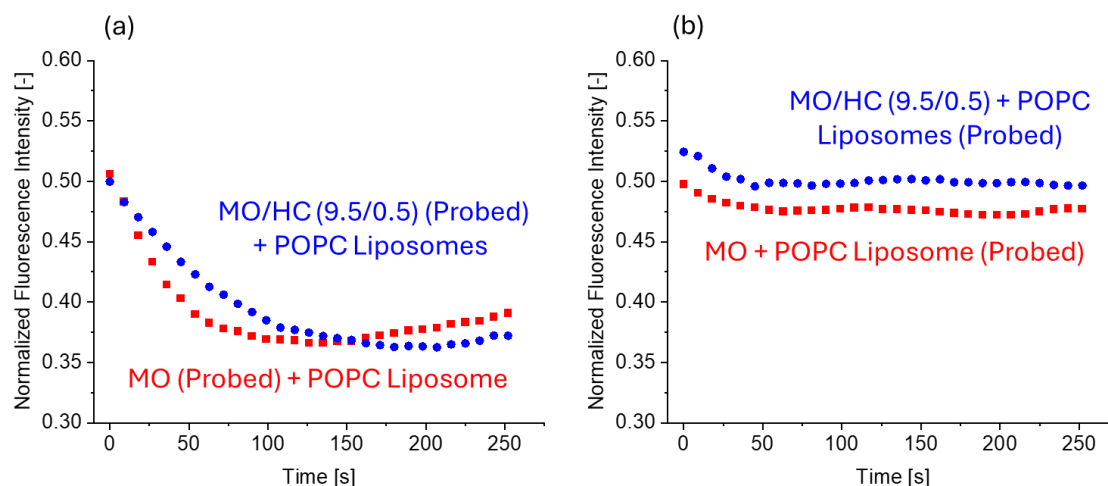


Figure 5-4 Fluorescence intensity of Laurdan of (a) probed MO and MO/HC cubosomes after mixing with POPC liposomes, (b) probed POPC liposomes after mixing with MO and MO/HC cubosomes. The fluorescence intensities were normalized to initial spectrum before mixing.

3.4 Generalized polarization GP_{340} of the Drug Loaded Cubosomes and Liposomes

To indicate the changes in membrane hydration state of the cubosomes and liposomes upon mixing, the changes in the GP_{340} values were assessed. Initially, the MO and MO/HC cubosomes displayed GP_{340} values of -0.296 and -0.297, respectively. These values reveal a highly hydrophilic environment due to the curved cubic membranes (Fracassi et al. 2023). The loading of HC did not alter the membrane environment dramatically up to 5 mol% as seen in chapter 2. For POPC, it showed values of -0.01, reflecting a less hydrated membrane condition. In **Figure 5-5**, the changes of the GP_{340} value in relation to HC loading were evaluated. The GP_{340} of the probed cubosomes and probed liposomes gradually transitioned towards the values of their counterpart as shown in the trend in spectrum changes. This result confirms the lipid exchange and the interaction between the cubosomes and liposomes. For both cubosomes, the GP_{340} values of the cubosomes increased after mixing. The increase in GP_{340} values is due to Laurdan experiencing less water relaxation around it due to the transition from cubic to lamellar phase. In previous works, the water relaxation of Laurdan in the $Pn3m$ cubic phase was shown to be much larger than that in the lamellar phase (Mangiarotti et al. 2021a). Also, the kinetics of the GP_{340} value in the HC loaded cubosomes were much slower than MO cubosomes. Considering that the incorporation of HC increases the cubosome lattice size due to the high affinity to bilayer, it is reasonable that the lipid

exchange with liposomal membranes is slower in MO/HC than in MO. In the case of GP_{340} values of POPC liposomes, it was observed that both cubosomes induce small decrease in their hydration state. Such results imply that the incorporation of the drug would primarily affect the carrier and induce small changes to the guest membrane (liposomes). The drug loaded cubosomes were shown to reach the final membrane state much slower than MO cubosomes indicating that the HC incorporation could alter the interaction of cubosomes with cell membrane models. This finding is an important fact to be considered in designing cubosomes as hydrophobic drug carriers.

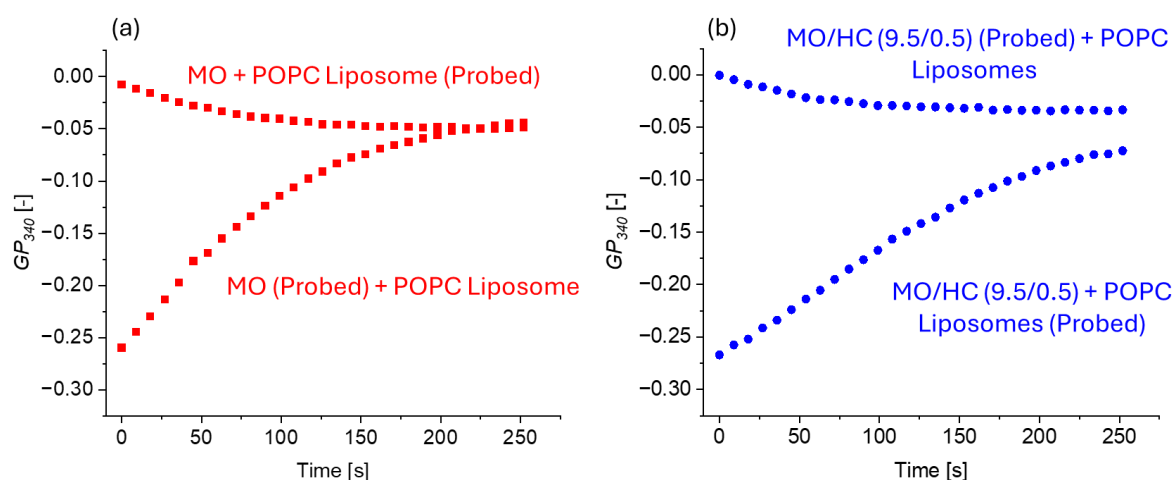


Figure 5-5 Changes to the GP_{340} values over time after of (a) probed MO cubosomes and probed POPC liposomes, (b) probed MO/HC cubosomes and probed POPC liposomes.

4. Summary

As a continuation of the characterization method in chapter 2 and methodology developed in chapter 3 and 4, in this chapter, the interactions between drug loaded cubosomes and POPC liposomes are investigated. By using TR-SAXS and Laurdan probe, the influence of drug loading on the interaction was demonstrated. Although the incorporation of the drug did not alter the duration and kinetics of the cubic to lamellar phase transition, the membrane property analysis using Laurdan fluorescence probes showed slower kinetics in the drug loaded cubosomes. This implies that the rate of lipid exchange between carriers and cell membranes was suppressed in the presence of drug molecules.

Chapter 6: General Conclusion

Dispersed cubic phase nanoparticles are a promising platform for drug delivery, due to their well-defined internal structures and high membrane surface area. Designing cubosomes as drug delivery carriers requires careful consideration of various factors such as structure, drug release, and interactions with cell membranes, which are heavily influenced by the properties of the cubic membrane. In this study, systematic characterization of the self-assembly properties was performed to indicate the influence of the membrane environment in dictating the structure and stability of the carrier. Using structural analysis methods and membrane bound fluorescence probes, the methodology to elucidate the interactions of cubosomes with model cell membrane was established. The findings of this study offer valuable insights into the interactions of cubosomes with model cell membranes and contribute to the enhancement of the design of cubosomes as for therapeutic delivery applications.

In chapter 2, the physicochemical properties of monoolein of MO and MO/OA self-assemblies are investigated after the incorporation of the hydrophobic drug, HC using Raman spectroscopy, cryo-TEM, and fluorescent probes. HC incorporation altered the surface property of MO and MO/OA nanoparticles, resulting in aggregation of the self-assemblies at high hydrocortisone loading. Through the examination of polarity, zeta-potential, and particle size of the dispersions, the influence of the drug on the properties such as polarity, zeta-potential, and particle size was highlighted and the relationship between these properties and colloidal stability were elucidated.

In chapter 3, through the usage of TR-SAXS and the changes to the GP_{340} values of Laurdan probed cubosomes, the development of the methodology to indicate changes to the physicochemical properties of cubosomes when interacting with cell membrane lipids was conducted. The results of the TR-SAXS experiments revealed that the MO cubosomes transitioned from the cubic phase to the lamellar phase upon mixing with the DOPC liposomes. Furthermore, the kinetics of apparent lipid exchange (k_{app}) and estimation of the apparent amount of DOPC in the cubosomes over the course of interaction could be obtained through the GP_{340} values.

In chapter 4, the methodology introduced in chapter 3 was further extended and used to study the interactions of MO cubosomes with model cell membranes at different

phase states. The effects of the carrier on the model cell membrane were also elucidated. TR-SAXS measurements showed that the time of the structural change of the cubic phase to lamellar phase was influenced by the fluidity of the liposome bilayers. After mixing the cubosomes and liposomes, the membrane hydration states of the cubosomes and liposomes transitioned to resemble the hydration state of their counterpart. In addition, the membrane hydration of the liposomes was shown to be an important factor in dictating the time needed to reach the final intermediate state after mixing.

In chapter 5, the characterization and methodology used in previous chapters was used to assess the effects drug loading on the interactions of MO cubosomes with POPC liposomes. The incorporation of the drug did not alter the duration and kinetics of the cubic to lamellar phase transition. However, slower lipid exchange kinetics in the drug loaded cubosomes compared to blank cubosomes were observed in the membrane state analysis experiments. These results demonstrate that incorporating drugs into cubosomes reduces the rate of lipid exchange between carriers and model cell membranes.

Suggestion for Future Works

1. Interactions of Cubosomes in Cell Mimetic Environment

The primary goal of this study was to develop the necessary methodology to examine the interactions of cubosomes with cell membranes. Liposomes were chosen as a model for cell membranes due to several considerations related to the stopped-flow step up in the TR-SAXS experiments. However, it is necessary to investigate the interactions of the cubosomes in cell mimetic environment. For example, protein forming corona could influence the properties of the cubosomes, which in turn could influence the interactions.

2. Expansion of Methodology Using Other Membrane Bound Fluorescence Probes

The methodology developed in this work is simple and effective in determining elucidating the changes in the cubic membrane as well as the estimation of the degree of lipid exchange, the preference of the allocation of Laurdan must be considered. The possible preference of Laurdan could result in overestimation in content of the apparent lipid exchange. Therefore, expansion of this approach using other membrane bound probes that are not likely to preferentially allocate in the membranes must be considered.

3. Expansion of Approach to Other Types of LNPs

Using the approach in this study, the interactions of other types of LNPs and the effects they induce on model cell membranes could be realized. This method could be employed to compare the interactions and kinetics of lipid exchange of different types of cubosomes composed of non-lamellar phase forming lipids or other nanostructured lipid carriers. Such a simple approach can be effective in the design of LNPs for various drug delivery applications.

Nomenclatures

2θ	=	Angles in XRD analysis	[Deg]
a	=	Lattice Parameter	[nm]
P	=	Fluorescence polarization of DPH	[-]
GP_{340}	=	General polarization calculating at exciting light at 340 nm	[-]
G	=	Correction factor	[-]
PDI	=	Polydispersity index	[-]
q	=	Scattering vector	[nm ⁻¹]
T_m	=	Melting temperature	°C
t_c	=	Time of convergence	[s]
ζ	=	Zeta potential	[mV]

List of Abbreviations

CHOL	=	Cholesterol
Cryo-TEM	=	Cryogenic Transmission Electron Microscopy
DAS	=	Decay Associated Spectra
DDS	=	Drug Delivery System
DLS	=	Dynamic Light Scattering
DOPC	=	1,2-dioleoyl-sn-glycero-3-phosphocholine
DPH	=	1,6-Diphenyl-1,3,5-hexatriene
DPPC	=	1, 2-dipalmitoyl-sn-glycero-3-phosphocholine
DPPE	=	1,2-Dipalmitoyl- <i>sn</i> -glycero-3-phospho-L-serine
F108	=	Pluronic F108
F127	=	Pluronic F127
FFT	=	Fast Fourier Transformation
HC	=	Hydrocortisone
k_{app}	=	Apparent lipid exchange rate constant
LNP	=	Lipid Nanoparticles
MO	=	Monolein
OD_{400}	=	Optical Density measure at 400 nm
OA		Oleic Acid
PDI	=	Polydispersity Index
POPC		1-Palmitoyl-2-oleoyl-sn-glycero-3-phosphocholine
SAXS	=	Small-Angle X-ray Scattering
TR-SAXS	=	Time-Resolved Small-Angle X-ray Scattering
TEM	=	Transmission Electron Microscopy
XRD	=	X-Ray Diffraction

References

- Abourehab, MAS, Ansari, MJ, Singh, A, Hassan, A, Abdelgawad, MA, Shrivastav, P, Abualsoud, BM, Amaral, LS, and Pramanik, S. 2022. "Cubosomes as an Emerging Platform for Drug Delivery: A Review of the State of the Art." *Journal of Materials Chemistry B* 10 (15): 2781–2819.
- Akhlaghi, SP, Ribeiro, IR, Boyd, BJ, and Loh, W. 2016. "Impact of Preparation Method and Variables on the Internal Structure, Morphology, and Presence of Liposomes in Phytantriol-Pluronic® F127 Cubosomes." *Colloids and Surfaces B: Biointerfaces* 145:845–53.
- Alsop, RJ, Khondker, A, Hub, JS, and Rheinstädter, MC. 2016. "The Lipid Bilayer Provides a Site for Cortisone Crystallization at High Cortisone Concentrations." *Scientific Reports* 6 (March): 1–10.
- Angelov, B, Angelova, A, Filippov, SK, Drechsler, M, Štěpánek, P, and Lesieur, S. 2014. "Multicompartment Lipid Cubic Nanoparticles with High Protein Upload: Millisecond Dynamics of Formation." *ACS Nano* 8 (5): 5216–26.
- Angelov, B, Angelova, A, Filippov, SK, Narayanan, T, Drechsler, M, Štěpánek, P, Couvreur, P, and Lesieur, S. 2013. "DNA/Fusogenic Lipid Nanocarrier Assembly: Millisecond Structural Dynamics." *Journal of Physical Chemistry Letters* 4 (11): 1959–64.
- Azhari, H. 2018. "Surface Modified Cubosomes for Drug Delivery across the Blood-Brain Barrier," no. October, 1–242.
- Azhari, H, Strauss, M, Hook, S, Boyd, BJ, and Rizwan, SB. 2016. "Stabilising Cubosomes with Tween 80 as a Step towards Targeting Lipid Nanocarriers to the Blood-Brain Barrier." *European Journal of Pharmaceutics and Biopharmaceutics* 104 (May): 148–55.
- Badran, M. 2014. "Formulation and in Vitro Evaluation of Flufenamic Acid Loaded Deformable Liposomes for Improved Skin Delivery." *Digest Journal of Nanomaterials and Biostructures* 9 (1): 83–91.
- Barauskas, J, Johnsson, M, Joabsson, F, and Tiberg, F. 2005. "Cubic Phase Nanoparticles (Cubosome): Principles for Controlling Size, Structure, and Stability." *Langmuir* 21 (6): 2569–77.
- Barriga, HMG, Ces, O, Law, R V., Seddon, JM, and Brooks, NJ. 2019. "Engineering Swollen Cubosomes Using Cholesterol and Anionic Lipids." *Langmuir* 35 (50): 16521–27.
- Barriga, HMG, Holme, MN, and Stevens, MM. 2019. "Cubosomes: The Next Generation of Smart Lipid Nanoparticles?" *Angewandte Chemie - International Edition* 58 (10): 2958–78.
- Boge, L, Hallstensson, K, Ringstad, L, Johansson, J, Andersson, T, Davoudi, M, Larsson, PT, Mahlapuu, M, Håkansson, J, and Andersson, M. 2019. "Cubosomes for Topical Delivery of the Antimicrobial Peptide LL-37." *European Journal of Pharmaceutics and Biopharmaceutics* 134 (November): 60–67.
- Bompard, J, Rosso, A, Brizuela, L, Mebarek, S, Blum, LJ, Trunfio-Sfarghiu, AM, Lollo,

- G, Granjon, T, Girard-Egrot, A, and Maniti, O. 2020. "Membrane Fluidity as a New Means to Selectively Target Cancer Cells with Fusogenic Lipid Carriers." *Langmuir* 36 (19): 5134–44.
- Boyd, BJ. 2003. "Characterisation of Drug Release from Cubosomes Using the Pressure Ultrafiltration Method." *International Journal of Pharmaceutics* 260 (2): 239–47.
- Brown, KG, Peticolas, WL, and Brown, E. 1973. "Raman Studies of Conformational Changes in Model Membrane Systems." *BIOCHEMICAL AND BIOPHYSICAL RESEARCH COMMUNICATIONS* 54 (1).
- Bui, TT, Suga, K, and Umakoshi, H. 2016. "Roles of Sterol Derivatives in Regulating the Properties of Phospholipid Bilayer Systems." *Langmuir* 32 (24): 6176–84.
- Chang, C, Meikle, TG, Drummond, CJ, Yang, Y, and Conn, CE. 2021. "Comparison of Cubosomes and Liposomes for the Encapsulation and Delivery of Curcumin." *Soft Matter* 17 (12): 3306–13.
- Chong, JYT, Mulet, X, Waddington, LJ, Boyd, BJ, and Drummond, CJ. 2011. "Steric Stabilisation of Self-Assembled Cubic Lyotropic Liquid Crystalline Nanoparticles: High Throughput Evaluation of Triblock Polyethylene Oxide-Polypropylene Oxide-Polyethylene Oxide Copolymers." *Soft Matter* 7 (10): 4768–77.
- Davis, JH, Clair, JJ, and Juhasz, J. 2009. "Phase Equilibria in DOPC/DPPC-D62/Cholesterol Mixtures." *Biophysical Journal* 96 (2): 521–39.
- Demurtas, D, Guichard, P, Martiel, I, Mezzenga, R, Hébert, C, and Sagalowicz, L. 2015. "Direct Visualization of Dispersed Lipid Bicontinuous Cubic Phases by Cryo-Electron Tomography." *Nature Communications* 6:1–8.
- Dong, Y Da, Larson, I, Hanley, T, and Boyd, BJ. 2006. "Bulk and Dispersed Aqueous Phase Behavior of Phytantriol: Effect of Vitamin E Acetate and F127 Polymer on Liquid Crystal Nanostructure." *Langmuir* 22 (23): 9512–18.
- Driever, CD, Mulet, X, Johnston, APR, Waddington, LJ, Thissen, H, Caruso, F, and Drummond, CJ. 2011. "Converging Layer-by-Layer Polyelectrolyte Microcapsule and Cubic Lyotropic Liquid Crystalline Nanoparticle Approaches for Molecular Encapsulation." *Soft Matter* 7 (9): 4257–66.
- Duff Putu, Jean Shoveller., Julio Montaner., Cindy Feng., Rachel Nicoletti., Kate Shannon ., GO. 2016. "Influence of Cholesterol and Bilayer Curvature on the Interaction of PPO-PEO Block Copolymers with Liposomes." *Physiology & Behavior* 176 (1): 139–48.
- Dutt, S, Siril, PF, and Remita, S. 2017. "Swollen Liquid Crystals (SLCs): A Versatile Template for the Synthesis of Nano Structured Materials." *RSC Advances* 7 (10): 5733–50.
- Dyett, BP, Yu, H, Strachan, J, Drummond, CJ, and Conn, CE. 2019. "Fusion Dynamics of Cubosome Nanocarriers with Model Cell Membranes." *Nature Communications* 10 (1).
- El-Enin, HA, and AL-Shanbari, AH. 2018. "Nanostructured Liquid Crystalline Formulation as a Remarkable New Drug Delivery System of Anti-Epileptic Drugs for Treating Children Patients." *Saudi Pharmaceutical Journal* 26 (6): 790–800.

- Elnaggar, YSR, Etman, SM, Abdelmonsif, DA, and Abdallah, OY. 2015. "Novel Piperine-Loaded Tween-Integrated Monoolein Cubosomes as Brain-Targeted Oral Nanomedicine in Alzheimer's Disease: Pharmaceutical, Biological, and Toxicological Studies." *International Journal of Nanomedicine* 10:5459–73.
- Esposito, E, Cortesi, R, Drechsler, M, Paccamiccio, L, Mariani, P, Contado, C, Stellin, E, Menegatti, E, Bonina, F, and Puglia, C. 2005. "Cubosome Dispersions as Delivery Systems for Percutaneous Administration of Indomethacin." *Pharmaceutical Research* 22 (12): 2163–73.
- Esposito, E, Eblovi, N, Rasi, S, Drechsler, M, Gregorio, GM Di, Menegatti, E, and Cortesi, R. 2003. "Lipid-Based Supramolecular Systems for Topical Application: A Preformulatory Study." *AAPS PharmSci* 5 (4): 1–15.
- Faried, M, Suga, K, Okamoto, Y, Shameli, K, Miyake, M, and Umakoshi, H. 2019. "Membrane Surface-Enhanced Raman Spectroscopy for Cholesterol-Modified Lipid Systems: Effect of Gold Nanoparticle Size." Research-article. *ACS Omega* 4 (9): 13687–95.
- Fini, A, Bergamante, V, Ceschel, GC, Ronchi, C, and Moraes, CAF. 2008. "Control of Transdermal Permeation of Hydrocortisone Acetate from Hydrophilic and Lipophilic Formulations." *AAPS PharmSciTech* 9 (3): 762–68.
- Fong, WK, Hanley, T, and Boyd, BJ. 2009. "Stimuli Responsive Liquid Crystals Provide 'on-Demand' Drug Delivery in Vitro and in Vivo." *Journal of Controlled Release* 135 (3): 218–26.
- Fong, WK, Hanley, TL, Thierry, B, Tilley, A, Kirby, N, Waddington, LJ, and Boyd, BJ. 2014. "Understanding the Photothermal Heating Effect in Non-Lamellar Liquid Crystalline Systems, and the Design of New Mixed Lipid Systems for Photothermal on-Demand Drug Delivery." *Physical Chemistry Chemical Physics* 16 (45): 24936–53.
- Fox, CB, Uibel, RH, and Harris, JM. 2007. "Detecting Phase Transitions in Phosphatidylcholine Vesicles by Raman Microscopy and Self-Modeling Curve Resolution." *Journal of Physical Chemistry B* 111 (39): 11428–36.
- Fracassi, A, Podolsky, KA, Pandey, S, Xu, C, Hutchings, J, Seifert, S, Baiz, CR, Sinha, SK, and Devaraj, NK. 2023. "Characterizing the Self-Assembly Properties of Monoolein Lipid Isosteres." *Journal of Physical Chemistry B* 127 (8): 1771–79.
- Gan, L, Han, S, Shen, J, Zhu, J, Zhu, C, Zhang, X, and Gan, Y. 2010. "Self-Assembled Liquid Crystalline Nanoparticles as a Novel Ophthalmic Delivery System for Dexamethasone: Improving Preocular Retention and Ocular Bioavailability." *International Journal of Pharmaceutics* 396 (1–2): 179–87.
- Guo, C, Liu, H, Wang, J, and Chen, J. 1999. "Conformational Structure of Triblock Copolymers by FT-Raman and FTIR Spectroscopy." *Journal of Colloid and Interface Science* 209 (2): 368–73.
- Gustafsson, J, Ljusberg-Wahren, H, Almgren, M, and Larsson, K. 1996. "Cubic Lipid–Water Phase Dispersed into Submicron Particles." *Langmuir* 12 (20): 4611–13.
- Heurtault, B, Saulnier, P, Pech, B, Proust, JE, and Benoit, JP. 2003. "Physico-Chemical

- Stability of Colloidal Lipid Particles.” *Biomaterials* 24 (23): 4283–4300.
- Hina Shrestha, Rajni Bala, and SAC. 2014. “Lipid-Based Drug Delivery Systems.” *Journal of Pharmaceutics* 2014.
- Israelachvili, JN, Mitchell, DJ, and Ninham, BW. 1977. “Theory of Self-Assembly of Lipid Bilayers and Vesicles.” *BBA - Biomembranes* 470 (2): 185–201.
- Ito, N, Watanabe, NM, Okamoto, Y, and Umakoshi, H. 2023. “Multiplicity of Solvent Environments in Lipid Bilayer Revealed by DAS Deconvolution of Twin Probes: Comparative Method of Laurdan and Prodan.” *Biophysical Journal* 122 (23): 4614–23.
- Izza, N, Suga, K, Okamoto, Y, Watanabe, N, Bui, TT, Wibisono, Y, Fadila, CR, and Umakoshi, H. 2021. “Systematic Characterization of Nanostructured Lipid Carriers from Cetyl Palmitate/Caprylic Triglyceride/Tween 80 Mixtures in an Aqueous Environment.” *Langmuir* 37 (14): 4284–93.
- Jabłonowska, E, Nazaruk, E, Matyszevska, D, Speziale, C, Mezzenga, R, Landau, EM, and Bilewicz, R. 2016. “Interactions of Lipidic Cubic Phase Nanoparticles with Lipid Membranes.” *Langmuir* 32 (37): 9640–48.
- Johnsson, M, Silvander, M, Karlsson, G, and Edwards, K. 1999. “Effect of PEO-PPO-PEO Triblock Copolymers on Structure and Stability of Phosphatidylcholine Liposomes.” *Langmuir* 15 (19): 6314–25.
- Jones, MN. 1995. “The Surface Properties of Phospholipid Liposome Systems and Their Characterisation.” *Advances in Colloid and Interface Science* 54 (C): 93–128.
- Kaddah, S, Khreich, N, Kaddah, F, Khrouz, L, Charcosset, C, and Greige-Gerges, H. 2018. “Corticoids Modulate Liposome Membrane Fluidity and Permeability Depending on Membrane Composition and Experimental Protocol Design.” *Biochimie* 153:33–45.
- Kalepu, S, and Nekkanti, V. 2015. “Insoluble Drug Delivery Strategies: Review of Recent Advances and Business Prospects.” *Acta Pharmaceutica Sinica B* 5 (5): 442–53.
- Kashapov, R, Gaynanova, G, Gabdrakhmanov, D, Kuznetsov, D, Pavlov, R, Petrov, K, Zakharova, L, and Sinyashin, O. 2020. “Self-Assembly of Amphiphilic Compounds as a Versatile Tool for Construction of Nanoscale Drug Carriers.” *International Journal of Molecular Sciences* 21 (18): 1–47.
- Kulkarni, C V. 2016. “Lipid Self-Assemblies and Nanostructured Emulsions for Cosmetic Formulations.” *Cosmetics* 3 (4).
- Kulkarni, C V., Wachter, W, Iglesias-Salto, G, Engelskirchen, S, and Ahualli, S. 2011. “Monoolein: A Magic Lipid?” *Physical Chemistry Chemical Physics* 13 (8): 3004–21.
- Lakic, B, Beh, C, Sarkar, S, Yap, SL, Cardoso, P, Valery, C, Hung, A, Jones, NC, Hoffmann, SV, Blanch, EW, Dyett, B, and Conn, CE. 2025. “Cubosome Lipid Nanocarriers for Delivery of Ultra-Short Antimicrobial Peptides.” *Journal of Colloid and Interface Science* 677 (July 2024): 1080–97.
- Larsson, K, and Tiberg, F. 2005. “Periodic Minimal Surface Structures in Bicontinuous Lipid-Water Phases and Nanoparticles.” *Current Opinion in Colloid and Interface*

Science 9 (6): 365–69.

- Lei, H, Gao, X, Wu, WD, Wu, Z, and Chen, XD. 2016. “Aerosol-Assisted Fast Formulating Uniform Pharmaceutical Polymer Microparticles with Variable Properties toward PH-Sensitive Controlled Drug Release.” *Polymers* 8 (5).
- Li, Y, Angelova, A, Hu, F, Garamus, VM, Peng, C, Li, N, Liu, J, Liu, D, and Zou, A. 2019. “PH Responsiveness of Hexosomes and Cubosomes for Combined Delivery of Brucea Javanica Oil and Doxorubicin.” *Langmuir* 35 (45): 14532–42.
- Mangiarotti, A, and Bagatolli, LA. 2021a. “Impact of Macromolecular Crowding on the Mesomorphic Behavior of Lipid Self-Assemblies.” *Biochimica et Biophysica Acta - Biomembranes* 1863 (12): 183728.
- Mathews, PD, Mertins, O, Angelov, B, and Angelova, A. 2022. “Cubosomal Lipid Nanoassemblies with PH-Sensitive Shells Created by Biopolymer Complexes: A Synchrotron SAXS Study.” *Journal of Colloid and Interface Science* 607:440–50.
- McMullen, TPW, Lewis, RNAH, and McElhaney, RN. 2004. “Cholesterol-Phospholipid Interactions, the Liquid-Ordered Phase and Lipid Rafts in Model and Biological Membranes.” *Current Opinion in Colloid and Interface Science* 8 (6): 459–68.
- Meikle, TG, Dyett, BP, Strachan, JB, White, J, Drummond, CJ, and Conn, CE. 2020. “Preparation, Characterization, and Antimicrobial Activity of Cubosome Encapsulated Metal Nanocrystals.” *ACS Applied Materials and Interfaces* 12 (6): 6944–54.
- Milogrodzka, I, Nguyen Pham, DT, Sama, GR, Samadian, H, Zhai, J, Campo, L de, Kirby, NM, Scott, TF, Banaszak Holl, MM, and ‘t Hag, L van. 2023. “Effect of Cholesterol on Biomimetic Membrane Curvature and Coronavirus Fusion Peptide Encapsulation.” *ACS Nano* 17 (9): 8598–8612.
- Moore, TJ, and Sharma, B. 2020. “Direct Surface Enhanced Raman Spectroscopic Detection of Cortisol at Physiological Concentrations.” *Analytical Chemistry* 92 (2): 2052–57.
- Morsi, NM, Abdelbary, GA, and Ahmed, MA. 2014. “Silver Sulfadiazine Based Cubosome Hydrogels for Topical Treatment of Burns: Development and in Vitro/in Vivo Characterization.” *European Journal of Pharmaceutics and Biopharmaceutics* 86 (2): 178–89.
- Muir, BW, Zhen, G, Gunatillake, P, and Hartley, PG. 2012. “Salt Induced Lamellar to Bicontinuous Cubic Phase Transitions in Cationic Nanoparticles.” *Journal of Physical Chemistry B* 116 (11): 3551–56.
- Mulet, X, Kennedy, DF, Conn, CE, Hawley, A, and Drummond, CJ. 2010. “High Throughput Preparation and Characterisation of Amphiphilic Nanostructured Nanoparticulate Drug Delivery Vehicles.” *International Journal of Pharmaceutics* 395 (1–2): 290–97.
- Nakano, M, Kamo, T, Sugita, A, and Handa, T. 2005. “Detection of Bilayer Packing Stress and Its Release in Lamellar-Cubic Phase Transition by Time-Resolved Fluorescence Anisotropy.” *Journal of Physical Chemistry B* 109 (10): 4754–60.
- Nakano, M, Sugita, A, Matsuoka, H, and Handa, T. 2001. “Small-Angle X-Ray Scattering and ¹³C NMR Investigation on the Internal Structure of ‘Cubosomes.’” *Langmuir*

17 (13): 3917–22.

- Nakano, M, Teshigawara, T, Sugita, A, Leesajakul, W, Taniguchi, A, Kamo, T, Matsuoka, H, and Handa, T. 2002. “Dispersions of Liquid Crystalline Phases of the Monoolein/Oleic Acid/Pluronic F127 System.” *Langmuir* 18 (24): 9283–88.
- Nguyen, TH, Hanley, T, Porter, CJH, and Boyd, BJ. 2011. “Nanostructured Liquid Crystalline Particles Provide Long Duration Sustained-Release Effect for a Poorly Water Soluble Drug after Oral Administration.” *Journal of Controlled Release* 153 (2): 180–86.
- Nowroozi, F, Almasi, A, Javidi, J, Haeri, A, and Dadashzadeh, S. 2018. “Effect of Surfactant Type, Cholesterol Content and Various Downsizing Methods on the Particle Size of Niosomes.” *Iranian Journal of Pharmaceutical Research* 17 (Special Issue 2): 1–11.
- Parasassi, T, Krasnowska, EK, Bagatolli, L, and Gratton, E. 1998. “Laurdan and Prodan as Polarity-Sensitive Fluorescent Membrane Probes.” *Journal of Fluorescence* 8 (4): 365–73.
- Parasassi, T, Stasio, G De, Ravagnan, G, Rusch, RM, and Gratton, E. 1991. “Quantitation of Lipid Phases in Phospholipid Vesicles by the Generalized Polarization of Laurdan Fluorescence.” *Biophysical Journal* 60 (1): 179–89.
- Peng, X, Zhou, Y, Han, K, Qin, L, Dian, L, Li, G, Pan, X, and Wu, C. 2015. “Characterization of Cubosomes as a Targeted and Sustained Transdermal Delivery System for Capsaicin.” *Drug Design, Development and Therapy* 9:4209–18.
- Quinn, PJ. 1981. “The Fluidity of Cell Membranes and Its Regulation.” *Progress in Biophysics and Molecular Biology* 38 (C): 1–104.
- Rakotoarisoa, M, Angelov, B, Espinoza, S, Khakurel, K, Bizien, T, and Angelova, A. 2019. “Cubic Liquid Crystalline Nanostructures Involving Catalase and Curcumin: BioSAXS Study and Catalase Peroxidatic Function after Cubosomal Nanoparticle Treatment of Differentiated SH-SY5Y Cells.” *Molecules* 24 (17): 3058.
- Rizwan, SB, Assmus, D, Boehnke, A, Hanley, T, Boyd, BJ, Rades, T, and Hook, S. 2011. “Preparation of Phytantriol Cubosomes by Solvent Precursor Dilution for the Delivery of Protein Vaccines.” *European Journal of Pharmaceutics and Biopharmaceutics* 79 (1): 15–22.
- Rizwan, SB, Dong, YD, Boyd, BJ, Rades, T, and Hook, S. 2007. “Characterisation of Bicontinuous Cubic Liquid Crystalline Systems of Phytantriol and Water Using Cryo Field Emission Scanning Electron Microscopy (Cryo FESEM).” *Micron* 38 (5): 478–85.
- Rosado, C, Silva, C, and Reis, CP. 2013. “Hydrocortisone-Loaded Poly(ϵ -Caprolactone) Nanoparticles for Atopic Dermatitis Treatment.” *Pharmaceutical Development and Technology* 18 (3): 710–18.
- Rui, X, Okamoto, Y, Watanabe, NM, Shimizu, T, Wakileh, W, Kajimura, N, and Umakoshi, H. 2024. “Preparation and Characterization of Macrophage Membrane Camouflaged Cubosomes as a Stabilized and Immune Evasive Biomimetic Nano-DDS.” *Journal of Materials Chemistry B*, 8702–15.
- Rui, X, Watanabe, NM, Okamoto, Y, Wakileh, W, and Umakoshi, H. 2024. “Xuehui Rui,

* Nozomi Morishita Watanabe, Yukihiro Okamoto, Ward Wakileh, and Hiroshi Umakoshi *.”

- Sagalowicz, L, Michel, M, Adrian, M, Frossard, P, Rouvet, M, Watzke, HJ, Yaghmur, A, Campo, L De, Glatter, O, and Leser, ME. 2006. “Crystallography of Dispersed Liquid Crystalline Phases Studied by Cryo-Transmission Electron Microscopy.” *Journal of Microscopy* 221 (2): 110–21.
- Sarkar, S, Dyett, B, Lakic, B, Ball, AS, Yeo, LY, White, JF, Soni, S, Drummond, CJ, and Conn, CE. 2023. “Cubosome Lipid Nanocarriers As a Drug Delivery Vehicle for Intracellular Mycobacterium Tuberculosis Infections.” *ACS Applied Materials and Interfaces* 15 (18): 21819–29.
- Sarkar, S, Tran, N, Soni, SK, Conn, CE, and Drummond, CJ. 2020. “Size-Dependent Encapsulation and Release of DsDNA from Cationic Lyotropic Liquid Crystalline Cubic Phases.” *ACS Biomaterials Science and Engineering* 6 (8): 4401–13.
- Scanavachi, G, Coutinho, A, Fedorov, AA, Prieto, M, Melo, AM, and Itri, R. 2021. “Lipid Hydroperoxide Compromises the Membrane Structure Organization and Softens Bending Rigidity.” *Langmuir* 37 (33): 9952–63.
- Scott, HL, Skinkle, A, Kelley, EG, Waxham, MN, Levental, I, and Heberle, FA. 2019. “On the Mechanism of Bilayer Separation by Extrusion, or Why Your LUVs Are Not Really Unilamellar.” *Biophysical Journal* 117 (8): 1381–86.
- Siekmann, B, Bunjes, H, Koch, MHJ, and Westesen, K. 2002. “Preparation and Structural Investigations of Colloidal Dispersions Prepared from Cubic Monoglyceride-Water Phases.” *International Journal of Pharmaceutics* 244 (1–2): 33–43.
- Spicer, PT, Hayden, KL, Lynch, ML, Ofori-Boateng, A, and Burns, JL. 2001. “Novel Process for Producing Cubic Liquid Crystalline Nanoparticles (Cubosomes).” *Langmuir* 17 (19): 5748–56.
- Spicer, PT, Small, WB, Lynch, ML, and Burns, JL. 2002. “Dry Powder Precursors of Cubic Liquid Crystalline Nanoparticles (Cubosomes).” *Journal of Nanoparticle Research* 4 (4): 297–311.
- Suga, K, Kondo, D, Otsuka, Y, Okamoto, Y, and Umakoshi, H. 2016. “Characterization of Aqueous Oleic Acid/Oleate Dispersions by Fluorescent Probes and Raman Spectroscopy.” *Langmuir* 32 (30): 7606–12.
- Suga, K, Otsuka, Y, Okamoto, Y, and Umakoshi, H. 2018. “Gel-Phase-like Ordered Membrane Properties Observed in Dispersed Oleic Acid/1-Oleoylglycerol Self-Assemblies: Systematic Characterization Using Raman Spectroscopy and a Laurdan Fluorescent Probe.” *Langmuir* 34 (5): 2081–88.
- Tadros, T, Izquierdo, P, Esquena, J, and Solans, C. 2004. “Formation and Stability of Nano-Emulsions.” *Advances in Colloid and Interface Science* 108–109:303–18.
- Tilley, AJ, Dong, Y Da, Chong, JYT, Hanley, T, Kirby, N, Drummond, CJ, and Boyd, BJ. 2012. “Transfer of Lipid between Triglyceride Dispersions and Lyotropic Liquid Crystal Nanostructured Particles Using Time-Resolved SAXS.” *Soft Matter* 8 (20): 5696–5708.
- Tilley, AJ, Drummond, CJ, and Boyd, BJ. 2013. “Disposition and Association of the Steric Stabilizer Pluronic® F127 in Lyotropic Liquid Crystalline Nanostructured

- Particle Dispersions.” *Journal of Colloid and Interface Science* 392 (1): 288–96.
- Tirosh, O, Barenholz, Y, Katzhendler, J, and Prie, A. 1998. “Hydration of Polyethylene Glycol-Grafted Liposomes.” *Biophysical Journal* 74 (3): 1371–79.
- Tiwari, G, Tiwari, R, Bannerjee, S, Bhati, L, Pandey, S, Pandey, P, and Sriwastawa, B. 2012. “Drug Delivery Systems: An Updated Review.” *International Journal of Pharmaceutical Investigation* 2 (1): 2.
- Tran, N, Zhai, J, Conn, CE, Mulet, X, Waddington, LJ, and Drummond, CJ. 2018. “Direct Visualization of the Structural Transformation between the Lyotropic Liquid Crystalline Lamellar and Bicontinuous Cubic Mesophase.” *Journal of Physical Chemistry Letters* 9 (12): 3397–3402.
- Tyler, AII, Barriga, HMG, Parsons, ES, McCarthy, NLC, Ces, O, Law, R V., Seddon, JM, and Brooks, NJ. 2015. “Electrostatic Swelling of Bicontinuous Cubic Lipid Phases.” *Soft Matter* 11 (16): 3279–86.
- Van’T Hag, L, Gras, SL, Conn, CE, and Drummond, CJ. 2017. “Lyotropic Liquid Crystal Engineering Moving beyond Binary Compositional Space-Ordered Nanostructured Amphiphile Self-Assembly Materials by Design.” *Chemical Society Reviews* 46 (10): 2705–31.
- Vandoolaeghe, P, Barauskas, J, Johnsson, M, Tiberg, F, and Nylander, T. 2009. “Interaction between Lamellar (Vesicles) and Nonlamellar Lipid Liquid-Crystalline Nanoparticles as Studied by Time-Resolved Small-Angle X-Ray Diffraction.” *Langmuir* 25 (7): 3999–4008.
- Veatch, SL, and Keller, SL. 2003. “Separation of Liquid Phases in Giant Vesicles of Ternary Mixtures of Phospholipids and Cholesterol.” *Biophysical Journal* 85 (5): 3074–83.
- Vitrac, H, MacLean, DM, Jayaraman, V, Bogdanov, M, and Dowhan, W. 2015. “Dynamic Membrane Protein Topological Switching upon Changes in Phospholipid Environment.” *Proceedings of the National Academy of Sciences of the United States of America* 112 (45): 13874–79.
- Watanabe, N, Goto, Y, Suga, K, Nyholm, TKM, Slotte, JP, and Umakoshi, H. 2019. “Solvatochromic Modeling of Laurdan for Multiple Polarity Analysis of Dihydrosphingomyelin Bilayer.” *Biophysical Journal* 116 (5): 874–83.
- Watanabe, N, Suga, K, Slotte, JP, Nyholm, TKM, and Umakoshi, H. 2019. “Lipid-Surrounding Water Molecules Probed by Time-Resolved Emission Spectra of Laurdan.” *Langmuir* 35 (20): 6762–70.
- Watanabe, N, Suga, K, and Umakoshi, H. 2017. “Comparison of Physicochemical Membrane Properties of Vesicles Modified with Guanidinium Derivatives.” *Journal of Physical Chemistry B* 121 (39): 9213–22.
- Wik, J, Bansal, KK, Assmuth, T, Rosling, A, and Rosenholm, JM. 2020. “Facile Methodology of Nanoemulsion Preparation Using Oily Polymer for the Delivery of Poorly Soluble Drugs.” *Drug Delivery and Translational Research* 10 (5): 1228–40.
- Yu, H, Angelova, A, Angelov, B, Dyett, B, Matthews, L, Zhang, Y, Mohamad, M El, Cai, X, Valimehr, S, Drummond, CJ, and Zhai, J. 2023. “Real-Time PH-Dependent Self-Assembly of Ionisable Lipids from COVID-19 Vaccines and In Situ Nucleic Acid

- Complexation.” *Angewandte Chemie - International Edition* 62 (35).
- Zaytseva, Y V., Zaytseva, I V., and Surovtsev, N V. 2022. “Conformational State Diagram of DOPC/DPPC62/Cholesterol Mixtures.” *Biochimica et Biophysica Acta - Biomembranes* 1864 (4): 183869.
- Zhang, L, Li, J, Tian, D, Sun, L, Wang, X, and Tian, M. 2020. “Theranostic Combinatorial Drug-Loaded Coated Cubosomes for Enhanced Targeting and Efficacy against Cancer Cells.” *Cell Death and Disease* 11 (1): 1–12.
- Zhao, J, Su, J, Qin, L, Zhang, X, and Mao, S. 2020. “Exploring the Influence of Inhaled Liposome Membrane Fluidity on Its Interaction with Pulmonary Physiological Barriers.” *Biomaterials Science* 8 (23): 6786–97.

List of Publications

[Papers]

1. Ward Wakileh, Nozomi Morishita Watanabe, Keishi Suga, Naoki Ikushima, Naoko Kajimura, Kaoru Mitsuoka, Yukihiro Okamoto, Hiroshi Umakoshi. Dispersibility and Surface Properties of Hydrocortisone-incorporated Self-Assemblies. *Colloids and Surfaces A: Physicochemical and Engineering Aspects*, 2023, 665, 131217.
2. Ward Wakileh, Nozomi Morishita Watanabe, Yuki Amatsu, Hiroshi Sekiguchi, Naoko Kajimura, Nanaki Kadonishi, Hiroshi Umakoshi. Investigation of Cubosome Interactions with Liposomal Membranes Based on Time-Resolved Small-Angle X-ray Scattering (TR-SAXS) and Membrane Hydration State Analysis. *The Journal of Physical Chemistry B*, *in press*. (2025)
3. Ward Wakileh, Nozomi Morishita Watanabe, Yuki Amatsu, Hiroshi Umakoshi. Examination of Effects of Hydrophobic Drug Incorporation on Cubosome-Cell membrane Model Interactions. *Chemistry Letters*, *Accepted*.
4. Ward Wakileh, Nozomi Morishita Watanabe, Zachary Nicolella, Yuki Amatsu, Naoko Kajimura, Hiroshi Umakoshi. Interactions of Cubosomes with Cell Membrane Lipids: Revealed Through Cubic Membrane Property Analysis. *Langmuir*, *Accepted* (2025)

[Related Papers]

1. Xuehui Rui, Yukihiro Okamoto, Nozomi Morishita Watanabe, Taro Shimizu, Ward Wakileh, Naoko Kajimura, Hiroshi Umakoshi. Preparation and characterization of macrophage membrane camouflaged cubosomes as a stabilized and immune evasive biomimetic nano-DDS. *Journal of Materials Chemistry B*, 2024, 12, 8702.
2. Xuehui Rui, Nozomi Morishita Watanabe, Yukihiro Okamoto, Ward Wakileh, Hiroshi Umakoshi. Exploring pH-Triggered Lamellar to Cubic Phase Transition in 2-Hydroxyoleic Acid/Monoolein Nanodispersions: Insights into Membrane Physicochemical Properties. *Journal of Physical Chemistry B*, 2024, 128, 9151–9162.

[International Conference/ Symposium]

1. Ward Wakileh, Nozomi Morishita Watanabe, Keishi Suga, Naoki Ikushima, Naoko Kajimura, Kaoru Mitsuoka, Yukihiro Okamoto, Hiroshi Umakoshi. Effects of Hydrocortisone Incorporation on the Physiochemical Properties of Monoolein and Oleic Acid Self-Assemblies, Membrane society of Japan, Membrane symposium, 2021. (Virtual Poster presentation)
2. Ward Wakileh, Nozomi Morishita Watanabe, Yuki Amatsu, Noboru Ohta, Hiroshi Sekiguchi, Yukihiro Okamoto, Hiroshi Umakoshi. Investigation of Cubosome Interactions with Liposomal Membranes Based on Time-Resolved SAXS and Membrane Property Analysis, International Congress on Membranes and Membrane Processes, Chiba, Japan, 9th -14th July, 2023. (Poster presentation).

Acknowledgements

I would like to extend my utmost gratitude to Prof. Dr. Hiroshi Umakoshi (Division of Chemical Engineering, Graduate School of Engineering Science, Osaka University) for his continuous guidance and encouragement during my studies at Osaka University. Professor Umakoshi believed in me and gave me the opportunity to pursue my studies in Japan, at the time when others did not. None of this work would have been possible without his unwavering support. Also, I would like to thank Prof. Dr. Nobuyuki Matsubayashi and Prof. Dr. Nobuyuki Nishiyama (Division of Chemical Engineering, Graduate School of Engineering Science, Osaka University) for their insightful comments and suggestions during the preparation of this thesis.

I am extremely grateful to Assist. Prof. Dr. Nozomi Morishita Watanabe (Division of Chemical Engineering, Graduate School of Engineering Science, Osaka University) for the countless hours she spent supporting me and providing me with valuable advice and comments. Professor Watanabe always tried her best to give me resources and opportunities to advance my research and hone my skills. At many points during this PhD, she saw the potential in me even when I could not believe in myself. Without her tremendous efforts and support, I would not be able to achieve this milestone.

My heartfelt thanks go to Assoc. Prof. Dr. Keishi Suga (Department of Chemical Engineering, Graduate School of Engineering, Tohoku University) for his valuable comments and helpful advice. I would like to thank Assoc. Prof. Dr. Yukihiro Okamoto (Division of Chemical Engineering, Graduate School of Engineering Science, Osaka University) for his advice and comments. In addition, I am grateful to Ms. Keiko Fukumoto for her kind support.

I am deeply thankful to all the collaborators for their invaluable expertise and input. Special thanks to Prof. Dr. Kaoru Mitsuoka and Dr. Naoko Kajimura (Research Center for Ultra-High Voltage Electron Microscopy, Osaka University) for their great assistance in the Cryo-TEM experiments. Also, I am grateful for Dr. Noboru Ohta and Dr. Hiroshi Sekiguchi (Japan Synchrotron Radiation Research Institute/SPring-8) for the tremendous support and advice in the TR-SAXS experiments.

Special thanks to all the members of the Bio-inspired Chemical Engineering Lab. I owe my deepest thanks to my colleagues Yuki Amatsu, Naoki Ikushima, Nanaki Kadonishi, Zach Nicolella, for their valuable contribution and collaboration across different projects during this PhD.

I would like to express my appreciation to my dad and aunts for always being very supportive and encouraging during my studies. Their active support has sustained me throughout this hard journey. Also, I am very thankful for all my friends in Amman, and all friends I made in Japan for making this journey unforgettable. Special thanks go to the staff at ARIS, Tasaka-san, Naoko-san and especially Ishikawa-san for their support and assistance. I am extremely grateful for the great friends in ARIS and all the great memories we have together there. To all the kind people at Ishibashi, thank you for your hospitality and kindness, especially the kind people at Tora, the late Sato-san (Taisho) and Yamato-san.

Finally, I am very grateful Japanese Government (MEXT) Scholarship for providing the financial support to complete my studies in Japan.